

NEUTRON CONTAMINATION FROM MEDICAL ELECTRON ACCELERATORS

| N | C | R | P |

NCRP REPORT No. 79

Neutron Contamination from Medical Electron Accelerators

**Recommendations of the
NATIONAL COUNCIL ON RADIATION
PROTECTION AND MEASUREMENTS**

Issued November 1, 1984

First Reprinting January 15, 1987

Second Reprinting October 15, 1990

Third Reprinting June 15, 1994

Fourth Reprinting August 15, 1995

***National Council on Radiation Protection and Measurements
7910 WOODMONT AVENUE / BETHESDA, MD. 20814***

LEGAL NOTICE

This report was prepared by the National Council on Radiation Protection and Measurements (NCRP). The Council strives to provide accurate, complete and useful information on its reports. However, neither the NCRP, the members of NCRP, other persons contributing to or assisting in the preparation of this report, nor any person acting on the behalf of any of these parties (a) makes any warranty or representation, express or implied, with respect to the accuracy, completeness or usefulness of the information contained in this report, or that the use of any information, method or process disclosed in this report may not infringe on privately owned rights; or (b) assumes any liability with respect to the use of, or for damages resulting from the use of, any information, method or process disclosed in this report.

Library of Congress Cataloging in Publication Data
National Council on Radiation Protection and Measurements.
Neutron contamination from medical electron accelerators.

(NCRP report, ISSN 0083-209X; no. 79)

Prepared by: Scientific Committee 60.

"Issued October 1, 1984."

Bibliography: p.

Includes index.

1. Electron beams—Therapeutic use—Congresses. 2. Neutrons—Congresses. 3. Particle accelerators—Safety measures—Congresses. 4. Radiotherapy—Safety measures—Congresses. I. National Council on Radiation Protection and Measurements. Scientific Committee 60. II. Title. III. Series. [DNLM: 1. Electrons. 2. Neutrons. 3. Particle Accelerators. 4. Radiometry—standards. 5. Radiotherapy—adverse effects. 6. Radiotherapy Dosage—standards. WN 250 N277n]

RM862.E4N38 1984 615.8'42 84-19848

ISBN 0-913392-70-7

Copyright © National Council on Radiation
Protection and Measurements 1984

All rights reserved. This publication is protected by copyright. No part of this publication may be reproduced in any form or by any means, including photocopying, or utilized by any information storage and retrieval system without written permission from the copyright owner, except for brief quotation in critical articles or reviews.

PREFACE

This report addresses a problem encountered with the use of electron accelerators in radiation therapy. The potential exists for the production of neutrons, in several different ways, when equipment used to generate electrons operates at energies above 10 MeV. The sources of these neutrons and their relative contributions are described. A further section is devoted to the potential hazard from the neutrons which are produced and which represent a contribution to the total radiation dose to the patient. This contribution is not normally included in the calculation of dose delivered to the treatment volume, as performed by the therapist and the medical physicist. The question of whether or not this additional dose constitutes an unacceptable risk to the patient is discussed.

The report addresses the hazard to operating personnel from neutrons produced outside the patient's treatment volume. Neutron measurement methods are also addressed. The report concludes with a survey of the published literature relevant to the subject.

The Council has noted the adoption by the 15th General Conference of Weights and Measures of special names for some units of the Système International d'Unités (SI) used in the field of ionizing radiation. The gray (symbol Gy) has been adopted as the special name for the SI unit of *absorbed dose*, *absorbed dose index*, *kerma*, and *specific energy imparted*. The becquerel (symbol Bq) has been adopted as the special name for the SI unit of *activity* (of a radionuclide). One gray equals one joule per kilogram; and one becquerel is equal to one second to the power of minus one. Since the transition from the special units currently employed-rad and curie-to the new special names is expected to take some time, the Council has determined to continue, for the time being, the use of rad and curie. To convert from one set of units to the other, the following relationships pertain:

$$1 \text{ rad} = 0.01 \text{ J kg}^{-1} = 0.01 \text{ Gy}$$

$$1 \text{ curie} = 3.7 \times 10^{10} \text{ s}^{-1} = 3.7 \times 10^{10} \text{ Bq} \text{ (exactly).}$$

iv / PREFACE

The present report was prepared by Scientific Committee 60. Serving on the committee during the preparation of this report were:

Richard C. McCall, Chairman
Stanford Linear Accelerator Center
Stanford, California

Members

Peter R. Almond
M. D. Anderson Hospital & Tumor Institute
Houston, Texas

George R. Holeman
Yale University
New Haven, Connecticut

John A. Devanney
Center for Devices and Radiological Health
Rockville, Maryland

Lawrence H. Lanzl
Rush-Presbyterian-St. Luke's
Medical Center
Chicago, Illinois

Everett G. Fuller
National Bureau of Standards
Washington, D.C.

Harry Ing, Advisor
Atomic Energy of Canada, Ltd.
Chalk River, Ontario

William P. Swanson, Consultant
Stanford Linear Accelerator Center
Stanford, California

NCRP Secretariat, James A. Spahn, Jr.

The Council wishes to express its appreciation to the members, advisor and consultant for the time and effort devoted to the preparation of this report.

Warren K. Sinclair
President, NCRP

Bethesda, Maryland
March 1, 1984

CONTENTS

Preface	iii
1. INTRODUCTION	1
2. NEUTRON PRODUCTION AND TRANSPORT	5
2.1 Physics of Photoneutron Production	5
2.1.1 Photo- and Electroproduction of Neutrons	5
2.1.2 Primary Photoneutron Spectra	26
2.2 Transport of Neutrons in Accelerator Head	34
2.2.1 Effects on Neutron Spectra	34
2.2.2 Neutron Fluence Attenuation	40
2.2.3 Absorbed Dose and Dose Equivalent Attenuation	42
2.3 Transport of Neutrons in a Concrete Room	46
2.3.1 Effect on Spectra	46
2.3.2 Spatial Distribution of Fluence, Absorbed Dose and Dose Equivalent	48
2.3.3 Room Shielding	49
2.3.4 Maze Design	52
2.3.5 Door Shielding	57
2.3.6 Reduction of Neutron Emission from Accelerators	59
3. HAZARDS FROM NEUTRONS	61
3.1 Patient Risk	61
3.1.1 Introduction	61
3.1.2 Source of Radiation Dose Outside the Treatment Volume	63
3.1.3 Significance of Leakage Exposure	67
3.2 Sources of Exposure for Operating Personnel	68
3.2.1 Door Leakage	68
3.2.2 Activation	69
3.2.2.1 Accelerator and Treatment Aids	69
3.2.2.2 Patient	70
3.2.2.3 Room Walls, Ceiling and Floor	70
3.3 Exposures During Installation	71
4. NEUTRON MEASUREMENTS	73
4.1 Introduction	73
4.2 Activation Detectors	73

vi / CONTENTS

4.2.1	Unmoderated Activation Detectors	73
4.2.1.1	Thermal Neutron Activation Detectors ..	74
4.2.1.2	Threshold Activation Detectors	74
4.2.2	Moderated Foil Detectors	78
4.2.3	Neutron Spectral Measurements	79
4.2.4	Data Collection	80
4.3	Etched Track Detectors	81
4.3.1	Introduction	81
4.3.2	Fission-Fragment Track-Etching Dosimeters	82
4.3.2.1	Photofission Corrections	85
4.3.3	Direct Interaction Track-etch Dosimeters	85
4.4	Diodes	88
4.5	Ionization Detectors	90
4.5.1	Introduction	90
4.5.2	Ionization Chambers	90
4.5.3	Proportional Counters	92
4.5.4	Geiger-Müller Counters	92
5.	LITERATURE REVIEW	94
	REFERENCES	98
	The NCRP	112
	NCRP Publications	119
	Index	128

1. Introduction

The National Council on Radiation Protection and Measurements (NCRP) has made recommendations for the protection of persons who may be exposed to radiation occupationally or otherwise. For implementation of these recommendations, it is necessary to examine the radiation environment of these individuals, to evaluate the factors determining the likelihood of their exposure, and to estimate the actual exposure. This report addresses these matters for neutron exposures resulting from the operation of medical electron accelerators. Contained in this report is a review of the source of neutrons generated from medical electron accelerators (betatrons, linear accelerators, and microtrons), an examination of the transport of the neutrons in the protective housing of the accelerator as well as in the structural shielding barrier, an outline of the hazards to operating personnel and patients, methods for reducing these hazards, and a description of methods of measuring neutrons from various types of medical accelerators. The report contains recommendations on practical methods of measuring neutrons, on factors for converting neutron fluence to dose and dose equivalent, and on reporting methods.

Neutron production in accelerators used for therapy can result in doses to patients and to operating personnel from direct exposure both to neutrons and to the resulting residual radioactivity. The various possible processes are shown schematically in Figure 1 (NCRP, 1964). Primary attention here will be given to neutron exposures, and thus those processes producing neutrons are important.

The minimum energy required to remove one neutron from a nucleus for most stable nuclei heavier than carbon lies between 6 and 16 MeV. A nucleus can absorb energy from a high-energy electron or a high-energy photon and emit a neutron if the energy of the electron or photon exceeds this minimum energy.

Neutrons can also be emitted during the process of photon- or electron-induced fission. The elements heavier than bismuth, including depleted uranium, undergo fission when bombarded with electrons or photons in the energy range used in radiotherapy. While there is no true threshold for photofission, this process is usually negligible, even in uranium, below about 5 MeV.

Above the neutron separation energy, (*i.e.*, the threshold energy)

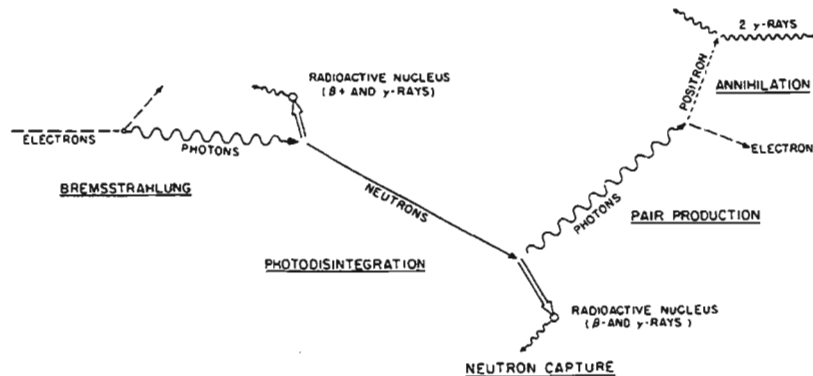


Fig. 1. Some interactions of radiation with matter (NCRP, 1964).

the cross section for neutron production increases with photon energy, E_γ , reaches a maximum value, then decreases with further increases of E_γ . The shape of this peak is characteristic of resonance reactions and is called the *giant resonance*. In all theories of photonuclear reactions, the giant resonance is attributed to electric dipole absorption of the incident photon, although quadrupole oscillations can modify the cross sections somewhat. Typically, the maximum value of the photonuclear cross section in most light elements is reached at about 20 to 25 MeV, and in heavy elements at lower photon energies, down to about 13 MeV in uranium. The full width at half maximum of the giant resonance is about 4 to 10 MeV for various nuclei and shows no simple dependence on mass number or atomic number. This topic will be explored in more detail in section 2.1.

In summary, the potential sources of neutron contamination are any materials on which the electron beam (or x-ray beam) is incident, such as the walls of the vacuum chamber in any accelerator, the walls of the wave guide in a linear accelerator, the x-ray target or beam extractor, filters, collimators, transmission ionization chambers, light localizers, the air path of the beam, and the patient. The potential sources of residual radioactivity are any places where neutrons are produced or absorbed.

The betatron was the first accelerator (greater than 10 MeV) to be developed and used for electron therapy (Skaggs *et al.*, 1946, 1948; Harvey *et al.*, 1952) and photon (*i.e.*, x-ray) therapy (Adams *et al.*, 1948; Quastler *et al.*, 1949) in which the energy of the radiations was sufficiently high to produce neutrons. Quastler *et al.* (1949), measured the slow neutron fluence rate and estimated the fast neutron fluence rate at the position of the patient while under treatment. In the betatron, the electrons are accelerated in a circular orbit. When the

electrons have reached an appropriate energy, the beam is directed either (1) through a field-free region and thus extracted from the betatron for electron therapy or (2) onto a high-atomic-number material which is the x-ray target.

At the present time, an electron linear accelerator would more likely be used for both electron and x-ray therapy. A design for a typical therapy room for a linear accelerator is shown in Figure 2(a). In a further development (Skaggs *et al.*, 1958), electron therapy with a linear accelerator is performed with a pencil-beam scanning technique. With this technique, much of the stray radiation, consisting of both bremsstrahlung and neutrons, is produced at an energy-selecting collimator. Downstream from this collimator, the electron beam is bent

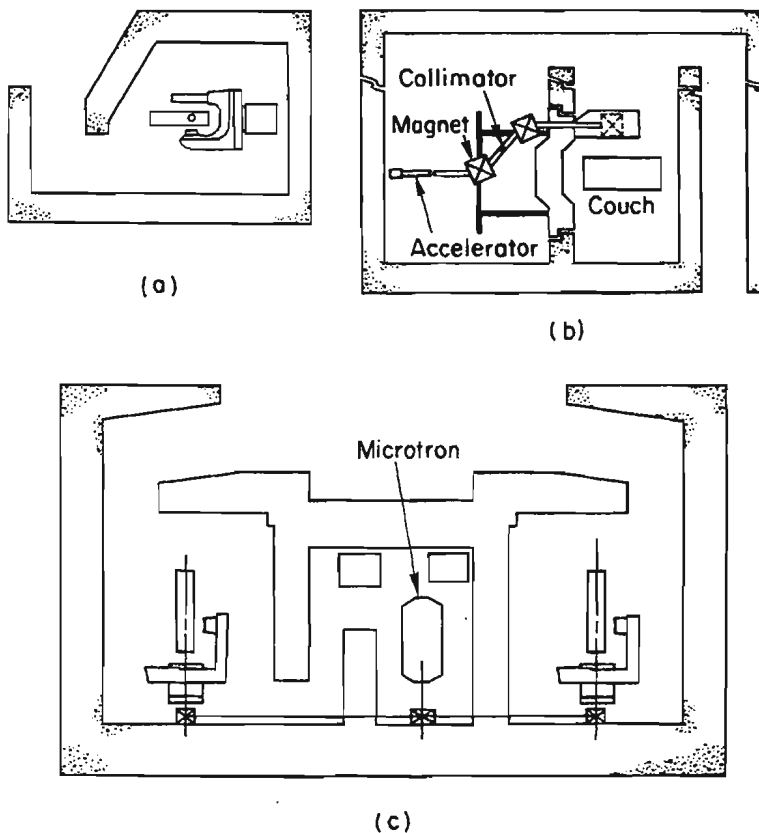


Fig. 2. Typical treatment room layouts for medical electron accelerators; (a) an isocentric linear accelerator, (b) an accelerator dedicated for electron therapy, and (c) a microtron serving two isocentric treatment heads in separate rooms.

through two magnets onto the patient without the need for beam collimators or flattening filters. Structural shielding is placed between the energy-selecting collimator and the patient treatment area. With this technique, patient exposure to neutrons is minimized. A typical therapy facility of this type is illustrated in Figure 2(b). Most modern commercial linear accelerators are built into an isocentric treatment gantry; *i.e.*, it is arranged so that the beam can be rotated around a point in space called the isocenter. The treatment head incorporates mechanisms to permit use of the electron beam or a target to produce x rays.

A third type of electron accelerator, the microtron, has recently appeared on the market. The microtron is also a circular machine, but has greater current capabilities than the betatron. The electron beam is usually transported to a separate therapy room into an isocentric treatment gantry. A typical microtron facility is illustrated in Figure 2(c), where one microtron is used for two separate therapy rooms.

At present, medical electron accelerators that operate at energies up to 50 MeV are in use. Below 10 MeV, neutron production is negligible; therefore, this report will be confined to machines that accelerate electrons to energies of 10 to 50 MeV.

2. Neutron Production and Transport

2.1 Physics of Photoneutron Production

2.1.1 Photo- and Electroproduction of Neutrons

The production of neutrons resulting from the interaction of photons or electrons with various nuclides is governed by the properties of the giant resonance of the photonuclear interaction. The area under this large peak in the plot of the nuclear photon absorption cross section as a function of photon energy E , is found to be approximately that given by the dipole sum-rule (Levinger and Bethe, 1950),

$$\int_0^{\infty} \sigma(E) dE = \frac{2\pi^2 e^2 \hbar}{Mc} \frac{NZ}{A} = 0.06 NZ/A \text{ (MeV-barns)} \\ = 60 NZ/A \text{ (MeV-mbarns).} \quad (1)$$

In this expression, e is the charge of the electron, \hbar is Planck's constant divided by 2π (MeV-s), M is the mean nucleon mass ($Mc^2 = 938.926$ MeV), c is the speed of light (cm^2s^{-1}), N the neutron number, Z the proton number, and $A = N + Z$ is the number of nucleons in a nuclide. The area under the empirical total absorption curve, referred to as the strength of the giant resonance, is sometimes expressed in units of this sum rule. The symbol used for this integral is σ_0 or $\sigma_0(E)$ if the integral is made only up to an upper energy limit of E .

Figure 3 gives a rough picture of the giant resonance for nuclides ranging from oxygen to lead. In this figure, the energy scale for each nuclide has been normalized so that the mean energy (energy weighted by cross section) for photon absorption below 30 MeV has been set equal to one. The actual mean energies for the specific nuclides are given in MeV by the figures in the center of the shaded region indicated for each nuclide. These shaded regions indicate the extent of the giant resonance, *i.e.*, they indicate roughly the region between the half-maximum points on the absorption cross-section curve. Note that in this figure the overall widths of the giant resonance vary by a factor of about two. The narrowest resonances are for those nuclides with closed shells, whereas the broadest are for those nuclides, (*e.g.*, ^{165}Ho)

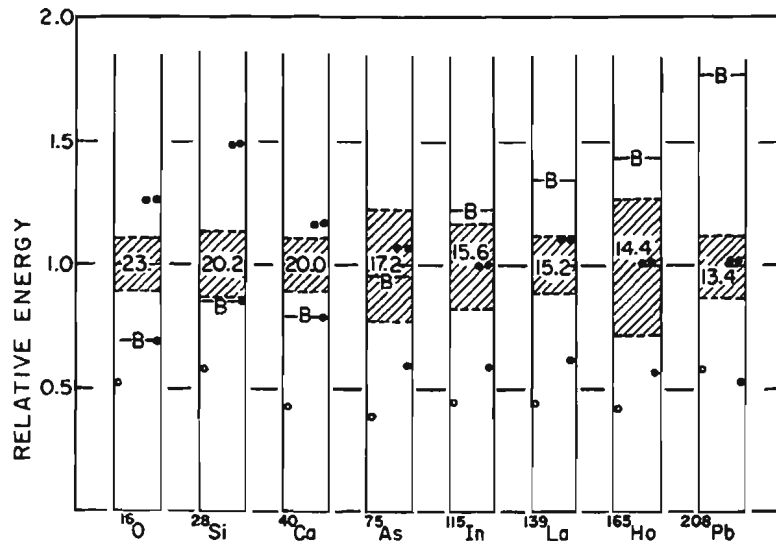


Fig. 3. Giant resonance summary. The energy scale for each nucleus has been normalized so that the giant resonance is one. The width of the giant resonance on this scale is indicated by the shaded regions. Separation energies are indicated by circles, open for protons and closed for neutrons. See text for complete description.

that have large permanent deformations. The overall extent of the giant resonance for the deformed nuclei is determined to a large extent by the splitting of the giant resonance resulting from the nuclear deformation. In this respect, the large width indicated for ^{75}As is interesting in that it can probably be associated with a dynamic deformation of this nucleus resulting from the zero-point vibrations of the nuclear surface.

The black dots and open circles shown for each nuclide in Figure 3 indicate, respectively, the neutron and proton separation energies, S_n and S_p . These are the energies that must be added to each nuclide to remove a neutron or a proton from it. The double black dots indicate the corresponding separation energies for two neutrons. Note that, while, for the light nuclides, the two-neutron separation energy is well above the giant resonance, in the heavier ones it occurs in the center of the giant resonance. For the latter nuclides, the $(\gamma, 2n)$ cross section can, therefore, make an appreciable contribution to the total absorption cross section. Note that this reaction results in the production of two neutrons for each photon absorbed. The lines designated by the letter "B" for each nuclide indicate the top of the Coulomb barrier for protons. In the light nuclides this barrier compensates for the difference in the separation energy for neutrons and protons. The total $(\gamma,$

p) yield might be expected to equal the total (γ , n) yield, were it not for the fact that the high neutron separation energy results in there being a paucity of states available for decay by neutron emission. In the heavy nuclides, the top of the Coulomb barrier comes well above the giant resonance and the decay is predominantly by neutron emission, since charged particles such as protons and alphas cannot easily penetrate the Coulomb barrier. Therefore, to a very good approximation, the sum of the neutron producing cross sections is the total nuclear absorption cross section for photons. This effect, when coupled with the low (γ , 2n) thresholds for the heavier nuclides, means that they are much more efficient photoneutron producers than are the lighter nuclides.

Principally as a result of the development of the quasi-monoenergetic, positron-annihilation-in-flight photon beams [see, e.g., (Beil *et al.*, 1969; Berman & Fultz, 1975)], reliable neutron production cross section measurements have been conducted for essentially all of the major stable nuclides, *i.e.*, those with relative isotopic abundances, for a given element, of 10 percent or greater. The data from these measurements for mass number A greater than 70, when combined with careful total photon absorption cross section measurements for the lighter nuclides (Ahrens *et al.*, 1975), have made it possible to establish firmly the systematics of the giant resonance over the entire periodic table. The mean energy and strength of the giant resonance derived from these measurements are given in Figures 4 and 5. It should be pointed out that, although the neutron production cross section measurements in general extend only to energies of about 30 MeV, the total strength of the giant resonance shown in Figure 5 has been obtained by integrating, over all energies, the Lorentz line fits (Berman, 1975) made to the empirical cross section data. In general, the magnitude of the integrated cross section under the Lorentz line extrapolation of the cross section to energies, above the range covered in a measurement, ranges from 10 to 15 percent of the integral over the measured cross section.

The neutron production cross section measurements made, using quasi-monoenergetic, positron-annihilation-in-flight photon beams, lead directly to data giving the (γ , 1n), (γ , 2n), . . . , (γ , in) reactions for the target nuclide. Each of these represents a sum over all the reactions that result in the production of "i" neutrons. For example,

$$\begin{aligned}\sigma(\gamma, 1n) &= \sigma(\gamma, n) + \sigma(\gamma, pn) + \sigma(\gamma, \alpha n) + \dots \text{etc.} \\ \sigma(\gamma, 2n) &= \sigma(\gamma, 2n)_a + \sigma(\gamma, p2n) + \sigma(\gamma, \alpha 2n) \dots \text{etc.}\end{aligned}\quad (2)$$

In these expressions, the first term represents the cross section for a

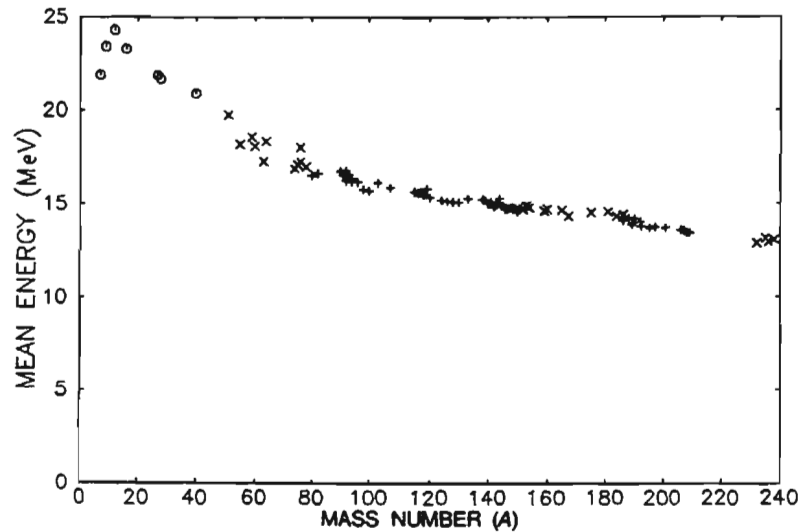


Fig. 4. Mean giant resonance energies. The plus signs represent the resonance energies of a single Lorentz line used to fit (γ, sn) cross section data, while the crosses are mean energies calculated from two Lorentz lines fitted to the cross section data. The circles are mean total absorption cross section energies calculated using data for energies below 30 MeV (Ahrens *et al.*, 1975).

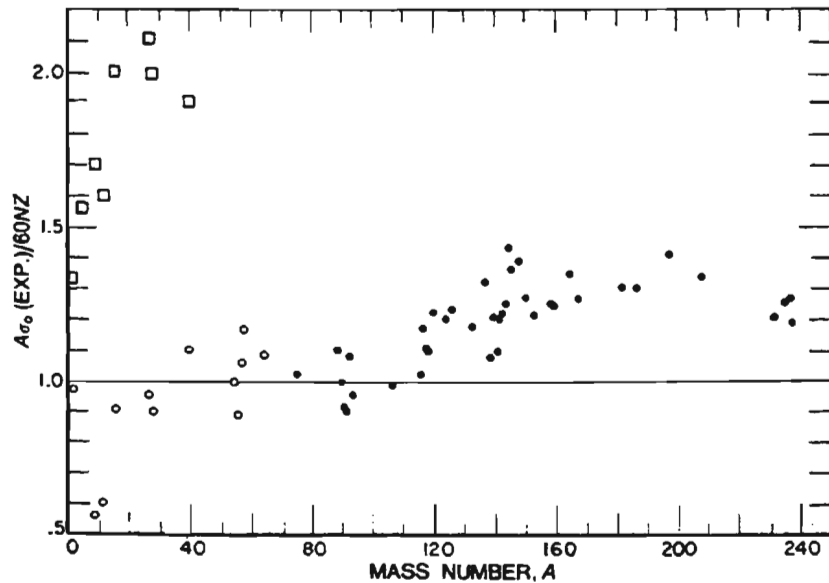


Fig. 5. The strength of the giant resonance in units of the classical dipole sum rule. Solid dots were obtained by integrating Lorentz line fits to (γ, sn) (see text for meaning) cross-section data. Open circles and squares are from total absorption cross-section measurements. For open circles, integration is taken to 30 MeV, for the squares it goes to 140 MeV.

reaction in which only "i" neutrons are emitted; e.g., $\sigma(\gamma, n)$ is the cross section for the reaction in which a nuclide of mass A and charge Z absorbs a photon and then emits a neutron to become a nuclide of mass $(A - 1)$ and charge Z . This nuclide is often radioactive, usually decaying by positron emission or by electron capture.

Except for a few special cases, the (γ, n) reaction makes the major contribution to the $(\gamma, 1n)$ cross section for photon energies below 35 MeV, i.e., in the giant resonance energy range. The only known exceptions to this are the $(\gamma, 1n)$ cross sections for the odd- Z , even- A nuclides ^6Li , ^{10}B , and ^{14}N . In these nuclides the (γ, pn) reaction is the major contributor to the $(\gamma, 1n)$ cross section because their (γ, pn) thresholds are close to or below their (γ, n) thresholds. For most nuclides then, the $(\gamma, 1n)$ cross section measured using modern quasi-monoenergetic, photon-beam facilities can be used as a very good approximation for the (γ, n) cross section. These cross section data tend to be much more reliable than the older results obtained from the analysis of measurements of bremsstrahlung-induced, radioactive yields.

The measured (γ, in) cross sections just described can be combined to obtain both $\sigma(\gamma, sn)$, the contribution of the photoneutron producing reactions to the total photon absorption cross section, and $\sigma(\gamma, xn)$, the total photoneutron yield cross section. These cross sections are given by

$$\begin{aligned}\sigma(\gamma, sn) &= \sigma(\gamma, 1n) + \sigma(\gamma, 2n) + \sigma(\gamma, 3n) + \dots \text{etc.} \\ \sigma(\gamma, xn) &= \sigma(\gamma, 1n) + 2\sigma(\gamma, 2n) + 3\sigma(\gamma, 3n) + \dots \text{etc.}\end{aligned}\quad (3)$$

Typical examples of $(\gamma, 1n)$ and (γ, xn) cross sections for a series of nuclides ranging from ^{12}C through ^{238}U are plotted in Figures 6 through 12. They are typical of the data available with quasi-monoenergetic photon beams. In all of these figures, the (γ, xn) cross section is indicated by crosses while the $(\gamma, 1n)$ or (γ, n) cross section is given by plus signs. Below the two nucleon separation energy the (γ, xn) cross section is equal to the sum of the single neutron emission cross sections. The superposition of a cross and a plus sign results in the low energy cross section points that appear to be plotted as asterisks in the lower energy positions of Figures 6 to 9 and 11. In some cases, cross-section data derived from measurement of bremsstrahlung yields extend to higher energies than do those made with the more modern techniques. In general, these measurements are not of as high a quality as the quasi-monoenergetic beam measurements and should only be used to extrapolate yield data to the higher energies.

The same nuclear reaction that can be induced by a photon can also be induced by the interaction of an electron with a nuclide. The

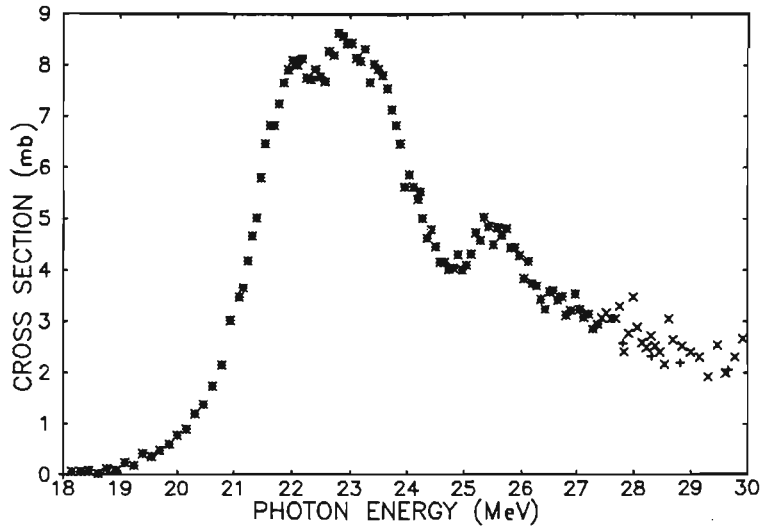


Fig. 6. The (γ, xn) and (γ, n) cross sections for ^{12}C . The (γ, xn) and (γ, n) cross sections are represented by crosses and plus signs, respectively. The data are based on those of Cook *et al.* (1966) and Fultz *et al.* (1966).

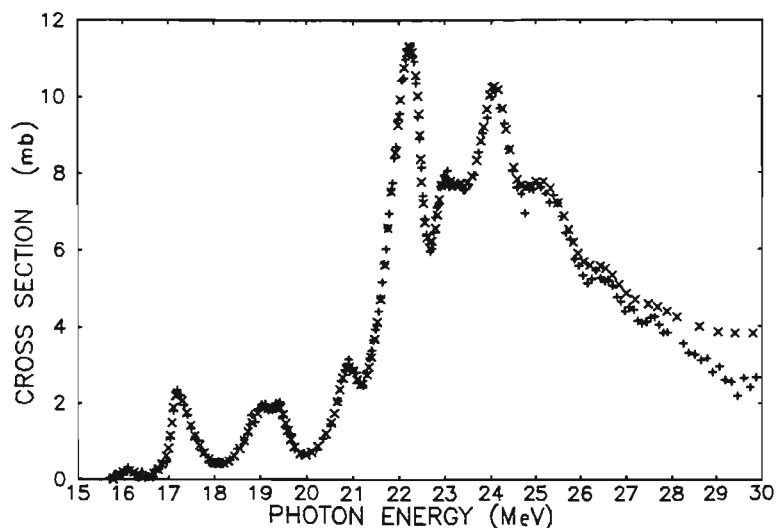


Fig. 7. The (γ, xn) and (γ, n) cross sections for ^{16}O . The (γ, xn) and (γ, n) cross sections are represented by crosses and plus signs, respectively (Veyssiére *et al.*, 1974).

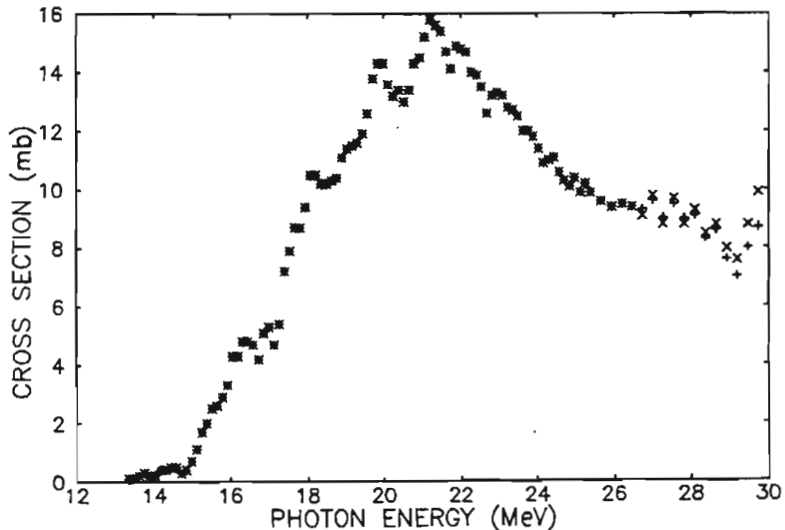


Fig. 8. The (γ, xn) and (γ, ln) cross sections for ^{27}Al . The (γ, xn) and (γ, ln) cross sections are represented by crosses and plus signs, respectively. Above 19.4 MeV the (γ, ln) cross section includes an unknown component due to the (γ, pn) cross section (Veyssiére *et al.*, 1974).

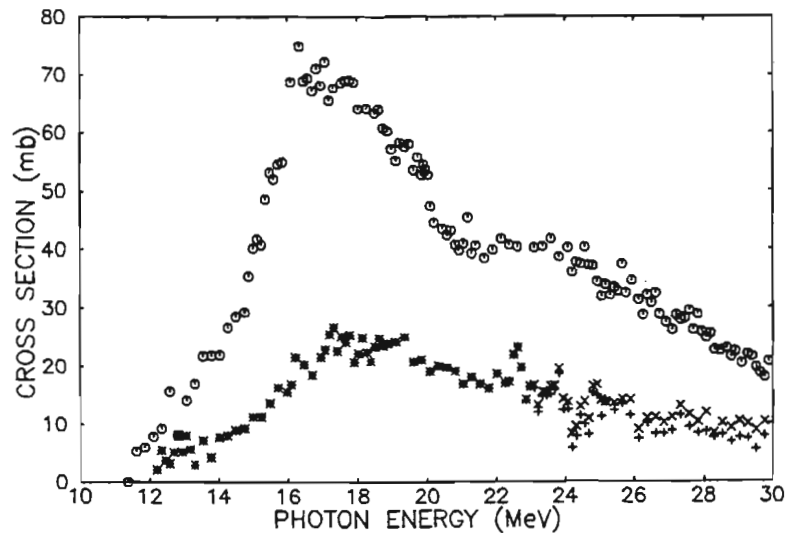


Fig. 9. Photoneutron cross sections for nickel isotopes. The (γ, xn) cross section for ^{60}Ni is given by the circles. The (γ, xn) and (γ, ln) cross sections for ^{58}Ni are given by the pluses and crosses, respectively. Above 19.6 MeV the (γ, ln) cross section includes an unknown component due to the (γ, pn) cross section (Fultz *et al.*, 1974).

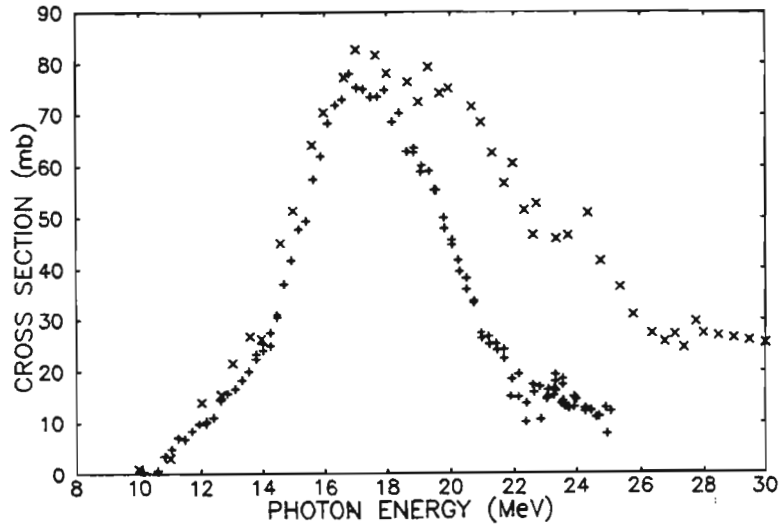


Fig. 10. Photoneutron cross sections for copper. The (γ, xn) cross section for natural copper is given by the crosses. The (γ, n) cross section for ^{63}Cu (abundance 69.2 percent) is represented by the plus signs. The (γ, xn) data are from Kneissl *et al.*, (1976); the $^{63}\text{Cu}(\gamma, n)$ data are from Sund *et al.*, (1968).

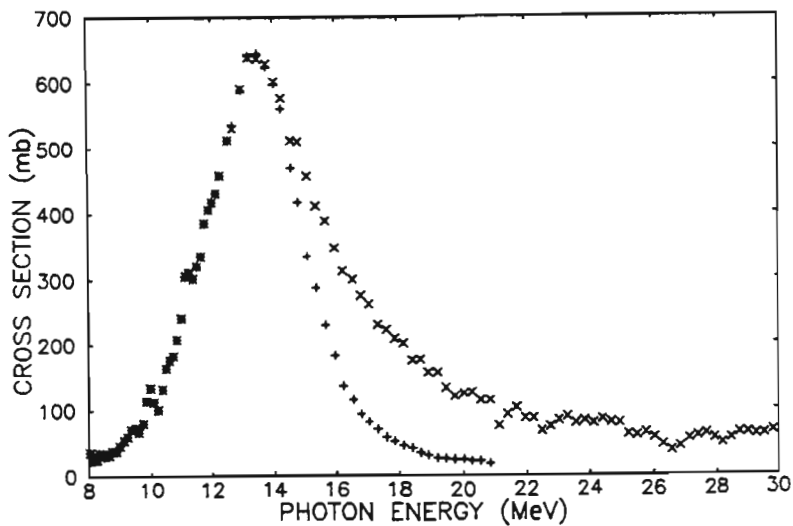


Fig. 11. The (γ, xn) and (γ, ln) cross sections for ^{208}Pb . The (γ, xn) and (γ, ln) cross sections are represented by crosses and plus signs, respectively. Above 14.9 MeV the (γ, ln) cross section includes an unknown component from the (γ, pn) reactions (Veysiére *et al.*, 1970).

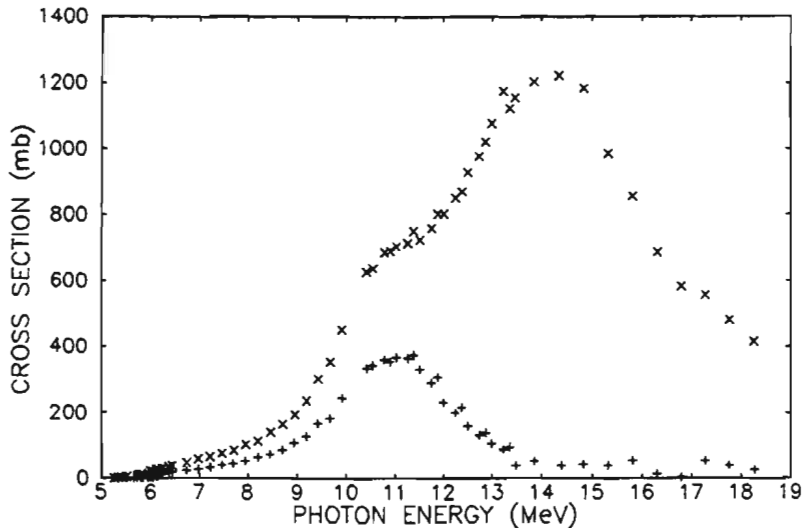


Fig. 12. The (γ, xn) and (γ, ln) cross sections for ^{238}U . The (γ, xn) and (γ, ln) cross sections are indicated by crosses and plus signs, respectively.

electrodisintegration cross section, *i.e.*, $\sigma(e, n:E_e)$, is analogous to the bremsstrahlung-weighted photodisintegration cross section, $\sigma_q(\gamma, n:E_e - mc^2)$, that would be measured using a bremsstrahlung spectrum generated by an electron with energy E_e . These two reactions are indicated schematically in the two diagrams given in Figure 13. Note that in both diagrams an electron with energy E_i enters from the left. In Figure 13a, the electron scatters through an angle θ in the Coulomb field of a radiator, nuclide R , to produce a real photon of energy $E_\gamma = E_i - E_f$. This photon then induces a photonuclear reaction in the target nuclide A , *e.g.*, $\gamma + A \rightarrow (A - 1) + n$. This diagram can be cut into two pieces anywhere along the photon's path between R and A . The reaction can take place either in a second nuclide R' in the radiator or in a sample meters away.

In the electrodisintegration diagram, Figure 13b, the same nuclide A is both the "radiator" and the target. In the sample shown, an electron again enters from the left and scatters through an angle θ in the Coulomb field of the nuclide A . In a few such events, rather than creating a real photon as in Figure 13a, a virtual photon of energy $E_\gamma = E_i - E_f$ will interact directly with the nuclide A to initiate a reaction, *e.g.*, $e + A \rightarrow (A - 1) + n + e'$. The notation $\sigma(e, n)$ is used for this reaction when the outgoing electron is not detected. When both the outgoing nucleon and electron are detected, the notation $\sigma(e, e'n)$ is used. Note that the diagram given in Figure 13b cannot be cut into two parts along the virtual photon line. Both the inelastic electron scattering and the electrodisintegration reactions result from the same

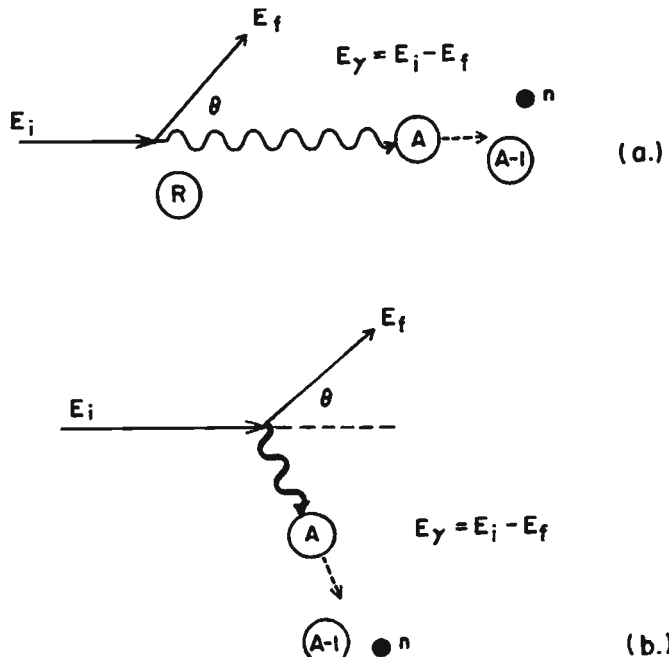


Fig. 13. Schematic representation of neutron production processes. Diagram (a) is for a (γ, n) reaction while (b) is for an (e, n) reaction. See discussion in text.

interaction of the incident electron with the target nuclide A . The electrodisintegration cross section is given by a sum of the integrals over the virtual-photon energy of the product of the appropriate virtual-photon spectra and photonuclear cross sections. Due to the lack of angular momentum resolved photonuclear cross section data and various technical difficulties in the calculations of virtual-photon spectra, it has not been possible to relate directly electro- to photodisintegration cross sections except for a few light nuclides and electron energies below 40 MeV.

In general, electrodisintegration cross sections are expected to be of the order of the fine structure constant, $\alpha \approx 1/137$, times the corresponding bremsstrahlung-weighted cross sections. This cross section, also called the cross section per equivalent quantum, is defined by the following expression:

$$\sigma_q(\gamma, n; E_b) = \frac{E_b \int_0^{E_\gamma} B(E_\gamma, E_b) E_\gamma^{-1} \sigma(\gamma, n; E_\gamma) dE_\gamma}{\int_0^{E_\gamma} B(E_\gamma, E_b) dE_\gamma}, \quad (4)$$

where $B(E_\gamma, E_b)$ is the energy per unit energy interval at an energy, E_γ , in a bremsstrahlung spectrum extending up to a maximum energy, E_b . The maximum energy is given by $E_b = E_i - mc^2$, where E_i is the energy of the electrons used to generate the bremsstrahlung and mc^2 is the electron rest mass, 0.511 MeV. Note that the integral in the denominator of this expression gives the total energy in the bremsstrahlung spectrum used to initiate the photonuclear reaction.

In order to put the electro- and photodisintegration reactions into some perspective, consider the yields from these two reactions resulting from the interaction of a beam of electrons with a "thin" target, i.e., a target in which the energy loss of the electrons passing through it is small enough so that the energy dependence of the reaction cross sections can be neglected. This condition defines a limiting energy loss for the electron ΔE_e which can be written as $\Delta E_e = \epsilon E_e$. The thickness of such a target is then given by $\Delta x = \epsilon E_e / \alpha(E_e) g/cm^2$, where $\alpha(E_e)$ is the total electron stopping power for the target. This is given by the sum of the collision, $\alpha_c(E_e)$, and radiative, $\alpha_r(E_e)$, stopping powers. In a small element of thickness Δx , the fraction of an electron's energy converted to bremsstrahlung is given by $\Delta x / X_r(E_e)$ where $X_r(E_e) = E_e / \alpha_r(E_e)$. Using these relationships, the reaction yields from the bremsstrahlung induced in the target, $Y_b(E_e)$, and from the direct electrodisintegration process, $Y_e(E_e)$, are given, e.g., by:

$$Y_b(\gamma, xn : E_e) = \frac{\Delta x}{X_r(E_e)} \frac{N \Delta x}{2A} \sigma_q(\gamma, xn : E_e - mc^2) \text{ neutrons/electron,} \quad (5)$$

$$Y_e(e, xn : E_e) = \frac{N \Delta x}{A} \sigma(e, xn : E_e) \text{ neutrons/electron,}$$

where $N = 6.022 \times 10^{23} \text{ mol}^{-1}$. Note that the ratio,

$$\frac{Y_b(\gamma, xn : E_e)}{Y_e(e, xn : E_e)} = \frac{\Delta x}{X_r(E_e)} \frac{1}{2} \frac{\sigma_q(\gamma, xn : E_e - mc^2)}{\sigma(e, xn : E_e)} \quad (6)$$

increases linearly with the target thickness. If the approximation is made that $\sigma(e, xn) / \sigma_q(\gamma, xn) = 1/37$ this expression becomes

$$\frac{Y_b}{Y_e} = \frac{\alpha_r(E_e)}{\alpha(E_e)} 68.5\epsilon, \quad (7)$$

i.e., it depends only on the target thickness and the ratio of the radiation to the total stopping power for the target. This yield ratio ranges from 10.2ϵ for Al at 10 MeV to 57.1ϵ for Pb at 50 MeV.

In terms of the expressions just discussed, the ratio of the neutron

16 / 2. NEUTRON PRODUCTION AND TRANSPORT

yield to the bremsstrahlung yield from a thin target is given by,

$$\begin{aligned} \frac{Y(xn)}{Y(brems)} &= \frac{N\Delta x}{A} \frac{\sigma_q(\gamma, xn)}{E_e} \left[0.5 + \frac{X_r(E_e)}{\Delta x} \frac{\sigma(e, xn)}{\sigma_q(\gamma, xn)} \right] \text{neutrons/MeV} \\ &\approx \frac{\epsilon}{\alpha(E_e)} \frac{N\sigma_q(\gamma, xn)}{A} \left[0.5 + \frac{\alpha(E_e)}{\alpha_r(E_e)} \frac{1}{137} \right] \text{neutrons/MeV}, \quad (8) \end{aligned}$$

where the only approximation involves replacing $\sigma(e, xn)/\sigma_q(\gamma, xn)$ by $1/137$. For 35 MeV electrons and $\epsilon = 0.05$, $Y(xn)/Y(brems)$ ranges from 1.88×10^{-6} neutrons per MeV of bremsstrahlung for carbon to 9.89×10^{-6} neutrons per MeV of bremsstrahlung for uranium. The quantities $\alpha_r(E_e)/\alpha(E_e)$ and $\alpha(E_e)$, are listed in Tables 1 and 2 (Berger and Seltzer, 1964). See also Berger and Seltzer, 1982.

Values of $\sigma_q(\gamma, xn:35 \text{ MeV})/A$ are plotted as a function of Z , the atomic number, in Figure 14. As is indicated by Figure 3 and Figures 6 through 12, 35 MeV is well above the peak of the giant resonance for all nuclides. The normalization of $\sigma_q(\gamma, xn:35 \text{ MeV})$ with the factor $1/A$, therefore, serves to remove most of the effect of the increase in strength of the giant resonance with the factor, NZ/A , given by the sum rule (see equation 1). This does not, however, remove the enhanced neutron yield due to the location of the $(\gamma, 2n)$ threshold relative to the giant resonance energy (see, e.g., Figure 3). The large normalized neutron yield for Be compared to C and O is the result of

TABLE 1—Ratio of radiative to total stopping power
 $\alpha_r(E_e)/\alpha(E_e)$

Element	E_e (MeV)					
	5	10	20	30	40	50
Be	.0280	.0586	.118	.173	.222	.266
C	.0390	.0797	.157	.224	.282	.333
N	.0410	.0805	.153	.215	.269	.316
O	.0459	.0895	.168	.234	.291	.341
Mg	.0714	.138	.253	.343	.415	.473
Al	.0774	.149	.270	.363	.436	.495
Fe	.149	.260	.418	.524	.599	.653
Cu	.164	.281	.444	.549	.623	.676
Ag	.243	.383	.552	.652	.716	.761
Sn	.254	.396	.563	.661	.725	.768
W	.341	.494	.650	.735	.790	.825
Au	.357	.508	.665	.747	.798	.833
Pb	.361	.511	.669	.750	.799	.834
U	.391	.540	.691	.769	.816	.848

TABLE 2—*Total electron stopping power**
 $\alpha(E_e)$, MeV-cm²/g

Element	E_e (MeV)					
	5	10	20	30	40	50
Be	1.566	1.673	1.844	2.001	2.152	2.302
C	1.761	1.914	2.164	2.396	2.622	2.847
N	1.915	2.157	2.523	2.840	3.128	3.405
O	1.919	2.172	2.564	2.907	3.227	3.526
Mg	1.750	1.979	2.383	2.773	3.158	3.543
Al	1.692	1.924	2.341	2.745	3.146	3.547
Fe	1.680	2.033	2.708	3.388	4.080	4.774
Cu	1.663	2.038	2.759	3.490	4.234	4.981
Ag	1.710	2.226	3.231	4.264	5.335	6.408
Sn	1.683	2.211	3.233	4.282	5.374	6.468
W	1.747	2.424	3.703	5.033	6.462	7.887
Au	1.770	2.469	3.839	5.242	6.694	8.190
Pb	1.779	2.493	3.907	5.337	6.783	8.303
U	1.783	2.530	4.006	5.512	7.059	8.673

* Later values for a broader range of electrons and energies in ICRU, 1984.

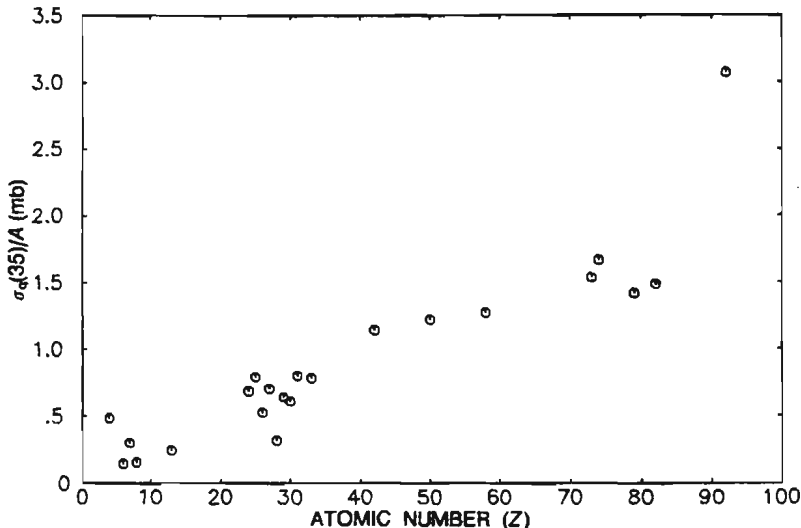


Fig. 14. Bremsstrahlung weighted photoneutron yield cross sections. The quantity plotted is $\sigma_4(\gamma, xn:35)/A$, where A is the atomic mass number. See text for discussion.

the $(\gamma, 2n)$ threshold in ${}^9\text{Be}$ being at 20.6 MeV, below the main giant resonance strength. In ${}^{12}\text{C}$ and ${}^{16}\text{O}$, these thresholds are on the high energy side of the giant resonance at 31.8 MeV and 28.5 MeV, respectively. The large value for ${}^{238}\text{U}$ is due to the large neutron multiplicity associated with the photofission cross section.

The low normalized yield for nickel at 35 MeV, 0.322 mb, is primarily

18 / 2. NEUTRON PRODUCTION AND TRANSPORT

due to the unique properties of ^{58}Ni . For a pure ^{58}Ni target, the normalized yield is even lower, 0.215 mb, giving, for the ratio of the neutron yield to bremsstrahlung yield for a target with $\epsilon = 0.05$, 1.28×10^{-6} neutrons per MeV of bremsstrahlung. The corresponding yield ratios for gold and lead are, respectively, 4.90×10^{-6} and 5.03×10^{-6} neutrons per MeV of bremsstrahlung. In spite of the low values of the ratio of neutron to bremsstrahlung yields for nickel, it is probably not practical to consider using nickel as a thick bremsstrahlung target or as a primary shielding material due to the necessity of having to provide additional shielding for radioactive decay products of the ^{57}Ni produced by the (γ, n) reaction in ^{58}Ni . The half life of ^{57}Ni is 36 hours and each decay results in the emission of a gamma ray with an energy of 1.38 MeV or higher. In addition, in 34 percent of the decays, positrons are emitted, each of which results in the production of two 511 keV annihilation photons.

In the discussion above, it has been assumed that the target with which the electron interacts is thin, i.e., $\epsilon \ll 1$. The actual value of ϵ chosen is such that, within the uncertainty desired for a calculated yield, the change in the electron's energy as it passes through the target can be neglected. When the target is not thin, the simple expressions given above must be replaced by the appropriate integrals of the various cross sections or yields over the electron energy distribution in the target. Note that for a thick target, thickness equal to or greater than the electron's range, the ratio of the neutron yield to the bremsstrahlung yield will be greater than the thin-target yields given by the expressions above. This results from the fact that the bremsstrahlung produced in an element at a given depth in a target can interact with all parts of the target at depths greater than the depth at which it was produced. This effect is included in the thin-target expressions, but those are valid only if the target is so thin that electrons passing through it lose, on the average, only a small fraction of their energy.

Tables 3 and 4 present data related to the production of neutrons in materials that are apt to be encountered in electron accelerator installations. Table 3 gives, for a series of elements ranging from beryllium to uranium, relative isotopic abundances, separation energy (S) associated with the principal neutron production reactions, and an abbreviated indication of the radioactive decay properties of the daughter nuclides produced in each reaction. Table 4 gives values of the cross section per equivalent quantum for the (γ, xn) reaction in a series of nuclides and elements. In all cases, the low-energy cross sections have been calculated from data obtained using quasi-monoenergetic positron annihilation-in-flight photon beams. In several

TABLE 3—Relative isotopic abundances, reaction separation energies and decay data

NUCLIDE			(γ, n) REACTION				(γ, pn) REACTION				($\gamma, 2n$) REACTION			
Chem. Symb.	Mass No.	Rel. Abund.	S_n MeV	$t_{1/2}$	Decay	Q MeV	S_{pn} MeV	$t_{1/2}$	Decay	Q MeV	S_{2n} MeV	$t_{1/2}$	Decay	Q MeV
H	2	0.02	2.23	s		—				—				
Be	9	100	1.67	s		18.92	s			20.56	53d	EC	0.86	
C	12	98.89	18.72	20.4min	β^+	1.98	27.41	s		31.84	19s	β^+	2.89	
	13	1.11	4.95	s			20.90	s		23.66	20.4min	β^+	1.98	
N	14	99.63	10.55	10min	β^+	2.21	12.49	s		30.62	11ms	β^+	17.3	
	15	0.36	10.83	s			18.38	s		21.39	9.96min	β^+	2.21	
O	16	99.75	15.66	122s	β^+	2.75	22.96	s		28.89	71s	β^+	5.15	
	17	0.03	4.14	s			16.27	s		19.81	122s	β^+	2.76	
	18	0.20	8.05	s			12.83	7.1s	β^-	10.4	12.19	s		
Mg	24	78.99	16.53	11.3s	β^+	4.06	24.11	2.6y	β^+	2.8	29.68	2.86	β^+	4.79
	25	10.00	7.33	s			19.02	s		23.86	11.3s	β^+	4.06	
	26	11.01	11.09	s			23.16	15h	β^-	5.5	18.43	s		
Al	27	100	13.06	$>10^6$ y	β^+	4.00	19.36	s		24.42	7.18s	β^+	4.28	
			6.4s	β^+	4.23									
Si	28	92.23	17.18	4.13s	β^+	4.81	24.64	10^6 y	β^+	4.0	30.49	2.21s	β^+	5.06
	29	4.67	8.74	s			20.06	s		25.65	4.13s	β^+	4.81	
	30	3.10	10.61	s			22.94	2.24min	β^-	4.6	19.08	s		
Cr	50	4.4	13.00	42min	β^+	2.63	21.14	16d	EC	4.0	23.58	21h	EC	1.7
	52	83.8	12.04	28d	EC	0.75	21.56	s		21.30	s			
	53	9.5	7.94	s			18.44	s		19.98	28d	EC	0.8	
	54	2.4	9.72	s			20.85	3.8min	β^-	4.0	17.66	s		
Fe	54	5.8	13.38	8.5min	β^+	3.74	20.91	21min	β^+	4.71	24.10	8.3h	β^+	2.37
							5.6d	EC	5.08					
	56	91.7	11.19	2.7y	EC	0.23	20.41	312d	EC	1.38	20.50	s		0.23
	57	2.1	7.65	s			17.83	s		18.84	27y	EC		
	58	0.2	10.04	s			20.60	2.6h	β^-	3.70	17.69	s		
Co	59	100.	10.45	71d	β^+	2.31	17.41	s		19.03	271d	EC	0.84	

TABLE 3. (Continued)

NUCLIDE			(γ , n) REACTION				(γ , pn) REACTION				(γ , 2n) REACTION			
Chem. Symb.	Mass No.	Rel. Abund.	S_n MeV	$t_{1/n}$	Decay	Q MeV	S_{pn} MeV	$t_{1/2}$	Decay	Q MeV	S_{2n} MeV	$t_{1/2}$	Decay	Q MeV
Ni	58	68.2	12.20	36h	β^+	3.27	19.55	79d	β^+	4.6	22.47	6.1d	EC	2.13
	60	26.1	11.34	10^5 y	EC	1.07	19.99	71d	EC	2.3	20.39	s		
	61	1.1	7.82	s			17.35	s			12.21	10^5 y	EC	1.10
	62	3.5	10.60	s			20.46	5.3y	β^-	2.8	18.42	s		
	64	0.9	9.66	100y	β^-	0.07	20.95	1.5min	β^-	5.3	16.50	s		
Cu	63	69.2	10.85	9.7m	β^+	3.95	18.72	s			19.74	3.4h	β^+	2.24
	65	30.8	9.91	12.7h	β^+	1.68	17.11	100y	β^-	0.07	17.83	s		
					β^-	0.58								
Zn	64	48.6	11.86	38min	β^+	5.5	14.04	9.7min	β^+	3.95	20.98	9.2h	EC	1.63
	66	27.9	11.06	244d	EC	1.4	18.84	13h	EC	1.67	19.04	s		
	67	4.1	7.05	s			16.33	s			18.11	244d	EC	1.32
	68	18.7	10.20	s			19.11	5.1min	β^-	2.64	17.25	s		
	70	0.6	9.21	56min	β^-	0.90	19.50	31s	β^-	4.62	15.70	s		
W	180	0.1	8.41	38min	EC	1.06	14.5	2.4h	EC	1.91	15.3	21d	EC	0.09
	182	26.3	8.06	121d	EC	0.19	14.67	8.1h	EC	0.86	14.75	s		
	183	14.3	6.19	s			13.28	s			14.25	121d	EC	0.19
	184	30.6	7.41	s			14.63	115d	β^-	1.81	13.60	s		
	186	28.6	7.20	75d	β^-	0.43	15.0	8.7h	β^-	2.87	12.95	s		
Pt	190	0.1	8.8	11h	EC	1.91	14.4	41h	EC	2.8	15.7	10d	EC	0.54
	192	0.8	8.7	2.9d	EC	1.00	15.0	12d	EC	2.0	15.1	s		
	194	32.9	8.38	4.3d	EC	0.06	15.30	74d	β^-	1.5	14.63	s		
									EC	1.1				

	195	33.8	6.11	s		13.47	s		14.49	4.3d	EC	0.06
	196	25.3	7.92	s		15.60	19h	β^-	2.3	14.03	s	
	198	7.2	7.5	18h	β^-	0.72	15.8	52s	β^-	3.2	13.4	s
								1.4h	β^-	1.2		
Au	197	100	8.06	6.2d	EC	1.49	13.71	s		14.72	183d	EC 0.23
					β^-	0.68						
Pb	204	1.4	8.4	52h	EC	0.97	14.5	12d	EC	1.37	15.3	10^8 y EC 0.05
	206	24.1	8.09	10^7 y	EC	0.06	14.80	3.8y	β^-	0.76	14.82	s
									EC	0.35		
	207	22.1	6.74	s		13.99	s		14.82	10^7 y	EC	0.06
	208	52.4	7.37	s		14.85	4.2min	β^-	1.53	14.11	s	
U	234	0.01	6.84	10^6 y		4.91	13.15	1.3d	β^-	1.34	12.60	72 y 5.41
	235	0.72	5.30	10^6 y		4.86	11.93	27d	β^-	0.57	12.14	10^6 y 4.91
	238	99.27	6.15	6.8d	β^-	0.52	13.6	9.1min	β^-	3.1	11.28	10^6 y 4.57

Note: Q values give the total energy available for the decay processes indicated. For positron decay the maximum positron energy is: $E_{\beta^+} = Q - 2mc^2$, where $mc^2 = 0.511$ MeV. No attempt has been made to give the energies of gamma rays that often follow decay by electron capture (EC) or beta decay. The energies of gamma rays following electron capture can approach the Q values listed above.

Sources of data: Relative abundances (Holden, 1977), Separation Energies (Wapstra and Bos, 1977), Decay Data (Lederer and Shirley, 1977).

Element	$\sigma_q(E_m)$, mb										Data Source
	E_m (MeV)										
	10	15	20	25	30	35	40	45	50		
Be	1.30	1.88	2.21	2.84	3.74	4.38*	5.04	5.52	6.08	Kneissl <i>et al.</i> , 1975; Jones and Terwilliger, 1953	
C			0.01	0.637	1.38	1.75*	2.02	2.19	2.38	Fultz <i>et al.</i> , 1966; Jones and Terwilliger, 1953	
N		0.186	0.598	1.96	3.51	4.22*	4.75	5.08	5.42	Berman <i>et al.</i> , 1970; Fast <i>et al.</i> , 1960	
O			0.097	0.820*	1.87	2.46				Berman, 1975; Veyssi��re <i>et al.</i> , 1974	
Mg		0.159	0.853	2.37						Fultz <i>et al.</i> , 1971; Alvarez <i>et al.</i> , 1971	
Al		0.015	1.00	3.29	5.33*	6.68	7.95	8.93	9.90	Veyssi��re <i>et al.</i> , 1974; Jones and Terwilliger, 1963	
Si			0.425	2.16	3.41					Veyssi��re <i>et al.</i> , 1974	
Mn		2.40	12.8	25.1	35.5	40.6				Alvarez <i>et al.</i> , 1973a	
Co		2.85	15.3	28.4	39.1	44.7				Alvarez <i>et al.</i> , 1973b	
Ni		0.961	6.9	12.4	16.8					Fultz <i>et al.</i> , 1974	
Cu	0.031	3.26	17.7	31.0	40.5*	45.9	50.8	54.0	57.4	Kneissl <i>et al.</i> , 1976; Jones and Terwilliger, 1953	
Mo	0.595	13.7	52.1	79.0*	98.5	110.	121.	130.	138	Beil <i>et al.</i> , 1974; Jones and Terwilliger, 1953	
Sn	0.346	20.3	74.2	108.	132.*	145.	157.	165.	174.	Fultz <i>et al.</i> , 1969; Lepr��tre <i>et al.</i> , 1981	
Ce	1.63	39.1	108.	141.*	165.	179.	192.	201.	211.	Berg��re <i>et al.</i> , 1969; Lepr��tre <i>et al.</i> , 1981	
Ta	4.65	75.5	174.	222*	257.	278.	296.	309.	323.	Berg��re <i>et al.</i> , 1968; Lepr��tre <i>et al.</i> , 1981	
Pt		13.3	103.	204.						Veyssi��re <i>et al.</i> , 1975	
Au	3.23	85.4	181.	226.						Veyssi��re <i>et al.</i> , 1970	
Pb	6.04	108.	206.	250.*	286.	308.	327.	340.	355	Veyssi��re <i>et al.</i> , 1970; Lepr��tre <i>et al.</i> , 1981	
U	29.4	273.	493.*	597.	681.	732.	778.	807.	840	Caldwell <i>et al.</i> , 1980; Lepr��tre <i>et al.</i> , 1981	

* Indicates region where data from the second reference were normalized to cross section given by the first reference.

cases the calculations have been extended to higher energies by normalizing cross sections determined from measurements of bremsstrahlung yield curves to the quasi-monoenergetic photon data in a small energy region near their upper energy limit. The approximate location of this transition band is given by the *'s entered in the appropriate rows of Table 4.

Up to this point, the discussion of the production of neutrons has been concerned exclusively with the basic nuclear reactions that result in neutron production, their cross sections, and the resulting neutron yields from the interaction of electrons with thin targets. These are the basic data that are needed for the more complicated calculations that lead to estimates of the neutron yields resulting from the interaction of electron and bremsstrahlung beams with thick targets. Some thick-target neutron-yield calculations are made by dividing up the thick target into a series of thin targets and then using statistical methods to determine what happens to each of a large number of electrons in each element of the target. All processes are considered: energy loss by collision, bremsstrahlung production, pair production, Compton scattering, etc. If an electron generates a bremsstrahlung photon, then the photonuclear cross-section data are used to calculate the probability that the photon is absorbed to produce a neutron in the remaining thickness of the target. Each electron is followed until it either escapes or loses all of its energy in the target. Such calculations are laborious and require the use of sophisticated Monte Carlo computer programs. In principle, however, they can be carried out for specific target compositions, shapes, and geometries.

Swanson (1978, 1979) has followed a different approach to calculate the neutron yield from "semi-infinite" slabs of 10 elements ranging from carbon to uranium. The semi-infinite approximation means that the slabs are thick enough and of sufficient area to absorb the entire electromagnetic shower generated by an electron entering normal to the surface. Swanson's calculations (1978) indicate that this approximation is valid to within 5 percent when targets 8 to 10 radiation lengths thick are bombarded with 17 to 100 MeV electrons. While the target is infinitely thick for the electromagnetic shower, it is assumed to be very thin for the neutrons that are generated within it, *i.e.*, it is assumed that no neutrons are reabsorbed in the target. The effect of the photonuclear interactions on the shower propagation is also neglected. This latter effect is expected to be small since, at the most, the photonuclear cross section is less than seven percent of the sum of all the "electronic" cross sections that enter the shower calculations. The results of these calculations are given in Figure 15 (Swanson, 1979). In view of the assumptions and approximations on which these

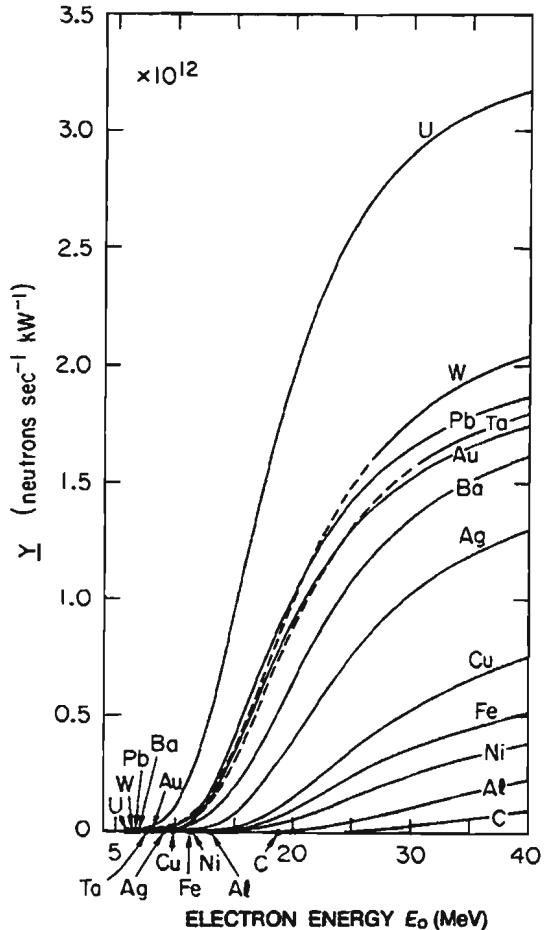


Fig. 15. Neutron yields from semi-infinite targets of various materials per unit incident electron-beam power as a function of incident electron energy E_0 . (Swanson, 1979).

calculations are based, the curves plotted in Figure 15 represent the maximum number of neutrons an electron can produce in interacting with any given element. In Table 5, neutron yields produced by 34-MeV electrons for a series of five target materials are compared for a wide range of target thickness. The sources of these data are: (a) Equation 5 of this report using a value $\epsilon = 0.1$, (b) experimental data of Barber and George (1959) and (c) the yields calculated by Swanson (1979) for semi-infinite target thickness.

Making use of the Monte Carlo calculations of Alsmiller and Moran

TABLE 5—Electron produced neutron yields for specified target thicknesses—34 MeV Electrons

The target thickness, t , is given in g/cm². The yields, Y , are in units of 10^{-4} neutrons/electron. The yields for Pb labeled Y_e were obtained from the value calculated by Swanson for semi-infinite target/thickness by means of the curve for 34 MeV electrons plotted in Figure 16.

Al		Cu		Ta		Pb			U		Notes
t	Y	t	Y	t	Y	t	Y	Y_e	t	Y	
1.18	0.0355	0.907	0.117	0.613	0.205	0.582	0.201		0.66	0.405	a.
24.2	4.31	13.3	13.0	6.21	18.1	5.88	21.3	23	6.17	47	
		26.6	23.7			11.4	46.8	46	12.4	101	
		39.9	29.2			17.3	64.7	63	18.6	139	
		53.1	33.5			22.9	77.7	73			
						34.4	90.0	87			
∞	8.8	∞	34.6	∞	91.5	∞	96.4	96.4	∞	166	c.

a. Calculated using Equation 5 of this work with a value of $\epsilon = 0.1$.

b. Experimental data of Barber and George (1959).

c. Based on calculated yields given by Swanson (1979); the “semi-infinite” target thickness “ ∞ ” is practically achieved for a target whose thickness is 8 to 10 radiation lengths.

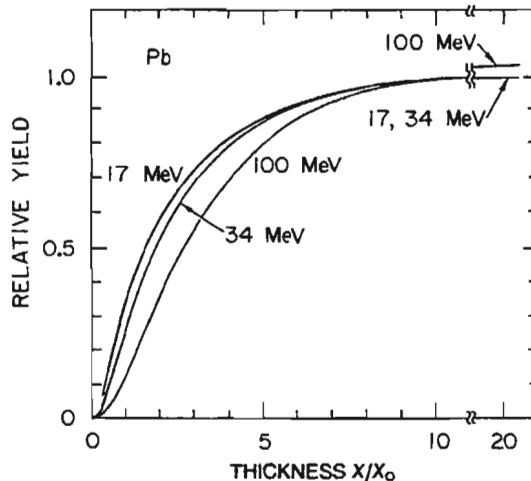


Fig. 16. Relative neutron yield produced by electron beams as a function of target thickness in radiation lengths X_0 (Swanson, 1978).

(1966) and of Hansen *et al.*, (1975), the plots of neutron yield as a function of lead target-thickness given in Figure 16 were obtained by Swanson (1978). Using this figure and the neutron yield from lead for a semi-infinitely thick target given in Figure 15, it is possible to obtain the neutron yield to be expected from a target of any given thickness. This has been done for the Pb targets used in the measurements of Barber and George (1959). The calculated and measured yields are compared in Table 5. The agreement between the calculated and measured yields for Pb, to within 7 percent, is quite satisfactory.

2.1.2 Primary Photoneutron Spectra

The spectrum of neutrons emitted following the absorption by a nuclide (A, Z) of a photon of energy E_γ is determined by the spectrum of states in the daughter nuclide ($A - 1, Z$) up to an excitation energy given by $E_x(\text{max}) = E_\gamma - S_n - \Delta_R$, where S_n is the neutron separation energy for (A, Z) and $\Delta_R \approx E_\gamma^2/2AMc^2$ is the center-of-mass recoil energy. In the decay of the photon-excited states in (A, Z) , the states in the daughter nuclide with energies less than or equal to $E_x(\text{max})$, that can be reached by the emission of low angular momentum neutrons, will be preferentially populated. When the level density of the appropriate states in the daughter nuclide is low, only a few states can participate in the decay process. The spectrum of photoneutrons then consists of only a few discrete lines whose energies in the center-

of-mass system are given by expressions of the form: $E_n(i) = E_\gamma - \Delta_R - S_n - E_x(A - 1, Z:i)$, where Δ_R is the energy in the center-of-mass system given the recoiling $(A - 1)$ nuclide and where $E_x(A - 1, Z:i)$ is the energy of the i 'th level in the nuclide $(A - 1, Z)$, measured with respect to its ground state.

When the density of states in the daughter nuclide is high, *i.e.*, many states of the appropriate angular momentum quantum numbers and parity are within an excitation energy interval comparable to the resolution of the neutron detector, the discrete spectrum of decay neutrons becomes continuous. At these excitation energies, the distribution of levels at an effective energy U in the daughter nuclide $(A - 1, Z)$ is usually taken to be that of a Fermi gas made up of Z protons and $(A - 1 - Z)$ neutrons confined within a volume equal to that of the nuclide [see, *e.g.*, (Preston, 1962)]. This density, $\omega(U)$, can be approximated by

$$\omega(U) = C_F U^{-2} \exp(2(aU)^{1/2}), \quad (9)$$

where the constants C_F and "a" depend on the number of neutrons and protons within the nuclide and on its size. In terms of the true excitation energy E_x , the effective excitation energy is given by $U - \Delta_p$, where Δ_p is the pairing energy correction (Gilbert and Cameron, 1965). This expression for the density of levels in the residual nuclide $(A - 1, Z)$ yields the following expression for the energy distribution, $dN(E_n)/dE_n$, of the decay neutrons resulting from the absorption of photons with energy E_γ by a target (A, Z) :

$$\frac{dN(E_n)}{dE_n} = K_f E_n \sigma_c(A - 1, Z:E_n) U^{-2} \exp(2(aU)^{1/2}), \quad (10)$$

where $U = E_\gamma - S_n - \Delta_p - E_n$ is the effective excitation energy. The term $\sigma_c(A - 1, Z:E_n)$ is the cross section for the capture of a neutron with kinetic energy E_n by the nuclide $(A - 1, Z)$ at the effective excitation energy U . This capture cross section cannot be measured. The constant K_f normalizes the spectrum to contain a specific number of neutrons. In analyzing photoneutron spectra, a theoretical ground-state neutron capture cross section is often used for σ_c or it is assumed to be a constant independent of neutron energy. In practice, the exact form of the expression used for σ_c makes little difference in the values of the constant "a" obtained from fitting empirical spectra since, over the portions of the spectrum where equation 10 is valid, σ_c is a slowly varying function of E_n compared to the other energy-dependent factors in the equation.

Another expression to describe the energy distribution of photoneu-

trons is based on Weisskopf's statistical treatment of nuclear level densities (Blatt and Weisskopf, 1952). The expression results from making a Taylor series expansion of the logarithm of the level density (the nuclear entropy) about the maximum excitation energy that can be reached in the daughter nuclide by neutron decay as a result of the absorption of a photon of energy E_γ by the parent nuclide. The resulting expression for the neutron spectrum is

$$\frac{dN(E_n)}{dE_n} = K_w \sigma_c (A - 1, Z; E_n) E_n \exp(-E_n/T), \quad (11)$$

where T is a "nuclear temperature." It should be noted that this temperature is associated with the residual nuclide that remains after the neutron has been emitted, not with the nuclide that originally absorbed the photon. The constant K_w normalizes the spectrum to contain a specific number of neutrons. Although this expression should give a valid description of only the low energy portion of the photoneutron spectrum, it has often been used to fit empirical spectral data over a good part of the total energy range covered by the data. The major deviation from the spectrum given by equation 11 is in the higher energy range where the neutrons are produced by the process described below.

In any nuclide ($A - 1, Z$) there are always a few low-lying states which bear a simple, single-particle relationship to the ground state of the neighboring nuclide (A, Z). It is, therefore, possible for a photon interacting with (A, Z) to induce a direct transition to one of these states, with the emission of a high-energy neutron. These neutrons are to be contrasted with those whose spectrum can be described by equation 10 or 11, which result from the neutron decay of the "giant-resonance state" reached when a nuclide (A, Z) absorbs a photon of energy E_γ . The direct spectrum of photoneutrons produced by a monoenergetic photon beam would consist of a series of discrete lines. In contrast to the isotropic angular distribution of the "statistical-decay" neutrons described by equations 10 or 11, the angular distribution of the "direct" neutrons is usually anisotropic with respect to the photon-beam direction.

Most of the available photoneutron spectra measurements were made with bremsstrahlung beams, i.e., the empirical spectra represent averages of monoenergetic photon spectra weighted with the product of the (γ, sn) cross section and the bremsstrahlung spectrum. Examples of photoneutron spectra for ^{16}O , ^{197}Au and Pb are given in Figures 17 through 19. Oxygen-16 is an example of a light nuclide where only a few states in the daughter nucleus have the appropriate parity and

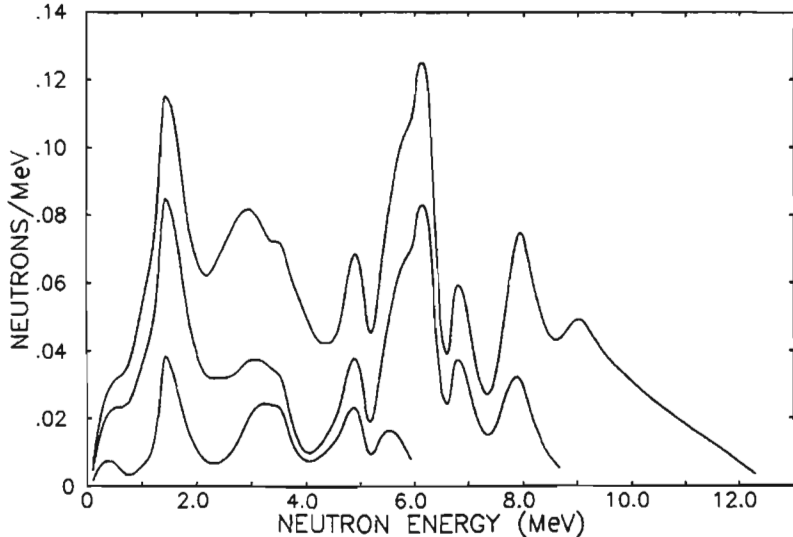


Fig. 17. Calculated bremsstrahlung-produced photoneutron spectra from ^{16}O . The three curves in order of increasing upper energy limit give the spectra produced by 21, 25 and 29 MeV bremsstrahlung spectra. The data are normalized such that the area under each spectrum is proportional to $\sigma_a(\gamma, xn; E_b)$, see Eq. 4. Spectra were calculated using the cross sections given by Caldwell (1967) for transitions to the ground and first three excited states of ^{15}O . The tabulated bremsstrahlung spectra of Penfold and Leiss (1958) were used.

angular momentum quantum numbers to participate to any great extent in the decay of the giant resonance of the parent nuclide.

Figures 18 and 19 give photoneutron spectra for lead and gold produced by bremsstrahlung spectra with a number of different peak energies. The spectra for lead are plotted on a linear-yield scale to facilitate comparison with the spectra for ^{16}O given in the previous figure.

The semilogarithmic plot used for the gold photoneutron spectra plotted in Figure 19 is the more usual form used to present spectral data for nuclides with mass numbers greater than 40. The data presented are those of Mutchler (1966). The neutron spectra measured for the two peak-energy bremsstrahlung spectra have been normalized such that the difference between these two spectra gives the spectrum that would be produced by a photon spectrum centered at about 14 MeV with a width at half maximum of about 2 MeV. Note that the slope of the difference spectrum for neutron energies below 3.5 MeV is different from the slope of the spectra measured using either 14 or 15 MeV bremsstrahlung. For energies near the peak of the giant

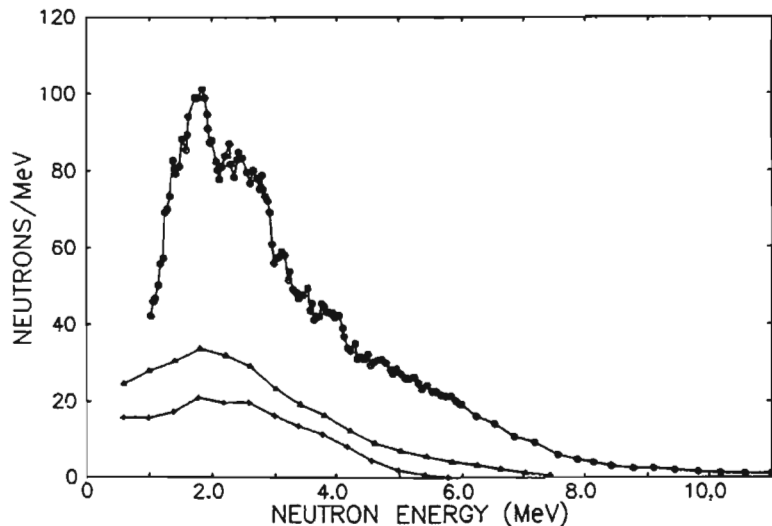


Fig. 18. Bremsstrahlung-produced photoneutron spectra from lead. The three sets of data are for 13, 15 and 31 MeV bremsstrahlung spectra. The area under each spectrum is proportional to $\sigma_q(\gamma, xn; E)$. The 31 MeV data are indicated by circles (McNeill *et al.*, 1970), those for 15 and 13 MeV indicated by triangles and plus signs, respectively (Mutchler, 1966).

resonance, the shape of the photoneutron spectrum depends on the shape and extent of the photon spectrum used to create the photoneutrons. Also note that all three spectra in Figure 19 show a rather pronounced change in slope in the vicinity of 3.5 MeV. The high-energy neutrons have been shown by Mutchler to be associated with direct transitions. These account for about 14 percent of the neutrons in the difference spectrum.

Two quite different photoneutron-production experiments have provided surveys of level density parameters that can be used to estimate photoneutron spectra. The first of these is the work of Mutchler (1966) in which the photoneutron spectra produced by bremsstrahlung with peak energies of 15, 14 and sometimes 13 MeV were measured at three angles for a series of 17 elements ranging from In to Bi. The angular distribution data were used to separate the measured spectra into evaporation and direct components and also to obtain the total photoneutron spectrum integrated over all angles. The measured spectra, as well as the separated evaporation components, were analyzed using various theoretical expressions, including those given by equations 10 and 11 above. The effect of using only the evaporation component in

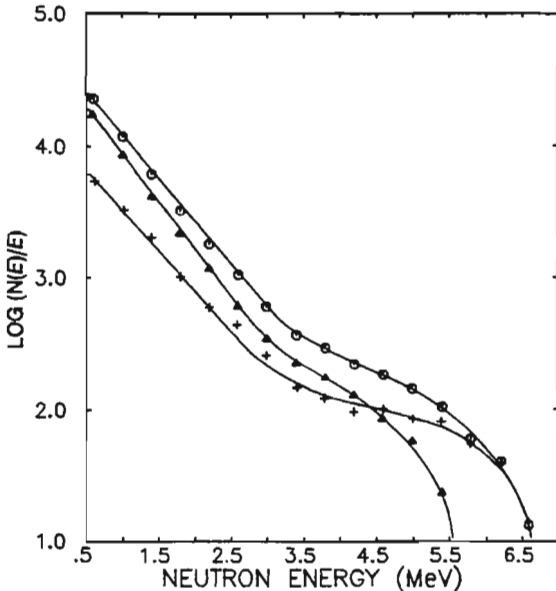


Fig. 19. Photoneutron spectra for gold (Mutchler, 1966). The spectra defined by circles and triangles, respectively, are produced by 13 and 15 MeV bremsstrahlung. The crosses give the difference spectrum due to a band of photons about 2 MeV wide centered at 14 MeV.

the analysis was to decrease the resulting values of T by about 10 percent and to increase the values of "a" by about 20 percent.

The second survey experiment is that of Barrett *et al.*, (1973), in which the neutron-energy-dependent moderation characteristics of a 1.6 meter cube of paraffin were used to determine the mean energy of the neutrons produced in a target irradiated by bremsstrahlung. For each of 38 elemental targets ranging from Ti to Bi, the mean energies of the neutrons produced by 18 different peak-energy bremsstrahlung spectra were determined. The peak bremsstrahlung energies ranged from 10 to 27 MeV. The resulting experimental points were then fitted with mean-energy curves calculated by using empirical photoneutron cross section data and photoneutron spectra based on both the Fermi gas (equation 9) and constant temperature [$\omega(u) \sim \exp(U/T)$] expression for the level density in the $(A - 1, Z)$ nuclide. The only adjustable constants used in the fitting procedure were the level density parameters, a or T , in the photoneutron spectral expressions. Empirical values were used for all other constants appearing in the expressions for the mean neutron energy. In the analysis, no attempt was made to

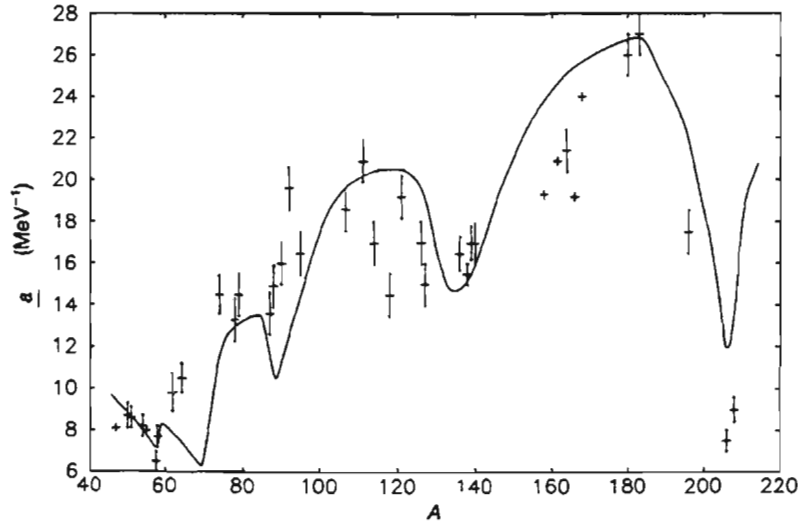


Fig. 20. Experimental values for the Fermi gas-level density parameter, a , as a function of mass number, A . A least-squares fit of the theoretical curve due to Newton (Newton, 1956), has been made to the experimental data by Barrett *et al.*, 1973.

include a direct neutron component in the spectra. The values of the level density parameter, a , determined in this experiment are plotted as a function of the nuclear mass number A in Figure 20.

The level density parameters resulting from the Mutchler (1966) and Barrett *et al.* (1973) experiments are listed in Table 6. On the whole, the values for the level density constant, a , obtained in the two experiments agree within the experimental uncertainties. Also listed in Table 6 are values of the nuclear temperature, T , obtained from time-of-flight measurements by Glazunov *et al.*, 1964. The neutron energies listed under E_b in Table 6 are those in which the transition takes place between the evaporation and direct spectra in Mutchler's data.

In contrast to the body of modern data that exist for the various neutron production cross-sections, the photoneutron spectral data are not very complete. This is particularly true for spectra produced by bremsstrahlung with peak energies above 25 MeV. There are a number of spectra available in the literature that were measured with nuclear emulsions for bremsstrahlung with peak energies from 20 to 30 MeV. However, the range of nuclides for which these measurements were made is limited. These measurements demonstrated the general features of the photoneutron spectrum which were later confirmed in

TABLE 6—Comparison of level density parameters

Target	E_a MeV	a MeV ⁻¹	T MeV	E_b MeV	θ^a Degrees	Reference
²³⁸ U	5.-16.		$0.33 \pm .03^b$	90		Glazunov <i>et al.</i> , 1964
²⁰⁹ Bi	7.5-16.		$0.84 \pm .04$	90		" "
	7.5-27.	9.0 ± 1.0	1.03	4π		Barrett <i>et al.</i> , 1973
	12.-14.	11.5 ± 0.8	$0.85 \pm .02$	4.0	4π	Mutchler, 1966
	13.-15.	13.6 ± 0.9	$0.81 \pm .02$	3.5	4π	" "
Pb	7.4-16.		$0.98 \pm .04$	90		Glazunov <i>et al.</i> , 1964
	7.4-27.	7.5 ± 1.5	1.2	4π		Barrett <i>et al.</i> , 1973
²⁰⁸ Pb	12.-14.	9.8 ± 1.0	$0.94 \pm .06$	5.0	4π	Mutchler, 1966
	13.-15.	7.7 ± 0.5	$1.2 \pm .04$	5.0	4π	" "
²⁰⁷ Pb	12.-14.	8.1 ± 1.0	$1.23 \pm .09$	4.0	4π	" "
	13.-15.	10.3 ± 1.2	$0.97 \pm .06$	4.0	4π	" "
²⁰⁶ Pb	12.-14.	8.3 ± 0.8	$1.25 \pm .09$	4.0	4π	" "
	13.-15.	8.4 ± 0.6	$1.14 \pm .06$	4.0	4π	" "
	197	Au	8.1-27.	17.5 ± 1.4	1.19	4π
	12.-14.		19.1 ± 2.8	$0.61 \pm .04$	3.5	Mutchler, 1966
	13.-15.		18.0 ± 2.2	$0.66 \pm .03$	4.0	" "
Pt	7.4-16.		$0.48 \pm .03$	90		Glazunov <i>et al.</i> , 1964
W	7.-27.	27.0 ± 1.3	0.50	4π		Barrett <i>et al.</i> , 1973
	13.-15.	22.1 ± 1.9	$0.60 \pm .01$	3.5	4π	Mutchler, 1966
¹⁸¹ Ta	7.6-27.	26.0 ± 1.3	0.49	4π		Barrett <i>et al.</i> , 1973
	12.-14.	25.4 ± 2.0	$0.54 \pm .02$	3.5	4π	Mutchler, 1966
	13.-15.	26.3 ± 2.3	$0.54 \pm .01$	3.2	4π	" "
Er	7.5-27.	$19.2 \pm ?$		4π		Barrett <i>et al.</i> , 1973
	13.-15.	20.2 ± 2.0	$0.62 \pm .03$	4.0	4π	Mutchler, 1966
¹⁶⁵ Ho	8.0-27.	21.4 ± 1.4	0.56	4π		Barrett <i>et al.</i> , 1973
	13.-15.	22.8 ± 4.2	$0.60 \pm .04$	3.0	4π	Mutchler, 1966
¹⁴¹ Pr	9.4-27.	17.0 ± 1.4	0.65	4π		Barrett <i>et al.</i> , 1973
	13.-15.	17.1 ± 2.6	$0.66 \pm .05$	3.0	4π	Mutchler, 1966
La	8.8-27.	15.5 ± 0.8	0.72	4π		Barrett <i>et al.</i> , 1973
	13.-15.	13.4 ± 0.7	$0.77 \pm .03$	3.5	4π	Mutchler, 1966
¹²⁷ I	9.1-27.	17.0 ± 1.5	0.70	4π		Barrett <i>et al.</i> , 1973
	3.-15.	15.9 ± 0.9	$0.68 \pm .01$	3.0	4π	Mutchler, 1966
Sn	8.8-27.	14.5 ± 1.4	0.73	4π		Barrett <i>et al.</i> , 1973
	13.-15.	14.5 ± 1.0	$0.66 \pm .01$	3.3	4π	Mutchler, 1966
In	9.0-27.	17.0 ± 1.4	0.57	4π		Barrett <i>et al.</i> , 1973
	13.-15.	16.9 ± 2.1	$0.67 \pm .02$	2.8	4π	Mutchler, 1966

^a The angle with respect to the photoneutron beam direction at which photoneutrons were observed. The notation 4π indicates that the experiment integrated over all outgoing neutron emission angles.

^b T_2 , temperature for fission spectrum, is $1.05 \pm .04$ MeV.

considerable detail by the time-of-flight measurements (Bertozzi *et al.*, 1958; Glazunov *et al.*, 1964; Mutchler, 1966; Kuchnir *et al.*, 1967).

Where no data exist, the photoneutron spectrum can be approximated by assuming that, for a monoenergetic photon, E_γ , it is given by an evaporation spectrum described by equation 10 with the value

of the constant, a , taken from Figure 20, plus a discrete peak at an energy, $E_n = E_\gamma - S_n$, containing 12 percent of the neutrons in the evaporation spectrum. If the photon energy is above the $(\gamma, 2n)$ separation energy, the spectrum of second neutrons should be obtained by summing evaporation spectra calculated using the probability that the daughter nuclide ($A - 1, Z$) is left at an excitation energy given by the spectrum of neutrons emitted by the target nuclide (A, Z). There should be no direct-neutron component in the second-neutron spectrum. The two spectra should be summed after being normalized, respectively, to the magnitude of the $(\gamma, 1n)$ and $(\gamma, 2n)$ cross sections at E_γ . The spectrum of neutrons produced by a bremsstrahlung spectrum with a maximum energy E_b is then given by summing (integrating over photon energy) the spectrum produced at each photon energy weighted with the bremsstrahlung spectrum, $B(E_\gamma, E_b)/E_\gamma$, (see, e.g., Penfold and Leiss, 1958). Because of the assumption that the direct-neutron spectrum consists of ground-state neutrons only, the resulting spectrum errs on the side of having somewhat higher-energy neutrons than will be found in a measured spectrum.

2.2 Transport of Neutrons in Accelerator Head

2.2.1 Effects on Neutron Spectra

The typical medical accelerator has massive photon shielding around the target which, when the accelerator is energized, serves to produce a collimated beam of x rays. Neutrons produced inside the head are approximately isotropic and penetrate the shielding in all directions. The photon shielding material is usually some heavy metal such as tungsten or lead; the head also contains a certain amount of iron and copper in bending magnets. These materials provide good photon shielding since they are all heavy elements. The only significant mechanisms of neutron energy loss in these heavy elements are inelastic scattering and $(n, 2n)$ reactions. The neutron interaction cross sections of W and Pb are illustrated in Figures 21 and 22, respectively (Howerton 1958).¹ Shown are the inelastic ($\sigma_{n,n'}$) and elastic (σ_{el}) scattering cross sections and the $\sigma_{n,2n}$ cross section. In the energy region of Figures 21 and 22 (the region of interest for medical electron accelerators) the sum of the inelastic and $(n, 2n)$ cross sections is called the nonelastic (σ_{non}) cross section. It can be seen that the

¹ These cross sections are chosen for illustrative purposes. When the best cross sections are desired, the latest compilation (BNL, 1979) should be used.

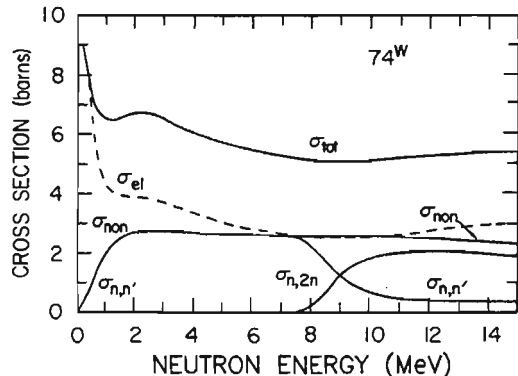


Fig. 21. Neutron interaction cross sections in natural tungsten as a function of neutron energy. These are adapted and simplified from Howerton, 1958.

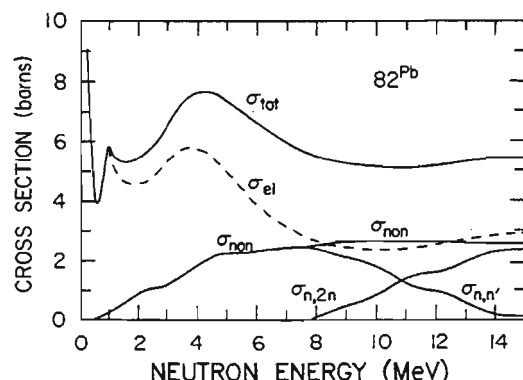


Fig. 22. Neutron interaction cross sections in natural lead as a function of neutron energy. These are adapted and simplified from Howerton, 1958.

inelastic scattering dominates energy losses at lower energies and that the ($n, 2n$) reactions dominate at higher energies. Inelastic scattering can occur only at energies above the lowest excited state of the shielding material (see Table 7). Tungsten is considerably more effective than lead in reducing neutron energy even though the nonelastic cross sections are almost the same since (a) W has 1.9 times more atoms cm^{-3} , and (b) inelastic scattering in W extends to much lower energies. Below 0.57 MeV, Pb is virtually transparent to neutrons.

The energy loss in any inelastic collision cannot be determined or predicted exactly, but there is a minimum energy loss which equals the energy of the lowest excited state. Often there is a large energy

TABLE 7—*Inelastic scattering thresholds*

Element	Atomic Mass Number	Abundance %	1st Excited State (MeV)
Pb	206	25.1	0.803
	207	21.7	0.570
	208	52.3	2.61
Fe	54	5.8	1.41
	56	91.7	0.847
W	182	26.4	0.100
	183	14.4	0.047
	184	30.6	0.111
	186	28.4	0.123

loss in a single collision, resulting in excitation of energy states above the ground state followed by a cascade of gamma rays. In the $(n, 2n)$ reaction, the minimum energy loss is equal to the binding energy of a neutron, and, since the energies of the two emerging neutrons tend to be similar, this reaction produces large numbers of low energy neutrons. The sum of the inelastic and $(n, 2n)$ cross sections is of the order of 1 or 2 barns for these materials, i.e., Pb, Fe and W. Therefore, a typical neutron penetrating the photon shielding material undergoes several collisions. In addition, a large amount of elastic scattering takes place in these materials at these energies. The elastic scattering results in negligible energy loss but has the effect of increasing the path length of the neutrons in the shielding material and offering greater opportunity for the inelastic and $(n, 2n)$ reactions to occur.

The shielding and geometry of the head of medical accelerators are very complicated. Since the head contains many moving and fixed devices, the shielding is never a solid sphere or cube or any other simple geometric configuration. Figure 23 is a schematic drawing of a typical therapy head for a medical accelerator. Since the shielding is designed primarily for photons, which are emitted predominantly in the forward direction, the shielding tends to be much thicker and heavier in this direction than in the other directions. This is not the distribution of shielding material appropriate for the neutrons, which are emitted nearly isotropically. The neutrons, however, are scattered so many times in the head that the head shielding may be approximated as a hollow sphere, with a wall thickness up to about 10 cm if tungsten is used and up to about 15 cm if lead is used as the shielding material. Usually, the shielding will be a mixture of these two materials. It is not safe to assume that different models of the same accelerator have identical head shielding, since the increasing price of

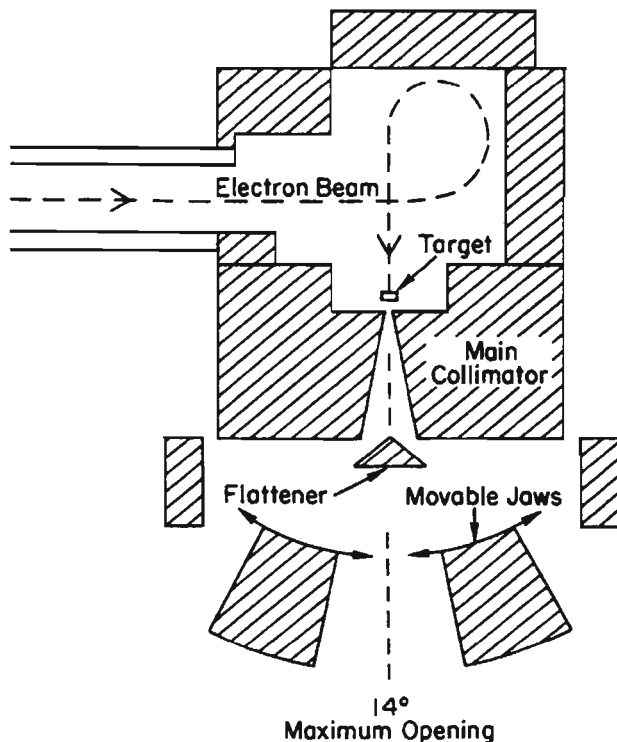


Fig. 23. Schematic drawing of a typical therapy head for a medical electron accelerator.

tungsten seems to be causing manufacturers to shift away from tungsten and toward the use of lead.

It is frequently stated that the photoneutron spectrum from machines in the medical accelerator energy range resembles the fission spectrum. Figure 24 shows that this is true for the primary neutron spectra (NCRP, 1964). These spectra are, however, quite different after they have penetrated the head shielding. In Figure 25 (McCall and Swanson, 1979) are shown the measured integral photoneutron spectra for 15 MeV electrons striking tungsten and for ^{252}Cf fission neutrons. The same figure includes the spectrum calculated by the Monte Carlo code MORSE (Straker *et al.*, 1970; 1976) from 15 MeV electrons bombarding tungsten after the neutrons have penetrated 10 cm of tungsten. (The notation "15 MeV W PN" is used to designate the photoneutron spectrum from 15 MeV electrons incident on a W

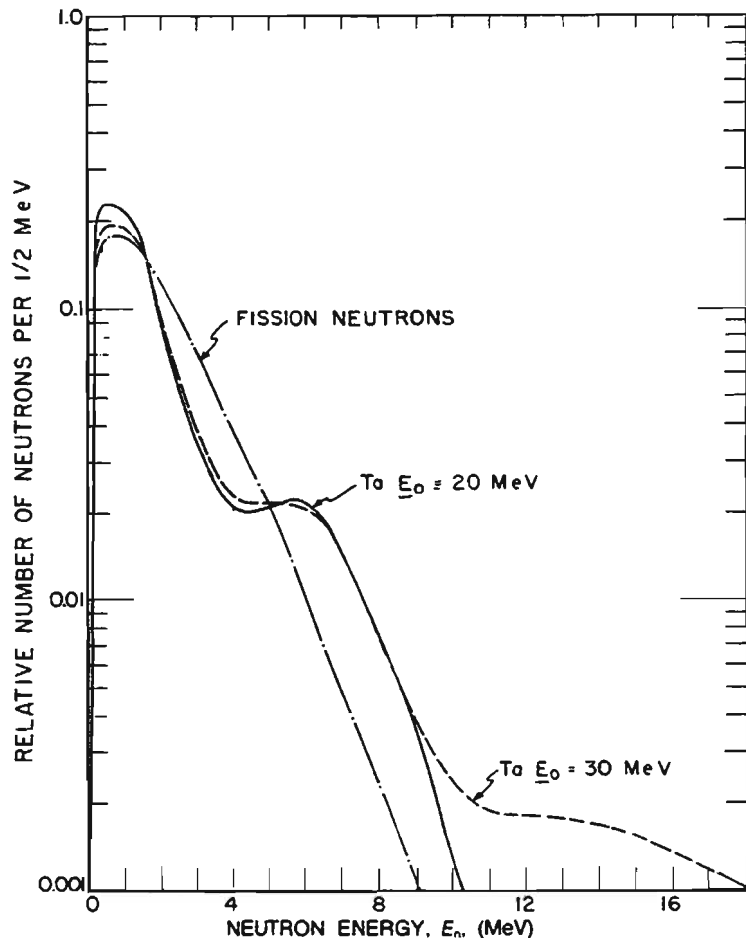


Fig. 24. Photoneutron spectra for tantalum with peak bremsstrahlung energies of 20 and 30 MeV. A fission neutron spectrum is shown for comparison (NCRP, 1964).

target). It is clear that the spectrum is very different after penetrating the 10 cm of tungsten. In particular, if neutron fluence from a 15 MeV medical accelerator is measured by use of a threshold detector calibrated with a bare ^{252}Cf source, the results will be significantly in error unless a correction is made for the changed spectrum. Also shown in Figure 25 is the further degradation, due to the concrete room in which medical accelerators are commonly located, when the detector is 1 meter from the source. This will be discussed in a later section. In

Figure 26, similar results are shown for 25 MeV electrons incident on Pb and shielding with 15 cm of Pb.

Another way of looking at the effects of the heavy metal head shielding on the spectrum of the neutrons is to consider the effect on the average energy of the spectrum. By average energy is meant the true average, *i.e.*, the total neutron energy divided by the total number of neutrons. Figures 27 and 28 show the effect of spherical shields of lead and tungsten around three different neutron sources (McCall *et al.*, 1979). It can be seen that the average energy drops off almost exponentially with increasing shield thickness. The slope of this exponential decrease is much steeper for tungsten than for lead and the slope gets steeper with increasing spectral energy. Since these materials become very transparent to neutrons with energy below that of the first excited state of the nucleus, it is clear that this exponential decrease will eventually begin to level off and that the average energy will remain almost constant for transmission through further thick-

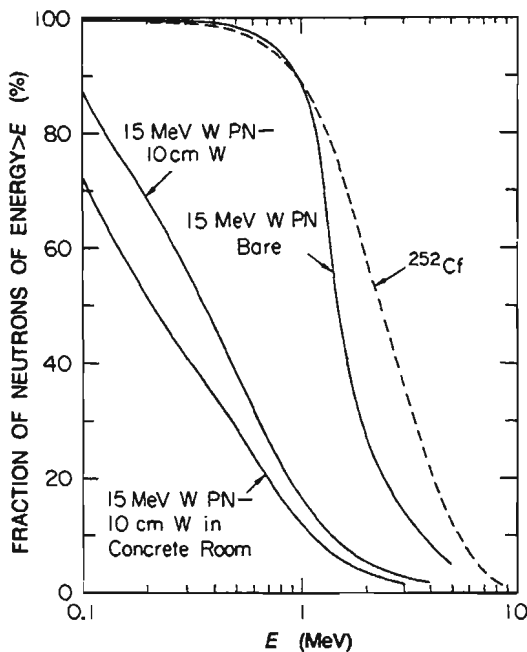


Fig. 25. Integral photoneutron spectrum for 15 MeV electrons striking a tungsten target (designated 15 MeV W PN bare). A fission spectrum (^{252}Cf) is shown for comparison. Also shown are the spectra obtained when 10 cm of tungsten shielding surrounds the tungsten target and when this assembly is placed in a concrete room (McCall and Swanson, 1979).

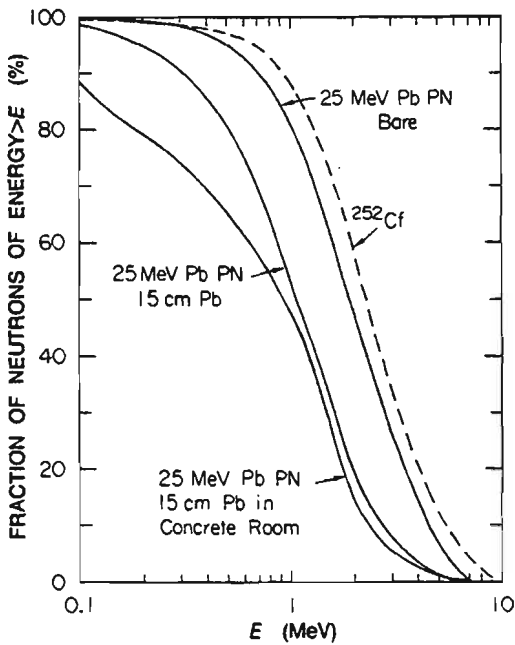


Fig. 26. Integral photoneutron spectrum for 25 MeV electrons striking a lead target. A fission spectrum (^{252}Cf) is shown for comparison. Also shown are the spectra obtained when 15 cm of lead surround the lead target and when the assembly is placed in a concrete room (McCall, 1979).

nesses of lead or tungsten. However, for the thicknesses encountered in medical accelerators, the exponential decrease is a reasonable approximation. A condensed method of showing the magnitude of these exponential decreases in average energy is given in Figure 29, where a half-energy layer (HEL) is defined analogous to a half-value layer in shielding work. It is that thickness of material which decreases the average energy by a factor of two (McCall *et al.*, 1979). The spectra used for calculations of the half-energy layers for Figures 28 to 30 are listed in Table 8. The average energies are those for the initial undegraded spectra.

2.2.2 Neutron Fluence Attenuation

Since capture cross sections for the heavy metals are small except at thermal neutron energies, there is little attenuation of neutron fluence in the accelerator head. In a machine with all-tungsten shield-

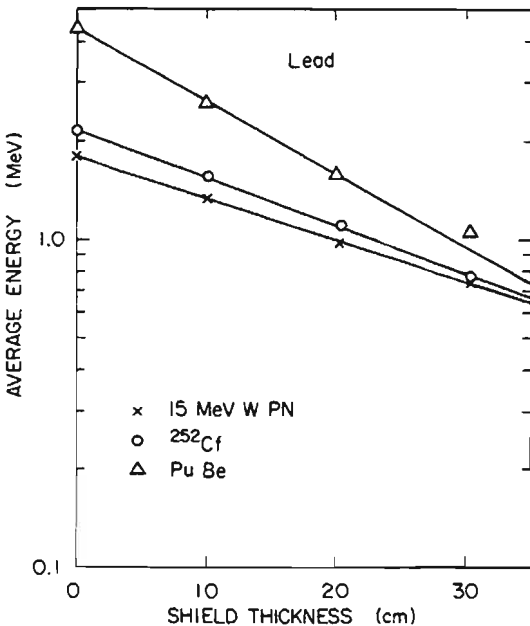


Fig. 27. The average energy of various neutron spectra as a function of the thickness of a spherical shell shield of lead surrounding the source (McCall *et al.*, 1979).

ing, as much as 15% of the fluence might be absorbed, but in a lead-shielded machine there would be essentially zero attenuation. There may, in fact, be a small buildup of neutron fluence due to the multiplying effect of $(n, 2n)$ reactions. In at least one of the newer commercial machines, the manufacturers have added borated hydrogenous shielding outside the photon shielding, and this additional shielding provides a considerable attenuation of neutron fluence. Each machine must be considered individually when calculating fluence attenuation since older and newer versions, even of the same model, may not be alike. One difference between neutron-head-leakage and photon-head-leakage should be noted. For photons, the attenuation of the shield is high and a small hole in the shielding may create a very narrow beam of photon radiation which is intense compared to the average level of photon fluence. For neutrons, however, the attenuation is quite low and even a gap in the shielding will not significantly increase the fluence in that direction. This is fortunate, perhaps, since it is difficult to measure beams of about 1 cm^2 area with neutron detectors, which typically have large dimensions.

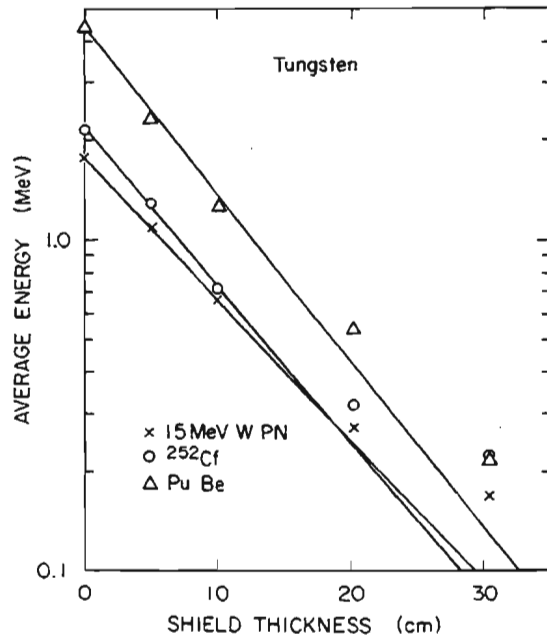


Fig. 28. The average energy of various neutron spectra as a function of the thickness of a spherical shell shield of tungsten surrounding the source (McCall *et al.*, 1979).

TABLE 8—Spectra used in Figures 28, 29, and 30

Spectra	Average Neutron Energy (MeV)
10 MeV W PN	0.65
15 MeV W PN	1.8
25 MeV W PN	2.2
25 MeV Pb PN	2.3
²⁵² Cf	2.15
Artificial	3.8
Pu (α , n) Be	4.4
Monoenergetic neutrons	1.5
Monoenergetic neutrons	6
Monoenergetic neutrons	8
Monoenergetic neutrons	10

2.2.3 Absorbed Dose and Dose Equivalent Attenuation

While the heavy metals do not attenuate neutron fluence significantly, they do reduce the absorbed dose or the dose equivalent to the patient because they cause a decrease in the energy of the neutrons. There have been many mistakes made in calculating the attenuation

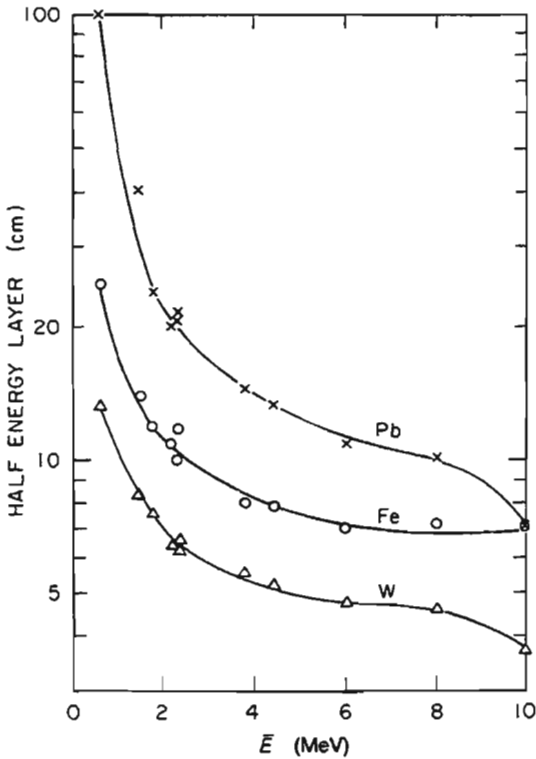


Fig. 29. The thickness of a spherical shell shield required to reduce the average energy of a neutron spectrum by one-half as a function of the unshielded average energy of the spectrum. Data are given for iron, lead and tungsten (McCall *et al.*, 1979). The spectra used are identified in Table 8.

of neutrons by heavy metal shields. One common mistake is to use the macroscopic neutron removal cross sections as listed, for example, in Appendix E of NCRP Report No. 38 (NCRP, 1971). As pointed out in NCRP Report No. 38, these cross sections can be used only if the heavy metal shield is followed by an adequate amount of hydrogenous shielding. Another common mistake is to use measured or calculated attenuation coefficients for slab shields in a situation where the shielding is more nearly a spherical shield around the source. In a slab-shield geometry, any neutron that is scattered is often effectively lost. Basically, a broad-beam slab geometry is intermediate between a narrow-beam slab geometry and the spherical-shell geometry. The photon shielding of medical accelerator heads is most nearly like a spherical shell; therefore, in this section, measured and calculated

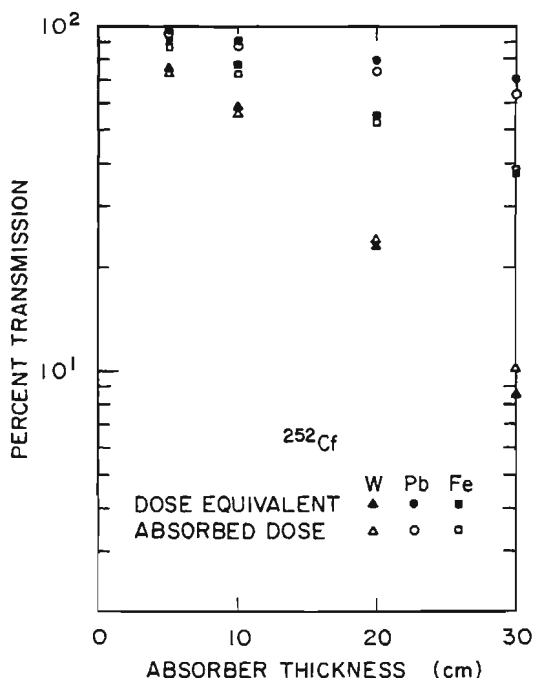


Fig. 30. The dose-equivalent transmission for spherical shell shields for a ^{252}Cf fission spectrum. Data are given for lead, tungsten and iron with source and detector at a constant distance (McCall *et al.*, 1979).

attenuation values for spherical shields around the source have been used. In Figure 30 the calculated absorbed dose and dose equivalent transmission are shown for Fe, Pb and W for the ^{252}Cf neutron spectrum (McCall, 1979).² A calculation using a photoneutron spectrum from 15 MeV electrons on tungsten would have given points indistinguishable from those in Figure 30. McCall *et al.*, (1979) have described a method of calculating dose equivalent attenuation in situations where there are no Monte Carlo calculations available. In the course of their work, they found a relationship between the average energy of a neutron spectrum and the factor for conversion of fluence to dose equivalent. This empirical relationship is shown in Figure 31a. The data can be fitted quite well to a straight line which is above and almost parallel to the line drawn through the fluence to dose equivalent conversion factors for monoenergetic neutrons given in ICRP-21

² The accuracy of the neutron cross sections for iron has been questioned (Hertel *et al.*, 1979). The transmission for iron may be significantly higher than that shown in Figure 31.

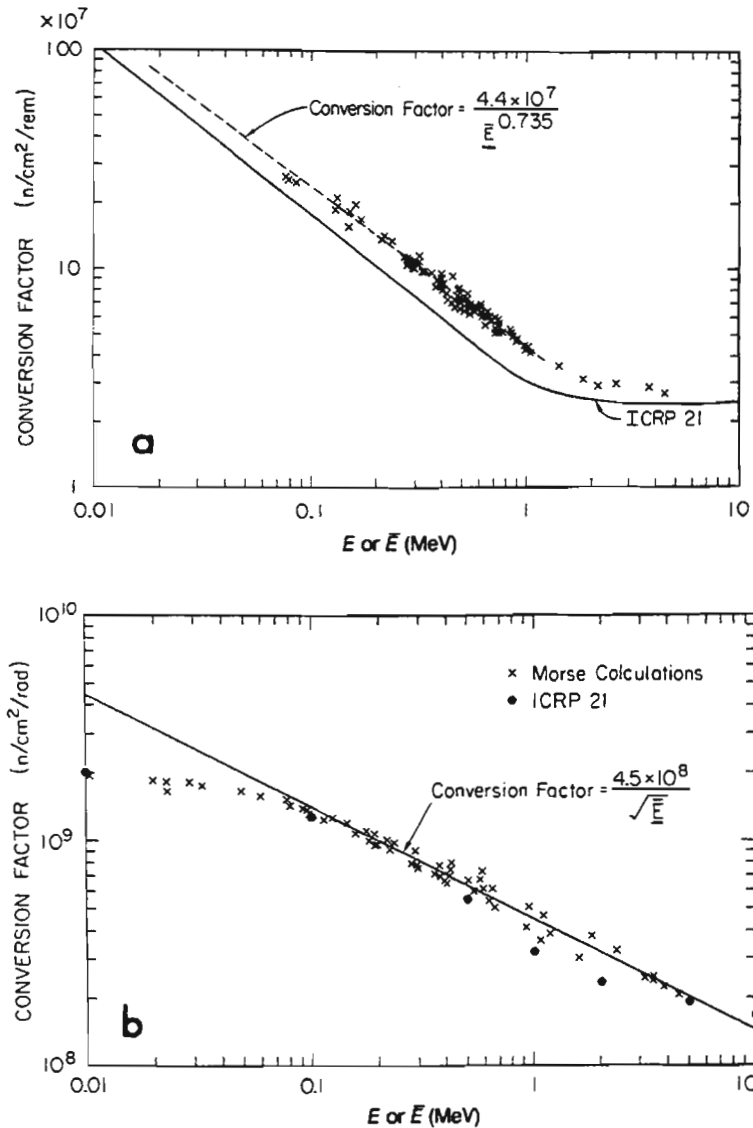


Fig. 31a. Fluence-to-dose equivalent conversion factors as a function of average neutron energy. The points are results of many different neutron spectra and shielding situations (McCall *et al.*, 1979). The dashed line is a least squares fit to the points. Also shown is the fluence to dose equivalent conversion factor for monoenergetic neutrons as given in ICRP Publication 21 (ICRP, 1973).

Fig. 31b. Fluence-to-absorbed dose conversion factors as a function of average neutron energy.

(1973). A similar relationship was found between the average energy and the factor for conversion of fluence to absorbed dose and is shown in Figure 31b. With this relationship and the half-energy layers shown in Figure 29, the dose equivalent transmission in a simple iron, lead, or tungsten shielding system can be calculated. As will be shown below, the effect of a concrete room can also be taken into account. An example is provided later, at the end of Section 2.3.1, which will illustrate how to use these figures for practical calculations.

2.3 Transport of Neutrons in a Concrete Room

2.3.1 Effect on Spectra

The effects of a concrete room on the neutron spectrum have been examined by only a few investigators. McCall *et al.*, (1979) investigated this problem by using the Monte Carlo code MORSE. The Monte Carlo calculations showed the effects of the concrete room on the spectrum as illustrated in Figures 25 and 26. There is a large increase in the number of low-energy neutrons which are scattered back out of the walls. The Monte Carlo method is not available to everyone; therefore a "cookbook" method was developed to take into account the neutron scattering in a concrete room (McCall *et al.*, 1979). The "cookbook" method is based on empirical relationships obtained from the results of many Monte Carlo calculations, one of which is shown in Figure 30. First, it was found that the neutron field could always be described as the sum of the neutrons coming directly from the source and a component scattered from the walls. The direct component, ϕ_{dir} , follows the inverse square law. The scattered component was found to be constant throughout the room and the scattered fluence, ϕ_{sc} , was determined from a relationship similar to that discovered earlier for thermal neutrons (Patterson and Wallace, 1958), *i.e.*,

$$\phi_{\text{sc}} = 5.4 \frac{aQ}{S}, \quad (12)$$

where Q is the number of fast neutrons,

S is the inside surface area of the room in cm^2 , and

a is a constant for a given accelerator (see below).

Eisenhauer *et al.* (1982) arrived at the same relationship for spherical rooms using an analytic approach and experimental albedos. Their

value was 5.6 instead of 5.4 as above. They also found experimentally that the relationship held for rectangular rooms. They were able to deduce that the typical neutron makes ~ 2.4 traversals of the room before it is captured or its energy falls below the cadmium cut-off energy.

The value of "a" in equation 12 is 0.85 for an all-W-shielded machine and 1.0 for an all-Pb-shielded machine, and is simply the fractional fluence transmission of the head shielding. The total epithermal, i.e., all neutrons with energy greater than the cadmium cut-off, 0.41 eV, fluence, ϕ , can then be given by

$$\phi = \phi_{\text{dir}} + \phi_{\text{sc}} = \frac{aQ}{4\pi R^2} + 5.4 \frac{aQ}{S}, \quad (13)$$

where R is the distance from the source to the detector in cm.

It was also found that the average energy of the scattered component is related to the average energy of the direct component as shown in Figure 32. For the range of energies of interest in medical accelerators, the relationship is adequately represented by $\bar{E}_{\text{sc}} = 0.24 \bar{E}_{\text{dir}}$. Then the average energy (\bar{E}) of the total spectrum can be given by

$$\bar{E} = \frac{\bar{E}_{\text{dir}} \phi_{\text{dir}} + \bar{E}_{\text{sc}} \phi_{\text{sc}}}{\phi_{\text{dir}} + \phi_{\text{sc}}} = \bar{E}_{\text{dir}} \left(1 - \frac{4.1 \times 4\pi R^2}{S + 5.4 \times 4\pi R^2} \right). \quad (14)$$

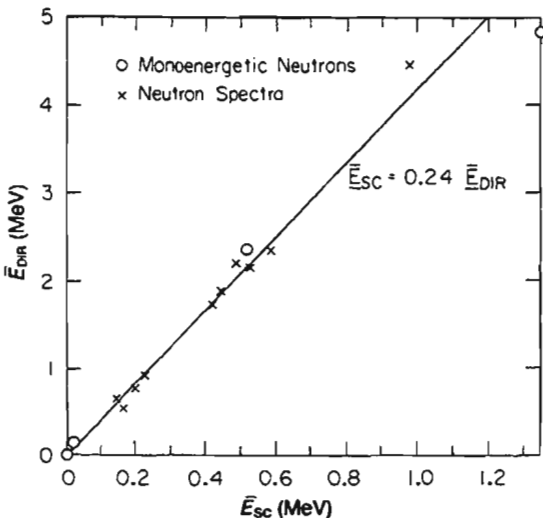


Fig. 32. The relationship between the average energy of a primary neutron spectrum and the scattered neutron spectrum from the walls of a concrete room containing that spectrum (McCall *et al.*, 1979).

To use the "cookbook" method, one then proceeds as follows:

1. The epithermal fluence (ϕ) is measured at the desired points, e.g., with moderated activation foils.
2. The average energy of the primary neutrons, (E_o), is determined by reference to the literature or with values taken from Table 8.
3. The average energy of the direct component is determined from E_o , the value of the HEL from Figure 29 and the number of HEL's in the head shielding.
4. S is calculated from the room dimensions.
5. E is calculated from equation (14) for each measured point.
6. The measured fluence is converted to dose equivalent, or absorbed dose, by use of Figure 31a or 31b, respectively.
7. Thermal fluence is measured separately, converted to dose equivalent or absorbed dose, and added to the above result to obtain total dose equivalent or absorbed dose. Thermal fluence is also constant throughout the room.

The "cookbook" method gives results that agree with Monte Carlo calculations to within $\pm 10\%$.

It may be instructive to illustrate such a calculation by an example. Assume that there is a 15 MeV accelerator with tungsten shielding in the room illustrated in Figure 2a. At a point in the patient plane two meters from the isocenter, an epithermal fluence is measured of 6.4×10^3 n/cm² per photon rad at the isocenter. By examination of the head shielding of the accelerator it is estimated that the head shielding can be approximated by 10 cm of W. From Table 8, E_o is 1.8 MeV and from Figure 29 the HEL = 7.5 cm. E_{dir} can be calculated by $1.8 \times (\frac{1}{2})^{10/7.5} = 0.71$ MeV. The inside surface area of the room is calculated as 1.6×10^6 cm² if the ceiling is 3.3 m high and the maze opening is treated as if it were a wall. The value R^2 in equation 14 is $100^2 + 200^2 = 5 \times 10^4$ cm² if the distance from target to isocenter is the usual 1 m. Equation 14 can then be used to calculate that E is 0.34 MeV. The conversion factor for a neutron spectrum with this average energy is 9.7×10^7 n/(cm²-rem) from Figure 31. The measured fluence is then interpreted as $6.4 \times 10^3 / 9.7 \times 10^7 = 0.066$ mrem per photon rad.

2.3.2 Spatial Distribution of Fluence, Absorbed Dose and Dose Equivalent

It has been shown (Patterson and Wallace, 1958; McCall *et al.* 1979) that, for a fast-neutron source, the thermal and scattered fast-neutron fluences are essentially constant throughout a concrete room. The shape of the room is not very critical in this respect although extremely

long narrow rooms can cause problems. Fortunately, the typical room used for medical accelerators is close enough to being cubical that this is a good approximation. The neutron fluence at any point in the room, then, is composed of scattered but fast neutrons from the walls with a spectrum which is constant throughout the room; a thermal component which is constant throughout the room; and a fast and possibly a thermal contribution, coming directly from the accelerator head, which will follow the inverse square law. It is clear, then, that the fluence measured as a function of the distance from the accelerator head will always drop off more slowly than the inverse square law would predict. The thermal and scattered contributions are lower in energy than the direct component and contribute less per neutron to the absorbed dose and the dose equivalent. Thus, the absorbed dose and dose equivalent will drop off more rapidly than the fluence as a function of the distance from the therapy head, but more slowly than the inverse square law would predict.

The "cookbook" approach of McCall *et al.*, (1979) can be used to calculate the distribution of fluence and dose equivalent in a therapy room. Another method of calculating the distribution of the fluence within the room is to use an extension of the method developed by Eisenhauer (1965), which was originally applied to a point source and a plane scattering surface such as concrete. In this method, the scattered neutron component is described by an image source, whose position is given in a manner analogous to specular reflection, and whose intensity is given by an albedo. If this method is extended to the six sides of a concrete room, the scattered component will be underestimated. If the second order term, *i.e.*, the reflection of the image sources, is then calculated, and this term added, a much better approximation of the scattered component is obtained. What is really desired is an infinite series of reflections as obtained with parallel mirrors. Eisenhauer *et al.*, (1982) have shown that this can be accomplished by replacing the albedo α by $\alpha/(1-\alpha)$. If this is done, excellent agreement with the MORSE Monte Carlo calculations can be obtained. It should be noted that there are many kinds of albedos and the one to be used depends on exactly what is to be calculated. For a good discussion of albedos see Selph (1973).

2.3.3 Room Shielding

Most radiotherapy accelerators are installed in concrete rooms to shield the outside world against radiation from the accelerator. There

are various components of radiation from the accelerator which have to be absorbed, such as leakage photons, direct-beam photons, and scattered photons. In addition, there are neutrons. The sum of these four components comprises the source term to be used in calculating the room shielding. This report concerns itself with the neutron contribution.

In calculating the neutron shielding, there is a complication in that most of the neutron dose equivalent attenuation data in the literature are for a slab shield geometry with either a point source or parallel beam of neutrons. Unfortunately, this shielding situation is rarely encountered in practice, where the following are more common:

1. An approximate point source of neutrons surrounded on all sides by the shield whose thickness is to be determined.
2. A neutron source or a scattered neutron field at one end of a concrete passage, with a shielding door to be designed for the other end.
3. A distribution of point sources in a long line or large circle with shielding on all sides, such as an accelerator. Thus, the source appears to be a line source.

The attenuation of the slab shield is greater than that for these three configurations, because almost any scattering event will direct the neutrons away from the detector. In other words, this is closer to being a "good geometry" than the above situations. The attenuation would be least in Case 1 above. Attenuation data for slab shields could be used for Cases 1 and 2 if a method were known to account for backscatter from the other 5 walls.

A second complication is that most of the published attenuation data apply to monoenergetic neutrons, whereas continuous spectra are encountered in practice. Calculations have been made with the Monte Carlo code MORSE (McCall, 1979) for continuous neutron spectra with the geometry of Case 1 (spherical-shell shielding). A plot of the dose equivalent tenth-value layer (TVL) versus the average energy, \bar{E}_{dir} , of the spectra ($\bar{E}_{\text{dir}} = E_0$ if there is no metal shielding around it) is shown in Figure 33. Also shown is a least squares fit to the calculated points. These are straight lines given by the equations $\text{TVL} = 15.5 + 5.6 \bar{E}_{\text{dir}} \text{ cm}$ for concrete, and $\text{TVL} = 6.2 + 3.4 \bar{E}_{\text{dir}} \text{ cm}$ for polyethylene. These values should provide a good approximation for shielding of neutrons from medical accelerators. The bottom line in Figure 33 is for monoenergetic neutrons. These curves illustrate that the common practice of using shielding data for monoenergetic neutrons, at the average energy of the continuous spectrum, is neither correct nor conservative. For comparison, NCRP Report No. 51 gives the tenth

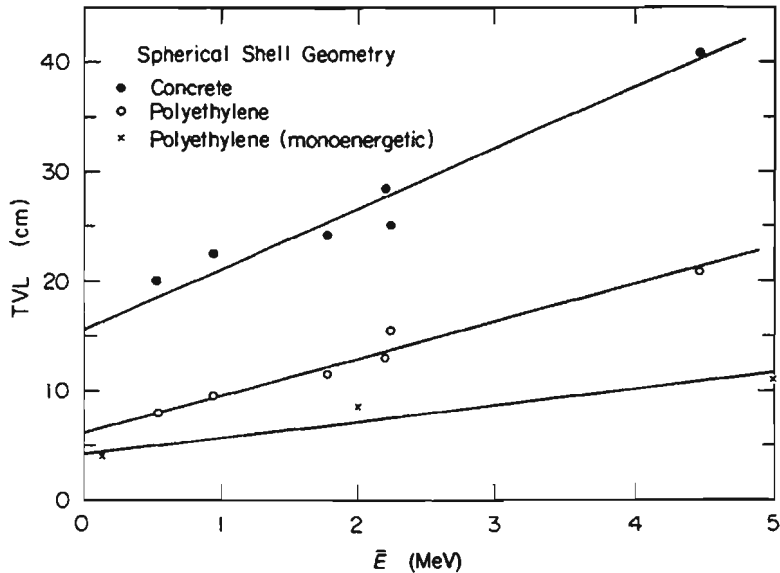


Fig. 33. The dose-equivalent tenth-value layer (TVL) for spherical shell shielding as a function of the average energy of the neutron source (McCall, 1979). The lines are least-squares fits to the calculated points.

value layer of neutrons³ produced by 16 MeV electrons striking a platinum target as 58 g/cm² or 25 cm in normal concrete (NCRP, 1977). This neutron spectrum would have an average energy of about 1.9 MeV, and, from Figure 33, the tenth-value layer would be about 26 cm. Had this comparison been made with the TVL for monoenergetic neutrons of 1.9 MeV, the agreement would have been poor. It should be noted that in Figure 33, Figure 36, and elsewhere in this report, where MORSE has been used to calculate shielding values, gamma-ray doses are not included. For shield thicknesses of two TVL's or more, this could cause the calculated dose equivalent to be too low by a factor of two or more.

Published data (e.g., Almond, 1979) show that the neutron contribution to the absorbed dose at 1 m from the target can be as much as about 0.05% of that due to the useful photon beam. If a quality factor of 10 is assumed, this contribution could be as much as 0.5%, i.e., 5 times the usual photon leakage specification. If the shielding value of concrete for photons and neutrons is examined, it is found that the

³This is not the value tabulated in NCRP Report No. 51, but is taken from Figure F-8 and is valid for the first four TVL's.

photons are always more penetrating than the neutrons for the energy range of interest here. For example, in Figure E-12 of NCRP Report No. 51, the dose equivalent index tenth-value layer for x rays in concrete varies from about 38 cm at 10 MeV to 47 cm maximum at higher energies (NCRP, 1977). The average energy \bar{E}_{dir} from medical accelerators would never be much above 1 MeV. Figure 33 shows that the tenth-value layer for the neutrons would be no more than 21 cm of concrete. Therefore, even if we consider the highest energy neutrons and the lowest energy x rays, for each x-ray tenth-value layer (38 cm), the neutrons are attenuated by a factor of $10^{38/21} = 65$. Since practical therapy rooms need concrete walls at least two x-ray tenth-value layers thick, adequate concrete shielding for the photons will always be adequate for the neutrons as well.

If a room is built using lead or iron as all or part of the shielding, further care must be taken since, as was described in previous sections, the shielding value of iron or lead for neutrons is very poor. The shielding calculations for thermal and fast neutrons in such a situation would be difficult. Some insight into the amount of shielding needed might be gained from the papers by Dudziak (1969) or Shure *et al.* (1969). These authors discuss the shielding values for heavy metals followed by a thickness of polyethylene. Since the value of the polyethylene is to provide hydrogen to moderate and capture the neutrons which have slowed down in the heavy metal, an equivalent thickness for concrete and polyethylene could be calculated with adequate accuracy.

2.3.4 Maze Design

Most therapy accelerator rooms are designed with at least a rudimentary maze or labyrinth; this avoids the use of massive doors which would have to be opened and closed by air or hydraulic systems. If the maze provides sufficient attenuation, the door needs to provide only radiation security. Often, however, there is not space for a good maze, or neutron shielding was not considered during its design. In addition, old accelerators are frequently replaced by higher energy machines which can generate neutrons, but no significant modification of the room design is carried out.

Examples of maze designs are shown in Figure 34. Figure 34a is a poor design because large areas directly illuminated by neutrons from the accelerator are visible from the door. Thus, neutrons can reach the door by a single scatter and are minimally attenuated in both energy and intensity. Figure 34b is an example of a good maze design.

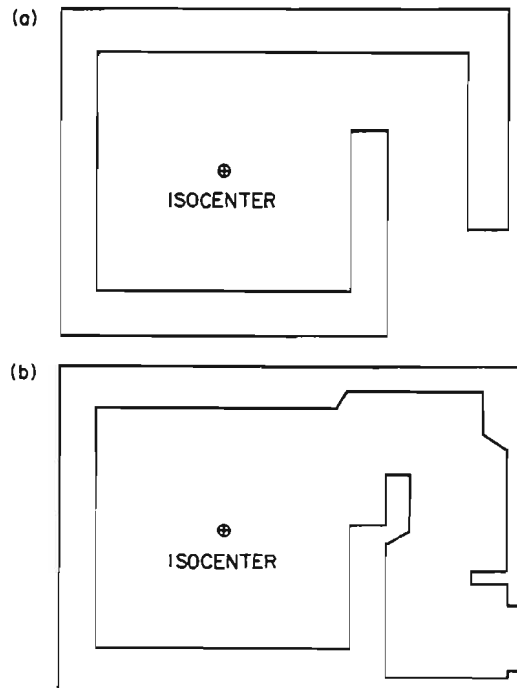


Fig. 34. Examples of maze configurations showing (a) a poor maze design and (b) a good maze design.

In this configuration, neutrons must scatter at least twice to reach the door. The same goal can be accomplished by a second bend in the maze, but more area and more concrete would be required.

There have been many studies of the penetration of mazes by neutrons (Spencer and Diaz, 1964; Spencer *et al.*, 1964; Song, 1965; Song, *et al.*, 1971; Maerker and Muckenthaler, 1967b; Maerker *et al.*, 1968). These studies, however, were directed at other problems which differ in one or more of the following respects from medical accelerator problems.

1. Neutrons were incident at a particular angle on a small part of one wall rather than at various angles over the entire maze entrance.
2. The mazes were long and narrow rather than being short and wide as found in therapy rooms.
3. Incident neutrons were of much higher energy than in the medical accelerator case.

4. The studies were designed to test a particular computer code which may not be generally available.

Thus, it is not at all clear how these results can be applied to the therapy-accelerator problem. In addition, very few published results of measurements are available for comparison. The albedo methods are simplest but would usually require computer calculations for proper applications. However, there are some simpler methods in the literature which are of adequate accuracy for shielding design. The first of these methods (Kersey, 1979) appears to be an empirical solution based on measurements in several therapy rooms. Essentially, the neutron dose equivalent at the maze entrance is calculated based on the inverse square law from the source. The attenuation in the maze is based on the center-line length of the maze and a value of 5 m of maze length to reduce the dose equivalent by a factor of 10.

As an example of the Kersey method, one can use the room shown in Figure 35. Assume that the neutron head leakage has been measured

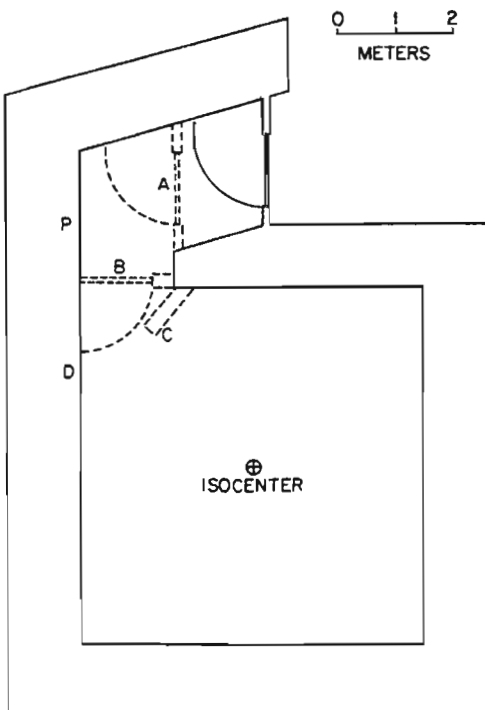


Fig. 35. A typical electron therapy accelerator room layout with an inadequate maze. Dashed lines at A, B, and C illustrate possible methods of decreasing the radiation dose at the door.

at 1 meter and found to be 0.5 mrem per useful photon rad (0.05% leakage). From Figure 35, the distance to the maze entrance (near B) is 3.7 meters. The center-line path length of the maze is also 3.7 meters. The neutron dose equivalent at the door would be given by

$$H = \frac{0.5}{3.7^2 \cdot 10^{3.7/5}} = 6.6 \times 10^{-3} \text{ mrem/photon rad.}$$

It should be noted that the Kersey method gives the total (thermal plus fast) neutron dose equivalent.

The second of these simplified methods (McCall *et al.*, 1980) is an albedo method which can be described as follows: On a room drawing, outline the portion of the walls, floor and ceiling that could be irradiated by direct neutrons from the accelerator, and be visible from the door. An effective center (the location is not critical) is selected for each of these four areas (floor, ceiling, and two corner walls). The incident and reflected angles are measured from these center points, and the simplification is made that all neutrons striking each effective area are concentrated in the point at the center. Next, the dose albedo, α (French and Wells, 1964) is used,

$$\alpha = \alpha(E_o) (\cos \theta_o)^n (\cos \theta), \quad (15)$$

where θ_o and θ are the incident and reflected angles, respectively, measured from the normal to the wall. For the range of neutron spectra from medical electron accelerators, a single value for $\alpha(E_o)$ of 0.11 can be used for concrete.

Next, the dose equivalent is assumed to follow the inverse square law both from the accelerator source to the effective centers, and from the effective centers to the door.

With the above simplifications, the dose equivalents from each of the irradiated areas (floor, ceiling and corner walls) are added. Obviously, many of the assumptions are questionable. Nevertheless, this is a calculation which can be done by hand, and it is sufficiently accurate for room shielding calculations.

Figure 35 can be used to exemplify this method. Neutrons can scatter from the wall at the top of the drawing at any location from the upper-right corner out to the point marked D, a distance of 3.6 meters, and go directly to the door. This part of the wall has an area of $3.6 \times 3.3 = 11.9 \text{ m}^2$ if the ceiling is 3.3 meters above the floor. A point P which is estimated to be the effective center of this area is selected. Point P is 4.7 meters from the isocenter and 3.3 meters from the door. With a protractor, the incident and reflected angles are found to be 47° and 22° , respectively. From Equation 15 above $\alpha = 0.11(\cos$

$47^\circ)^2(\cos 22^\circ) = 0.079$. The dose equivalent from this wall would then be

$$H = \frac{0.5}{4.7^2} \times \frac{0.079 \times 11.9}{3.3^2}$$

$$= 2.0 \times 10^{-3} \frac{\text{mrem}}{\text{photon rad}}.$$

The contributions from the other wall, the ceiling, and the floor are calculated similarly and all four contributions are added to give a total of

$$H = 2.4 \times 10^{-3} \frac{\text{mrem}}{\text{photon rad}}.$$

The dominance of the contribution from the wall facing the door is not unusual. This dose equivalent rate is for fast neutrons only.

The Kersey method was developed for only one model of accelerator. Results were found to agree with measurements to within a factor of two. The method was applied to other accelerators in a subsequent report (McCall *et al.*, 1980) and, while agreement was not as good, it always over-estimated the dose at the door, so it is conservative. This method also has the advantage of simplicity. The same report shows the McCall method to be somewhat more accurate but also more time-consuming. It also presented a third method which was subsequently found to be in error and the method should not be used.

It should be noted that both of the suitable methods make assumptions that are physically incorrect, but their results are adequate for shielding design.

To estimate the total radiation field at the door, Kersey suggests that the neutron capture γ -ray dose rate might be as much as $1/5$ of the total neutron dose equivalent rate. McCall *et al.*, (1980) made measurements outside the doors of several accelerator rooms and found that the three dose equivalent components—fast neutrons, thermal neutrons, and neutron capture γ rays—were of comparable magnitude unless there was considerable shielding in the door. Tochilin and LaRiviere (1979) and LaRiviere (1982a; 1982b) present data that are in rough agreement with both of the above. Maerker and Muckenthaler (1967a) observed that, in the middle of a concrete tunnel with a fluence rate ϕ n/(cm²-sec) of thermal neutrons, the dose rate of capture γ rays was approximately $10^{-6} \dot{\phi}$ rem/h. Since 1 mrem/h of thermal neutrons is equivalent to 260 n/(cm²-sec) (ICRP, 1973), the capture γ -ray dose rate is roughly $1/4$ of that due to thermal neutrons. When some existing data were tested (McCall, 1979) it was found that this rule-of-thumb

overestimated the measured capture γ -ray dose rate by a factor of 1.4 to 3.0. Since the door is at the end of a tunnel, rather than in the center, this is about as would be expected.

2.3.5 Door Shielding

The amount of shielding necessary at the door is closely related to the maze design. Most therapy room doors have a certain amount of lead shielding which is designed to attenuate scattered x rays. This topic has been adequately covered previously (NCRP, 1976; 1977). Assuming that scattered x rays have been adequately absorbed, the radiation field at the door will be a mixture of fast (but low-energy) neutrons, thermal neutrons, and neutron-capture gamma rays. The neutron-capture gamma rays are emitted from captures in the maze walls and the door itself. As stated above, in a room with a poorly designed maze, the neutron-capture gamma ray component may be $\frac{1}{5}$ or more of the total dose equivalent. The neutron-capture gamma rays are of very high energy, ranging up to ~ 10 MeV. The 2.2 MeV gamma ray from capture in hydrogen will be a prominent, but not a dominant, feature in the spectrum. Massive doors would be required to attenuate the capture gamma rays significantly. For example, from the results of surveys of half a dozen accelerators (McCall *et al.*, 1980) a TVL of 5–7 cm of lead was estimated. Later, a more careful measurement (LaRiviere, 1980) gave a TVL of 6.1 cm of lead. The only other reported measurements (Kersey, 1979) showed much lower energy gamma rays (TVL ~ 6 mm Pb) but these measurements were for rooms with much better mazes where scattered photons would be expected to be more important. As described in the previous section, proper maze design eliminates the need for the construction of very heavy doors.

For existing accelerators or for new accelerators being placed in existing rooms, it is sometimes impossible to build adequate mazes. In such cases, Figure 35 might represent a typical room. For accelerators with a nominal energy of 15 MeV and a workload of 80,000 rad/week, dose equivalents of 2–10 rem/year (neutrons plus photons) have been found at the door (McCall, 1979). There is often high occupancy just outside the door; therefore, it is necessary to reduce these radiation levels by factors of 4 to 20. Useful measures to be taken depend upon the amount of shielding needed. The configuration is like that in Case 2 of Section 2.3.3. Monte Carlo calculations for this case have been made (McCall, 1979) for concrete and polyethylene shielding; the results are shown in Figure 36. The average energy of the neutrons is

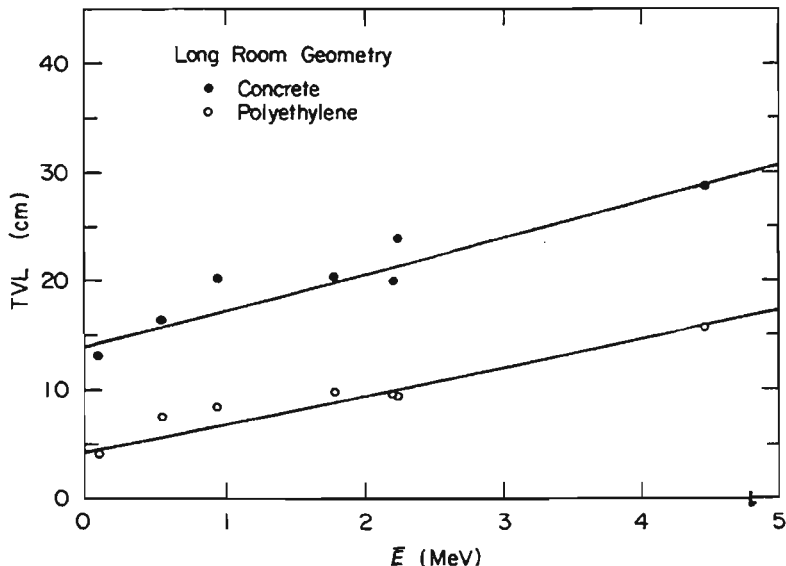


Fig. 36. Dose-equivalent tenth-value layer (TVL) for a geometry approximating a shielding door at the end of a maze as a function of average energy of the neutrons at the door. The lines are least-squares fits to the calculated points (McCall, 1979).

low—in the neighborhood of 100 keV for all accelerators. Two inches of polyethylene on the door would reduce the fast neutron component by a factor of about 10. If one inch of the polyethylene were borated (the outer inch), thermal neutrons would essentially be eliminated. However, there would be very little change in the neutron-capture gamma-ray dose rate, so that the total reduction in dose equivalent would be by a factor of about $1/3$ to $1/5$. If a larger reduction is needed, other measures must be taken. One possibility is to cover the maze walls with borated materials. Boron has a high neutron-capture cross section and produces ~ 1 gamma ray of 0.478 MeV energy per capture (NCRP, 1971). In concrete, about 2 gamma rays per capture are produced (Schmidt, 1970) and their energy is considerably higher—up to 10 MeV. The maximum reduction in capture gamma-ray dose to be expected would be about $1/2$. A more elegant solution would be to keep the thermal neutrons away from the door. Several possibilities for accomplishing this are illustrated in Figure 35. At position A, an auxiliary door has been added. Since the door material absorbs neutrons and reflects neutrons back into the room, the fast- and thermal-neutron fields at the outer door are reduced. At the same time, neutron-capture gamma-ray production near the outer door is reduced and

distance will make the others less important. This auxiliary door should incorporate 2 inches of polyethylene with the outer inch borated. A total reduction of the dose equivalent at the door by about a factor of 10 should be obtained. At position B a similar door is shown. This door would not shield as effectively, since the neutrons striking it are of somewhat higher energy and would not be attenuated so efficiently. Also, some neutrons would be scattered directly toward the outer door. At position C a "finger" wall is shown that can sometimes be added (Worsnop, 1979). This finger functions by shadowing part of the end wall area which can scatter neutrons directly toward the outer door. Since it can only partially shadow this area, it is probably not worthwhile to make this finger too thick. One foot of concrete or 3 inches of polyethylene might be reasonable maximum thicknesses. The reduction factor to be expected will depend on the geometry in each case. A solid-core wooden door rather than a metal door should be chosen. An industrial wooden door is 1 $\frac{1}{4}$ inches thick and would be expected to attenuate the fast neutrons at the door by a factor of about 0.75. Four cm of wood provides approximately the same neutron shielding as 1 cm of polyethylene.

2.3.6 Reduction of Neutron Emission from Accelerators

There are only two ways to reduce neutron emission from accelerators. Either reduce the number of neutrons produced per useful photon rad or put shielding around the accelerator to absorb the neutrons. The latter is the more obvious solution but is difficult to accomplish in the space available. In the first commercial accelerator to incorporate neutron shielding, LaRiviere has reported that the neutron-leakage dose equivalent was decreased by a factor of about 0.70 in the 15 MeV photon mode and by a factor of about 0.53 in the 19 MeV photon mode (LaRiviere, 1980).

Reduction of the relative numbers of neutrons produced can be accomplished within limits. McCall *et al.* (1978b) reported that changes in an accelerator design resulted in a 20% decrease in the neutron production per photon rad at the isocenter. McCall and Swanson (1979) analyzed the sources of neutron production in a typical therapy head. This analysis shows that neutron production could be reduced by absorbing the unwanted photons in a medium Z material such as Fe rather than Pb or W. The reduction in neutron production could be by a factor of 4 to 6. However, it takes much more Fe than Pb or W to provide the necessary shielding and there is insufficient space to take advantage of this reduction completely. In addition, there

are good reasons for making the target at least partially of a high-Z material. It is unlikely that neutron production in the therapy head could be reduced by more than a factor of two by appropriate choice of materials.

It is important that neutron production between the electron gun and the target be reduced as much as possible. Electrons striking collimators, beam scrapers, etc. produce photons which interact with the local shielding to produce photoneutrons. How large this source of neutrons might be is unknown, but calculations indicate that in some accelerators neutron production might be as large as from those sources occurring at and beyond the target (McCall and Swanson, 1979). The electrons lost at slits and collimators, of course, contribute nothing to the useful photon beam. It should be noted that these extraneous photon sources strike very thick shielding of heavy metals and produce the maximum possible number of neutrons. If these photon sources were shielded only in the direction of the patient, neutron production would be much lower, although extra concrete might be needed in the room shielding to attenuate the photons. Some state regulations, however, often require photon shielding in all directions from the target.

Another possibility, which has not been adequately explored, is the use of different field flatteners for large and small treatment fields. In order to flatten, e.g., a 22 MeV bremsstrahlung beam out to 14° (the corner of 35×35 cm field at 100 cm), the central-axis dose rate must be attenuated to about 1.8×10^{-13} rad/electron, an attenuation factor of about 0.15. To flatten the same beam at 4° —the corner of a 10×10 cm field at 100 cm—the central axis dose rate must be attenuated to about 5.5×10^{-13} rad/electron, an attenuation factor of about 0.46 (McCall, 1978). This would mean that the same useful photon dose rate could be provided with only $\frac{1}{3}$ the current in the latter case. The neutron production per useful photon rad would be reduced by the same factor. There would also be a small reduction in neutron production due to the fact that the flattener is thinner. If a significant fraction of treatments were with small fields, it might be a worthwhile modification to provide separate flatteners for large and small fields.

3. Hazards from Neutrons

3.1 Patient Risk

3.1.1 *Introduction*

The risk of harmful effects associated with a radiation dose can be divided into two categories: genetic and somatic. Genetic effects are those effects manifested in the progeny of an exposed individual whereas the somatic effects are those manifested in the individual. When radiation is used as a therapeutic modality in the treatment of malignant diseases, the patient is exposed to the risk of both genetic and somatic effects. The physician must be familiar with the risk of the particular treatment and must be able to convey the sense of the risk and the potential benefit to the patient, so that, together, they can arrive at an informed treatment decision. There are a number of sources available to guide the physician in arriving at risk factors (NAS, 1972; 1980; UNSCEAR 1977; 1982) and the principal benefit is the hope of a complete cure or, at least, a temporary remission of the effects of the disease.

Numerical estimates of risk can bear upon the choice between alternatives; therefore, it is necessary to estimate the risks (Pochin, 1978). However, it is not always possible to make numerical estimates since the appropriate data may not be available. Prior to the early 1950's most external-beam radiation therapy for deep-seated tumors was performed with 200 to 300 kV x rays. Very often therapy was terminated, not because the tumor had received a sufficient dose, but because the overlying skin had reached its tolerance dose. The physical advantages of high-energy radiation, including build up, increased depth dose, and reduced side scatter, have led to the virtual replacement of orthovoltage (200–300 kV) x-ray units with units of 1 MeV and higher energies.

The ratio of tumor integral dose to patient integral dose increases as the energy of the photons used increases, and as the type of administration increases from a single field to multiple fields to a

moving field (Wachsmann *et al.*, 1962). There is evidence that the cure rate for cervical cancer is higher when cobalt-60 gamma rays (1.25 MeV photons) rather than orthovoltage x rays are used, and that this rate is significantly higher for 22 MeV x rays (Bush, 1980). Why are the cure rates so much better with higher-energy radiation than with cobalt-60? Johns states that the question cannot be answered unequivocally, but he believes that "the differences in results are mainly due to the quite different dose patterns for the same dose to the tumor volume; the high energy beam deposits much less radiation in the normal tissue in the region between the skin and the tumor". (Johns, 1979).

With advances in therapeutic technology and use of combined modalities (surgery, radiotherapy, chemotherapy, hyperthermia, etc.), the survival time has been extended to many years for specific diseases. This extended survival time has stimulated the need to reevaluate the risks associated with the therapeutic techniques. To compound this situation, the radiation environments associated with supposedly similar treatment beams may actually differ from each other, thereby rendering different probabilities of risk for the treatment beams. For example, the photoneutron production and the leakage radiation associated with a 25 MeV photon beam generated by a betatron may differ from that for a 25 MeV photon beam generated by a linac. Since the radiation risks to the patient are related to the radiation environment generated by the therapeutic source, a knowledge of this environment is paramount before any associated risks can be evaluated.

The neutrons produced by radiation therapy beams are of relatively low intensity (See Sect. 3.1.3), and, consequently, the risks can be assumed to be those associated with low-level radiation. The reports of the Biological Effects of Ionizing Radiation Committee (BEIR) (NAS, 1972; 1980) and the reports of the United Nations Scientific Committee on the Effects of Atomic Radiation (UNSCEAR, 1977; 1982) address mainly the risks associated with low-level, low-LET radiation. They do not attempt to elaborate or discuss in any detail the risks associated with low levels of high-LET radiation. In addressing the therapeutic uses of radiation, the UNSCEAR report states that the seriousness of the primary disease requires that little consideration be given to any deleterious late effects of radiation that might occur many years after a successful treatment. The report goes on to state, however, that it is important to obtain estimates of the radiation dose within healthy organs and tissue irradiated in the treatment regimen, so that estimates of the frequency of such late effects can be made (UNSCEAR, 1977).

3.1.2 *Source of Radiation Dose Outside the Treatment Volume*

In radiation therapy, specified tissues are to be irradiated to a specified absorbed dose according to a specified time-dose pattern. Because of the limitations in treatment techniques, it is impossible to administer the prescribed absorbed dose exclusively to these tissues. For the purposes of this report, it is sufficient to discuss the dose to the treatment volume rather than the dose to the tumor. The volume of the patient included within the primary beam which encloses the tissues to be treated is called the treatment volume.

Any absorbed dose the patient receives outside the treatment volume must be considered undesirable. There are several sources of absorbed dose outside the treatment volume in addition to primary beam absorption in overlying and underlying tissues.

1. Photons leaking through the head shielding.
2. Photons scattered out of the treatment volume.
3. Neutrons originating in the treatment head and leaking through the head shielding.
4. Neutrons produced in the treatment volume by (γ , n) reactions and then penetrating outside the treatment volume.
5. Radiation due to radioactive isotopes produced in the body.

These various components are not completely independent of each other and it is the total risk to the patient which should be considered.

The first of the sources above is probably the best known, since it is a problem previously encountered with lower-energy x-ray generators. Most commonly, photon head leakage has been required by regulatory authorities to be less than 0.1% of the useful beam dose rate, when both are measured at the usual working distance from the target. The limit of 0.1% of the useful dose first appears in NCRP Report No. 3 (NCRP, 1936). The recommendation in its modern form appeared in ICRP Publication 4 (ICRP, 1962). It has been stated that the value was chosen rather arbitrarily as a value that could easily be met for the equipment of that time (Rawlinson and Johns, 1977). Others remember the reasons as being somewhat different, and it appears that the true reasoning behind the choice of 0.1% may be lost forever.

The second of the above sources has been considered in relation to the photon leakage dose (Rawlinson and Johns, 1977; Rawlinson, 1979). These authors made measurements and calculations of the ratio of the integral dose due to photon scatter to the integral dose due to photon head leakage. This ratio ranged from ~28 for large fields to ~5 for small fields using both ^{60}Co γ rays and 25 MV x rays. For this

work they assumed head leakage was a constant 0.1% of the useful dose rate at the depth of maximum dose rate. Calculations by Ing and Shore (1982) are in good agreement. These ratios must be considered as minimal since this assumption neglects the decrease of leakage dose rate with distance from the target and the effect of additional shielding of the patient by the adjustable collimators when they are partially open.

The third source above has been considered by several groups. Most of the work has concentrated on measurements of the neutron leakage dose rate in the plane of the patient. These results have been summarized by Almond (1979). The attenuation of such neutrons, from a 14 MeV and a 25 MeV machine, in a water phantom, has been calculated by McCall and Swanson (1979). They obtained half-value layers (HVLs) of 2.2 cm and 3.5 cm of water, respectively, from the calculated distributions of dose delivered by recoil charged particles. Such calculations have been confirmed by incorporating the depth dose curves for monoenergetic neutrons given in NCRP Report No. 38 (NCRP, 1971) weighted by the neutron-leakage spectrum. For neutrons from head leakage whose average energy is typically less than 1 MeV, the dose delivered by gamma rays produced by neutron interactions in the body is not negligible. These gamma rays have a flatter dose distribution (See NCRP, 1971) and tend to increase the HVL. For instance, the addition of the gamma dose to the neutron dose (giving the total "neutron-generated" dose) changes the half-value thickness for the 25-MeV machine to 5.0 cm of water. Pohlitz has measured the attenuation of photoneutrons produced in 5 mm Pb sheets placed in the x-ray beam at a distance of 125 cm from a betatron target (Pohlitz, 1959). The measurements were made with In foils placed in a $50 \times 50 \times 50$ cm³ paraffin phantom directly behind the lead. For betatron energies of 18 and 35 MeV, the half-value layers obtained were 5.8 and 4.3 cm of paraffin, respectively. In a subsequently-reported measurement, a HVL at 35 MeV of 3.9 cm in paraffin was obtained for betatron leakage neutrons at a distance of 108 cm (Pohlitz, 1960). When multiplied by the ratio of hydrogen concentrations, the paraffin HVLs of 5.8, 4.3 and 3.9 cm become 6.7, 5.0, and 4.5 cm, respectively, in water. Although these half-value layers are not very accurate, they can, nevertheless, be used to estimate the self-shielding of the patient to obtain the integral dose delivered by leakage neutrons. Brahme *et al.*, obtained an HVL of about 5 cm in tissue-equivalent plastic for photoneutrons from a 50 MeV microtron in good agreement (Brahme *et al.*, 1980). For a 20 cm thick patient (actually H₂O) and perpendicular incidence, the integral doses, obtained by integrating the attenuation curve, are 0.42, 0.34, 0.31, 0.25 and 0.16 of

the values obtained assuming no attenuation of half-value thicknesses of 6.7, 5.0, 4.5, 3.5 and 2.2 cm respectively.

Ing and Shore calculated the integral dose from head leakage neutrons in a 4×10^4 g phantom for a particular 25 MeV linear accelerator and an assumed leakage of 0.091% (neutron rad per photon rad at 1 m) (Ing and Shore, 1982). A value of 12 g-rad per photon rad was obtained for a beam 100 cm^2 in area. For these irradiation conditions and the same phantom size, the integral dose estimated using a HVL of 5.0 cm is $9.1 \times 10^{-4} \times 0.34 \times 4 \times 10^4 \text{ g} = 12 \text{ g-rad per photon rad}$, which is in good agreement. Swanson also estimated the integral dose in a phantom slightly different from that used by Ing and Shore (1982), and obtained a value of 4.0 g-rad for a 100 cm^2 beam and a head leakage of 0.03%, which is also in good agreement when the difference in assumed leakage is taken into account (Swanson, 1980).

The leakage of 0.091% used by Ing and Shore, (1982) represents the highest value measured for that particular type of accelerator, in which it is known that a large (and variable) fraction of the neutrons incident on the patient is produced at the two bends of the beam and in the collimator after the bend. In their calculation, Ing and Shore have included this component to derive their integral dose. On the other hand, the leakage (0.03%) assumed by Swanson probably represents the lower limit for those accelerators and includes only neutrons from the head. According to another study, the typical leakage from this machine is 0.059% which is almost exactly the average of the above values and would give an integral dose of 7.8 g-rad (Almond, 1979). Ing and Shore concluded that with a quality factor of 10, the integral dose equivalent from such 25 MeV machines could approach that from scattered photons for small fields. However, if production in the two "bends" are excluded and only neutron leakage from the head is considered, the integral dose equivalent from leakage neutrons is only about half of the unwanted integral dose equivalent from scattered photons (Ing and Shore, 1982).

The fourth source of radiation outside the treatment field was first studied by Laughlin who estimated that the dose equivalent from neutrons produced in the patient was of the order of 0.05–0.4% of the photon dose depending on field size (Laughlin, 1951). Horsley *et al.* (1953) made some rough calculations and decided it was not a significant problem. More recent Monte Carlo calculations by Ing *et al.* (1982) indicated that the patient integral dose outside the treatment volume due to neutrons produced in the patient is of the order of 100 times smaller than that due to photons scattered out of the treatment volume. Adams and Paluch found that the dose equivalent from neutrons produced in water by a $10 \text{ cm} \times 10 \text{ cm}$ beam of photons from

a 70 MeV synchrotron was about 1 mrem/photon rad at the edge of the beam. They found that neutrons were attenuated at 90° to the beam direction with a half-value layer of 4.0 cm in water (Adams and Paluch, 1965). No information was given about scattered photon doses except that at 20 cm from the edge of the beam, the scattered photon dose was about 10 times the dose equivalent from neutrons produced in the treatment volume. If a quality factor of 10 is assumed, this is in good agreement with the calculations of Ing *et al.* (1982). Calculations by Laughlin *et al.* (1979) are reported, with corrections by Bading *et al.* (1982), that are in very good agreement with those of Ing *et al.* (1982). Measurements and calculations by Allen and Chaudhri (1982) are confined to the treatment volume but agree closely with the results of Horsley *et al.* (1953). They also reach the conclusion that the dose as a result of photonuclear reactions in the patient is insignificant.

Frost and Michel studied distributions of neutrons and protons produced in a paraffin phantom by a 34 MeV betatron beam. They report additional dose-equivalent components of 7.1% and 2.4% (rem/treatment rad) for these particles, respectively, assuming a quality factor $Q = 10$ for both, or a total of 9.5% (rem/treatment rad) (Frost and Michel, 1964). While they point out that the protons produced have a very limited range, their data show that the fast-neutron component has a penumbra of about 12–13 cm in paraffin. This is the distance in which the neutron dose drops from 85% to 15% of the maximum. Measurements of the transverse neutron fluence show penumbras in the range 12–15 cm in paraffin for neutrons produced by a 24 MeV betatron beam in a paraffin phantom (Pohlitz, 1959). These authors do not give the fraction outside of the beam and this is difficult to obtain accurately from their published data, but one could expect a majority of the neutron dose to be deposited outside the treatment area if the field size is comparable to or less than the penumbras found.

The fifth source of radiation dose is that due to radioactive isotopes produced in the body. The predominant isotopes will be those from (γ , n) reactions in C, O, N, P and Ca. All of the isotopes produced are short-lived positron emitters ($T_{1/2} \ll 1$ h). The relative importance of the various isotopes depends on the accelerator energy and the relative amount of bone in the irradiated volume. This problem has been investigated with a 35 MeV betatron (Frost and Michel, 1967). They found very small doses due to this source, of the order of 0.01% of the useful photon dose in the worst case.

In summary, the dose the patient receives outside the treatment volume from the five sources considered are as follows:

1. *Photon head leakage*—Varies, but if recommendations are followed, it is usually less than 0.1% useful dose (NCRP, 1968).
2. *Scattered photons*—Integral dose is 5–30 times larger than that produced by 0.1% head leakage.
3. *Head leakage neutrons*—Maximum integral dose equivalent could be about half of that from scattered photons for any therapeutic treatment condition.
4. *Neutrons produced in patient*—Negligible.
5. *Radioactive isotopes produced in the patient*—Negligible.

3.1.3 Significance of Leakage Exposure

It was shown in the previous section that the integral dose equivalent from leakage photons, assuming the maximum 0.1% leakage, was at most about 20% of that due to scattered photons from the treatment volume. It was also shown that leakage neutron dose equivalent could be about half that due to scattered photons in the worse case. The maximum integral dose equivalent from leakage then would be about 70% of that due to scattered photons. In any realistic situation where there is a distribution of treatment field sizes the average relative contribution from leakage photons would be less.

The significance of neutrons from head leakage and photonuclear reactions in the body relative to changes in the scattered photon intensity with beam energy is evident (Ing *et al.*, 1982; Ing and Shore, 1982). For a ^{60}Co beam 100 cm^2 in area, these authors claim that the integral dose delivered by scattered photons outside the treatment volume is 20% of that inside the treatment volume. Their results also show that when the photons are produced by a 25 MeV machine, the integral dose outside the treatment volume from scattered photons is 10%, while the integral dose from leakage neutrons and photoneutrons in the body (even for the large assumed neutron leakage for the machine) is only 1% giving a total “unwanted” integral dose of 11%. Thus, the decreased photon scattering accompanying an increase in beam energy more than compensates for the additional contributions from neutrons produced by the photonuclear reaction.

Using the above estimates of the magnitude of neutron dose and the best available neutron risk coefficients, it is estimated that 5×10^{-6} fatal malignancies per year due to the neutrons may follow a typical treatment course of 5000 rad of 25 MeV x rays. This is about $\frac{1}{60}$ th of the average incidence of malignancies of the general population. Thus, the cancer risk to the radiotherapy patient from accelerator-produced

neutrons poses an additional risk to the patient that is negligible in comparison (Nath *et al.*, 1984). On the other hand, there are documented advantages of high-energy radiations, *i.e.*, betatron radiation which does have leakage neutrons, over cobalt-60 radiation which has no neutron component. For many tumor types, no data are available, but data show that, for stage III carcinoma of the cervix, 12 years after diagnosis, 33% of the patients, who have been treated by the betatron, survive, whereas, only 15%, who have been treated with cobalt-60, survive (Bush, 1980). It would appear that any higher risk of carcinogenesis associated with high energy photon therapy is negligible compared with the increased benefits relative to lower energy photon irradiation.

Recently a task group was appointed by the American Association of Physicists in Medicine to consider the risk to the patient from leakage neutrons (AAPM, 1982). Their conclusion was that the patient risk was extremely small and that more stringent leakage restrictions were undesirable (Nath *et al.*, 1984).

3.2 Sources of Exposure for Operating Personnel

3.2.1 *Door Leakage*

Most rooms will be adequately shielded against neutron leakage, except at the door (See Section 2.3.3). Rooms with inadequately designed mazes and doors, may have a radiation problem just outside the door. This is an area often occupied by technicians and nurses waiting for the treatment to be completed. The accelerator control console is often close to the door. Since a large fraction of the neutron component is below 500 keV, personnel dosimetry will be difficult. Film dosimeters containing nuclear-track film will detect only a negligible fraction of the fast neutron dose. Albedo dosimeters would be very direction dependent for these low energy neutrons. Photon and thermal neutron components of the radiation field outside the door are easier to measure by standard personnel dosimetry methods such as paired ${}^6\text{LiF}$ and ${}^7\text{LiF}$ thermoluminescent dosimeters (TLD). The sensitivity of such TLDs is good enough to measure a dose equivalent of <5 mrem due to thermal neutrons. While the thermal neutrons are only one component of the radiation field, TLD personnel dosimeters would be useful in detecting any changes in shielding, operating

procedures, etc., that affect the hazards from neutrons. Estimates of total dose equivalent will probably have to be based on periodic area surveys and occupancy times. Measurement methods are discussed in Section 4.

3.2.2 Activation

When a photon produces a neutron through a (γ , n) reaction, the product nucleus may be radioactive and the neutron may be absorbed forming a second radioactive nucleus. If the resulting radiation levels are significant, they could contribute to the radiation dose of the operating personnel. There is a small amount of information available indicating that this occurs. In a study of film badge exposures of technologists working on a 25 MeV accelerator compared with those working on 4 and 6 MeV accelerators, it was found that measurable exposures were seen only for those working on the higher-energy accelerator and would have been about 100 mR/y for a full-time technologist (Hoffman and Nath, 1982). Annual exposures of about 50 mR/y for technologists on an 18 MeV accelerator and 200 mR/y for those on a 25 MeV machine were observed (Almond, 1981).

The induced radioactivity can conveniently be discussed according to its location, namely:

1. Accelerator components and treatment aids.
2. Patient.
3. Room walls, ceiling and floor.

3.2.2.1 Accelerator and Treatment Aids. There is little information in the literature on this topic. It is clear that the parts of the accelerator which are most apt to become radioactive are the target, collimators (if any), field flattener and inside surfaces of the head shielding. These components are well-shielded and would only be a problem when the machine is disassembled for repairs. The induced activity in treatment aids of a 25 MeV linear accelerator has been studied (Glasgow, 1980). These treatment aids included plastic trays, lead and Cerrobend shielding blocks, aluminum plates, lucite trays, and wax and brass devices. One minute after a 300 rad treatment all of these, except for the brass items, exhibited a dose rate at contact of less than 2 mR/h. A brass wedge showed the highest dose rate of 26 mR/h at contact. The major portion of this dose rate was from ^{62}Cu ($T_{1/2} = 9.78$ min). Glasgow measured hand and body exposures of the radiation therapy technicians and found hand exposures exceeded body exposures by a ratio varying from 2/1 for a 4 MeV machine to 10/1 for a 23 MeV betatron.

Unpublished data from several accelerator manufacturers indicate maximum exposure rates of 1–4 mR/h at accessible points on their accelerators after continuous operation for 10–30 min (LaRiviere, 1980; Taumann, 1980; VanDyk, 1981).

3.2.2.2 Patient. While activation of the patient has been observed after radiotherapy (Mayneord *et al.*, 1949; Frost and Michel, 1967; Spring and Väyrynen, 1970; Strandén, 1977a; Hughes *et al.*, 1979), none of the authors have reported dose rates emanating from the activated patient. In all cases, ^{15}O ($T_{1/2} = 2.04$ min) and ^{11}C ($T_{1/2} = 20.3$ min) were the only significant isotopes observed. Kenney (1981) measured surface dose rates on two patients after a radiotherapy treatment with the following results:

45 MeV x rays, 338 cm² field, 210 rad dose resulted in a 12 mR/h reading, declining to 1.9 mR/h after 10 minutes.

25 MeV x rays, 311 cm² field, 286 rad dose resulted in a 13 mR/h reading, declining to 2.5 mR/h after 10 minutes.

It would appear that the dose to a technologist from such levels would be quite low. Since the carbon/oxygen ratio varies from fat to muscle, it is apparent that the $^{11}\text{C}/^{15}\text{O}$ ratio would vary from patient-to-patient and for different treatment sites.

3.2.2.3 Room Walls, Ceiling and Floor. Since the elemental composition of concrete varies depending on the source and nature of the portland cement, sand and aggregate used, the amount of induced radioactivity probably varies also. Various reactions are possible which can result in radioactive nuclei, *e.g.*, (γ, n) , $(n, 2n)$, thermal (n, γ) , (n, p) , etc. However, it is probable that thermal neutron capture is the dominant reaction. Experimental data are very sparse and most of the investigators have started their measurements 1 hour after shutdown. For a medical accelerator, where the normal operation is 1–3 minutes followed by immediate entry, these studies are not applicable. The dominant γ -ray emitting isotopes produced in a particular room were reported to be ^{28}Al ($T_{1/2} = 2.3$ min), ^{49}Ca ($T_{1/2} = 8.8$ min) and ^{24}Na ($T_{1/2} = 15$ h) (Tochilin and LaRiviere, 1978). These isotopes are all produced by thermal (n, γ) reactions but ^{28}Al can also be produced by ^{29}Si (γ, p) ^{28}Al and by ^{28}Si (n, p) ^{28}Al . The relative importance of these reactions is unknown at this time. For a busy radiotherapy accelerator, it is estimated a technologist would receive 10–15 mR/week. Most of this exposure would be from ^{28}Al . Calculations and measurements were for 15 and 18 MV photon-mode accelerators but, since the three dominant reactions are all due to thermal neutron capture, the same isotopes will probably be dominant for all accelerators in the therapy energy range. The magnitude of the activation will be a function of

the room size, the neutron yield of the accelerator, the distribution of on-off time, and, perhaps the chemical composition of the concrete.

3.3 Exposures During Installation

The process of installing a medical accelerator may cause special problems with respect to neutron leakage. Both the institution receiving the equipment and the company installation crew should take appropriate action to ensure that the personnel involved do not receive excess radiation exposure.

The neutron leakage around an accelerator is determined for the machine in its final configuration, *i.e.*, with all machine covers and shielding in place, with accelerator sections, bending magnets, and defining slits, etc. in their correctly aligned positions, and the room shielding and maze configuration designed for the minimal neutron leakage. During installation, many, if not all, of the above conditions may not be met. Machine covers and shielding are likely to be removed, the alignments may not be optimized, and higher neutron leakage than specified can occur, resulting in higher doses outside the accelerator room. In addition, workloads and occupancy factors are likely to be much different from those established for routine clinical work. This can result in higher neutron doses outside the accelerator room. These elevated doses will occur if the installation crew and physicist spend many hours making beam measurements and adjustments on the machine. In addition, the installation crew may spend time in areas not normally occupied during beam-on time, such as rooms for modulators, power and water supplies, etc.

These considerations lead to specific procedures that should be performed during installation.

1. Neutron surveys should be done in the control area and in the working space occupied by the installation crew at all stages of the installation, when a beam is being generated, to determine safe occupancy time. In addition, if there is evidence of unusual conditions, such as the accelerated electron beam striking slits or bending magnets, etc. that are normally not irradiated, special surveys should be made.
2. On entering the accelerator room after the beam has been on, a conventional survey should be taken to identify any hot spots of induced radioactivity and to determine general room background.
3. Most state and local regulatory bodies require that the local Radiation Safety Officer be responsible for these measurements

and for controlling the area. It is customary for the installation crew to have their own personnel dosimeters; however, the local radiation safety office should also issue personnel dosimeters and keep records of personnel exposure in the area.

4. If neutron dose rates are too high in occupied areas it may be possible to put up some temporary shielding. For example, sheets of plywood might be used to improve mazes temporarily (See Section 2.3.5).

4. Neutron Measurements

4.1 Introduction

In neutron monitoring there are several main tasks (LBL, 1973):

1. Measurement of fluence ($n \text{ cm}^{-2}$).
2. Measurement of the neutron spectrum as a function of energy⁴ ($n \text{ cm}^{-2} \text{ MeV}^{-1} \text{ s}^{-1}$).
3. Measurement of the total dose equivalent or dose equivalent rate (rem or rem s^{-1}).
4. Determination of the response of neutron detectors to other types of radiation when they are used in a mixed field.

It is sufficient for medical accelerators to divide the neutron energy spectrum into only two energy regions: thermal (0 to 0.5 eV) and fast ($>0.5 \text{ eV}$).

No single instrument or detector will perform all of the above tasks or cover both of the above energy regions. Therefore, detectors must be chosen which will perform the required tasks based on some knowledge of the energy regions involved.

In this report, we will not attempt an exhaustive discussion of neutron measurements, but will discuss methods which have been used to measure neutrons from medical electron accelerators. Methods using active detectors such as BF_3 proportional counters have been omitted since the photon fluence inside an accelerator room is too high for successful use. They can, however, be used to make measurements outside the room.

4.2 Activation Detectors

4.2.1 Unmoderated Activation Detectors

Activation detectors consist of a material which becomes radioactive when exposed to neutrons. The radioactivity may result from capture reactions, inelastic scattering leading to an isomeric state, (n,p), (n,α), or ($n,2n$) reactions, induced fission or spallation reactions. In all cases,

⁴There are several different formulations for expressing neutron spectra. See Sections 2.1 and 2.2 for examples.

the detector is exposed to the neutron field and then taken to a β - or γ -ray detector for counting. In some cases, chemical separation of the radioactive material must be performed before counting. The radioactivity of the activated detector can be measured by detection of the beta rays with end window or pancake Geiger counters, or measurement of the gamma rays by sodium iodide crystals or germanium detectors. The physics of activation detectors and the details of their use have been described by others (ICRU, 1977; Price, 1958). There are many advantages to the use of activation detectors;

1. Because individual detectors are inexpensive, many of them can be deployed at the same time. They are normally re-usable after allowing time for the radioactivity to decay.
2. They are relatively small and can give good geometric resolution for neutron fields with large variations over small distances.
3. Since they are passive, they are immune to electrical interference and most environmental effects, and can accurately average in time over pulsed or rapidly varying fields.

The disadvantages of activation detectors include:

1. Unwanted activation products may interfere with saturation activity determinations.
2. The time involved in analysis delays obtaining the results.
3. Sophisticated counting equipment may be needed, depending upon the activation products.

Those activation detectors which respond only to neutrons above thermal energies are usually referred to as threshold detectors.

4.2.1.1 Thermal Neutron Activation Detectors. Some useful thermal neutron activation detectors and their properties are listed in Table 9. There are many others which could be used, some of which will be discussed later. Indium and gold are among the most common detector materials used since they are readily available and have high neutron absorption (Barbier, 1969). To compensate for the finite sensitivity of these detectors to higher energy neutrons, covers or shields of material such as cadmium which would absorb the thermal neutrons were introduced, allowing the separation of the thermal neutrons from those neutrons above the effective energy cutoff of the cover. Indium is much more sensitive, but the relatively short half-life of the product ($T_{1/2} = 54$ min) requires that the counting equipment be relatively close to the point of measurement. The 2.7 day half-life of ^{198}Au , on the other hand, allows counting to be delayed for several days.

4.2.1.2 Threshold Activation Detectors. Threshold activation detectors may, in principle, respond to neutrons of any energy from thermal into very high energies. Most energy thresholds of these detectors, however, are hundreds of keV or higher. Resonance reactions may be

TABLE 9—*Useful thermal neutron detectors**

Nuclide or Element	Reaction	Half Life of Nuclide Produced	$\sigma_0 \times 10^{24}$ for Production cm^2
${}^3\text{He}$	(n,p) ${}^3\text{H}$	12.3 y	5327
${}^6\text{Li}$	(n,t) ${}^4\text{He}$	stable	945
${}^{10}\text{B}$	(n, α) ${}^7\text{Li}$	stable	3837
${}^{23}\text{Na}(\text{IS})^b$	(n, γ) ${}^{24}\text{Na}$	15.0 h	0.534
${}^{45}\text{Sc}(\text{IS})^b$	(n, γ) ${}^{46}\text{Sc}$	85 d	22.3
${}^{61}\text{V}$	(n, γ) ${}^{62}\text{V}$	3.8 min	4.9
${}^{55}\text{Mn}(\text{IS})^b$	(n, γ) ${}^{56}\text{Mn}$	2.58 h	13.3
${}^{59}\text{Co}(\text{IS})^b$	(n, γ) ${}^{60}\text{Co}$	5.24 y	36.6
${}^{63}\text{Cu}$	(n, γ) ${}^{64}\text{Cu}$	12.8 h	4.5
${}^{115}\text{In}$	(n, γ) ${}^{116m}\text{In}$	54 min	157
${}^{157}\text{Gd}$	(n, γ) ${}^{158}\text{Gd}$	stable	242000
${}^{197}\text{Au}(\text{IS})^b$	(n, γ) ${}^{198}\text{Au}$	2.70 d	98.8
${}^{236}\text{U}$	fission	many	577

* Adapted from ICRU (1969).

^b (IS) denotes natural monoisotopic element.

used for detection of the lower energy fast neutrons; however, many detectors may be required for adequate representation of the neutron spectrum in this range. For a discussion of resonance detectors, their use and analysis, the reader may refer to an International Atomic Energy Agency report on fluence measurements (IAEA, 1970).

Fast neutron fluence is commonly measured with threshold detectors which require neutrons above some minimum energy for activation. Most detectors have thresholds above 2 MeV. There is an energy region between that of the resonance detectors ($E < 0.01$ MeV) and that of threshold detectors, including fission detectors with a threshold of about 0.7 MeV, where it is difficult to make measurements.

ICRU Report 26 gives the cross sections of many commonly used reactions (ICRU, 1977). Table 10 gives the half-lives of the product nuclides and threshold energies of several useful threshold reactions. Some of the more useful threshold reactions are discussed further below.

The ${}^{32}\text{S}(\text{n},\text{p}){}^{32}\text{P}$ reaction has been used to measure fast neutron flux around accelerators. The technique has several useful characteristics (Patterson and Thomas, 1972):

1. Total integral fluence for a period up to one week can be obtained.
2. ${}^{32}\text{P}$ is a beta emitter and can be separated from the sulfur by careful ignition of the sample to volatilize the sulfur as sulfur dioxide, if greater sensitivity is required.
3. The cross section is well known and is given in Appendix E, ICRU Report 26 (ICRU, 1977).

TABLE 10—*Fast neutron threshold reactions**

Reaction	Half Life	Effective threshold MeV
$^{19}\text{F}(\text{n},2\text{n})^{14}\text{F}$	110 min	12.1
$^{24}\text{Mg}(\text{n},\text{p})^{24}\text{Na}$	15.0 h	7.0
$^{27}\text{Al}(\text{n},\text{p})^{27}\text{Mg}$	9.46 min	4.5
$^{27}\text{Al}(\text{n},\alpha)^{24}\text{Na}$	15.0 h	7.1
$^{31}\text{P}(\text{n},\text{p})^{31}\text{Si}$	2.62 h	2.4
$^{32}\text{S}(\text{n},\text{p})^{32}\text{P}$	14.3 d	2.7
$^{46}\text{Ti}(\text{n},\text{p})^{46}\text{Sc}$	83.8 d	3.8
$^{54}\text{Fe}(\text{n},\text{p})^{54}\text{Mn}$	313 d	3.3
$^{55}\text{Mn}(\text{n},2\text{n})^{54}\text{Mn}$	313 d	11.5
$^{56}\text{Fe}(\text{n},\text{p})^{56}\text{Mn}$	2.59 h	6.1
$^{60}\text{Ni}(\text{n},\text{p})^{60}\text{Co}, ^{60m}\text{Co}$	71.3 d, 9.15 h	2.8
$^{60}\text{Ni}(\text{n},2\text{n})^{57}\text{Ni}$	36.0 h	12.3
$^{63}\text{Cu}(\text{n},2\text{n})^{62}\text{Cu}$	9.76 min	12.4
$^{64}\text{Zn}(\text{n},\text{p})^{64}\text{Cu}$	12.7 h	4.0
$^{66}\text{Cu}(\text{n},2\text{n})^{64}\text{Cu}$	12.7 h	11.2
$^{103}\text{Rh}(\text{n},\text{n}')^{103m}\text{Rh}$	56.1 min	0.7
$^{107}\text{Ag}(\text{n},2\text{n})^{106}\text{Ag}$	24.1 min	10.7
$^{115}\text{In}(\text{n},\text{n}')^{115m}\text{In}$	4.50 h	1.4
$^{127}\text{I}(\text{n},2\text{n})^{126}\text{I}$	12.8 d	11.5
$^{232}\text{Th}(\text{n,f})$ fission products		1.4
$^{237}\text{Np}(\text{n,f})$ fission products		0.7
$^{238}\text{U}(\text{n,f})$ fission products		1.4

* Adapted from ICRU, 1977.

4. ^{32}P has a relatively long half-life of 14.3 days.

The $^{27}\text{Al}(\text{n},\alpha)^{24}\text{Na}$ reaction can be used to detect neutrons above 7.1 MeV. The useful characteristics include the following (Patterson and Thomas, 1973):

1. ^{24}Na has a convenient half-life of 15 hours.
2. ^{24}Na emits two energetic photons (1.37 and 2.75 MeV) making it possible to use thick samples.
3. Samples are readily available.
4. Cross section information is available in Appendix E of ICRU Report 26 (ICRU, 1977).

The $^{12}\text{C}(\text{n},2\text{n})^{11}\text{C}$ reaction can be used to monitor neutrons above about 20 MeV. The reaction has the following useful characteristics (Patterson and Thomas, 1973):

1. ^{11}C is a positron emitter with an E_{\max} of 0.98 MeV and a half-life of 20.34 minutes.
2. The carbon can be used in the form of plastic scintillators and activity is easily counted in the laboratory.
3. The cross section is well known.

Various types of fast neutron activation detectors have been used

to monitor neutrons in the vicinity of high-energy-electron accelerators (Laughlin, 1951; Ernst and Ovadia, 1956; Frost and Michel, 1964; Brenner, 1965; Adams and Paluch, 1965; Fox and McAllister, 1977; Stranden, 1977b; Deye and Young, 1977; Price *et al.*, 1978a; 1978b; Gur *et al.*, 1978a; 1978b; 1979; Nath *et al.*, 1979; McGinley and Sohrabi, 1979). Neutron fluence was measured near the target area of a 35 MeV betatron using a variety of threshold detectors; however, due to photon interference only aluminum and red phosphorus provided useful information (Brenner, 1965). Price, Holeman and Nath further developed the phosphorus in the form of a P_2O_5 detector and evaluated the photon interference (Price *et al.*, 1978b). The P_2O_5 detector has been used in the beam and adjacent to the beam of several medical accelerators (Price *et al.*, 1978a; McGinley and Sohrabi, 1979). The extent of photon interference, *i.e.*, responses produced by photons that may be mistaken for responses produced by neutrons, is difficult to assess when activation detectors are used to measure neutron fluences around medical accelerators. The interference may result from (γ, n) , $(\gamma, 2n)$, (γ, p) , and (γ, np) reactions producing activation of the detector or detection of the neutrons resulting from these reactions. When P_2O_5 is exposed to an accelerator field, it has been shown that all activation products have either short half-lives or are stable except for ^{31}Si and ^{32}P (Price *et al.*, 1978b). There are no direct photonuclear reactions which will produce these two products. The photon interference has been evaluated experimentally at a 25 MeV medical linear accelerator and found to be less than 4% (Price *et al.*, 1978b).

An important assumption in the determination of the fast neutron fluence is the shape of the neutron energy spectrum used in evaluating the activities produced in the phosphorus. Several different neutron sources have been considered, in order to estimate the uncertainty in determining the fast neutron fluence using the phosphorus technique when the neutron energy spectrum is unknown, with favorable results (Price *et al.*, 1978a; 1978b). If attempting to assess the total neutron dose equivalent relying only on phosphorus activation data, knowledge of the complete neutron spectrum is required. The error involved in determining the total neutron dose equivalent is highly dependent upon the accuracy of the assumed spectrum. Threshold detectors, with thresholds above 2 MeV, are difficult to use for measuring spectra from medical linear accelerators (Tochilin and LaRiviere, 1979). It can be shown that the major portion of a shielded neutron leakage spectrum, from a 15 MeV photon mode machine, falls below 2 MeV. Errors are introduced into the P_2O_5 technique as the neutron spectrum becomes moderated. However, in the beam, where there is a larger fraction of higher energy neutrons and for higher energy machines

(such as 25 MeV) using an assumed spectrum, the P_2O_5 technique has been demonstrated to give accurate results (Price *et al.*, 1978a; 1978b).

4.2.2 *Moderated Foil Detectors*

One method of measuring fast neutrons is to use hydrogenous material to moderate the neutrons and produce a thermal fluence inside the moderator. A detector which responds to the thermal neutrons is placed in the center of this moderator. The response, as a function of neutron energy, depends upon the shape and composition of the moderator. One such detector uses a thermal-neutron activation foil. Materials which have been used for the moderator include polyethylene, paraffin, and water. There have been many different foils used for activation detectors within these moderators, including indium and gold. Moderators may be designed to allow the measurement of fluence or dose equivalent, independently of neutron energy; in each case, however, the desired aim is only approximated. There is usually a decrease in sensitivity for both low and very high energies.

Among moderators that have been designed to achieve a constant response per unit fluence for neutrons of different energies, is a cylinder of polyethylene 15 cm in diameter and 15 cm high covered with cadmium (0.5–0.8 mm) which absorbs all incident thermal neutrons (Stephens and Smith, 1958; Smith, 1960). These moderators are relatively inexpensive to make and a large number of them can be distributed for simultaneous exposure. They are commercially available.

There are several examples of moderated detectors which have been designed to have a constant response per unit of dose equivalent of neutrons independent of energy. All commercial versions of these have been designed to incorporate active thermal neutron detectors, for example, BF_3 proportional counters. However, it is possible to use them also with passive thermal neutron detectors, such as activation foils (Rogers and VanDyk, 1981). This type of moderator-detector combination is often called a rem meter. Examples are the Andersson-Braun, and the Hankins rem meters (Andersson and Braun, 1963; Hankins, 1968b). The disadvantages of the rem meter types of moderator are that they are usually too complicated for the user to build and must be purchased. They are not very sensitive, so they require long exposure times, and they are too expensive to buy in the quantities needed for large number of measurements at one exposure.

All of these moderated foil detectors have some distinct advantages in use around medical accelerators. First, the pulsed nature of the

radiation causes no problem. Second, the detectors are insensitive to interference from associated radio frequency fields and to interference from photons except for possible photoneutron reactions in the detector materials, themselves. There have been several publications which have considered the photon response of moderated foil detectors due to photoneutron production in the detector (McCall *et al.*, 1976; Kushelevsky and Shani, 1976; Axton and Bardell, 1978). The disadvantages of moderated foil detectors include the relatively large size which limits the geometrical definition, their weight and bulk in moving them from site to site, and the decay time necessary before the foils can be used again.

4.2.3 Neutron Spectral Measurements

The Bonner multisphere spectrometer has been used for measurement of neutron spectra over a wide energy range (Bramblett *et al.*, 1960). It consists of the bare thermal neutron detector, a 0.03 inch thick cadmium cap, and six polyethylene moderating spheres (2, 3, 5, 8, 10 and 12 inch diameter). The spectrometer has been used by laboratories throughout the world to measure neutron spectra from heavily shielded reactors as well as from accelerators (Hankins and Pederson, 1963; Distenfeld *et al.*, 1967; Burrus, 1962; O'Brien *et al.*, 1965; McGuire, 1966; Stevenson, 1967; Overly *et al.*, 1967; Hankins, 1968a). A variety of different detectors has been used inside the polyethylene spheres, e.g., thermal activation foils, active detectors and thermoluminescent dosimeters (Distenfeld *et al.*, 1967; O'Brien *et al.*, 1965).

The neutron spectrum is unfolded by an iterative technique (O'Brien *et al.*, 1965; Watkins and Holeman, 1968; Sanna, 1976). The spectrometer has been thoroughly investigated using known test spectra, including comparison with results from the time-of-flight technique, and found to be a reliable low-resolution system (Stevenson, 1967; Awschalom, 1966; Overly *et al.*, 1967; Hankins, 1968a; Weinstein *et al.*, 1969; Watkins and Holeman, 1968; Holeman *et al.*, 1977).

Spectral measurements in a medical linac beam were attempted but failed because of interference from (γ, n) reactions in the cadmium, unequal photonuclear cross sections of the ^6Li and ^7Li TLD's used, and possible (γ, n) reactions in the polyethylene spheres. For spheres located outside the linac photon beam, there was no indication of such interference (Holeman *et al.*, 1977). Other investigators have studied the in-beam interference with conflicting results (Axton and Bardell,

1972; 1978; 1979; Kushelevsky and Shani, 1976;). See Table 11 for a comparison of various in-and near-beam measurements of neutron dose equivalent rates.

4.2.4 Data Collection

For every irradiation of activation detectors, one should record the following (IAEA, 1970):

1. The location of each detector.
2. The irradiation interval, specifying the starting and finishing times of this interval.
3. The machine parameters.

In cases where they are variable, the following additional data may be useful:

1. Experimental layout.
2. Machine configuration.

If the data are to be reanalyzed in the future for some reason, it has been recommended that the following data be preserved (IAEA, 1965; IAEA, 1970):

1. *Detector data*: mass, dimensions, chemical and isotopic composition.
2. *Positioning data*: description or drawing of irradiation geometry, type and dimensions of detector holders, covers and shields.
3. *Irradiation data*: duration of irradiation, time from the end of the irradiation until counting, counting time, variations in exposure, if any.
4. *Counting data*: equipment, counting efficiency, calibration methods, traceability of calibration standards used, activity at the

TABLE 11—Comparison of various methods for neutron measurements in and near the treatment beam of a 25 MeV linear accelerator

Method	Neutron Dose Equivalent Rate (rem/min)			Reference
	At Isocenter	at 50 cm to the side	at 1 m to the side	
P ₂ O ₅	3.04	1.52	0.8	Price <i>et al.</i> , 1978a; 1978b
Multisphere	—	1.04	0.82	Nath <i>et al.</i> , 1979
Moderator-Au*	2.25	1.97	—	McCall, 1977
Track Etch	—	1.40	—	Wilenzick <i>et al.</i> , 1973

Note: Photon beam dose rate was 400 rad/min at a distance of 105 cm.

* Moderators and gold activation foils interpreted with the aid of Monte Carlo calculation.

time of counting, the calculated saturation activity at the time of counting, the calculated saturation activity per gram of target material (specifying the decay constant used in the calculation), measured or estimated amounts of impurity-induced activities or interference.

5. *Correction data:* corrections applied, if any.
6. *Final data:* value of cadmium ratio, if determined, values of fluence (specifying the integral cross section values used and appropriate references), error values associated with the various measured and calculated quantities, dose conversion factors used to convert from fluence to absorbed dose or dose equivalent, and quality factors used or assumed.

4.3 Etched Track Detectors

4.3.1 Introduction

The etched track detectors are based upon the fact that microscopic radiation damage tracks are formed in solids which have been irradiated with heavy particles. If the solids are then etched, the tracks are etched faster than the undamaged portion and become visible under a microscope (Young, 1958). Tracks can be made visible in a variety of dielectric materials including minerals (mica), natural and artificial inorganic glasses, and, especially, organic polymers which have proven to be considerably more sensitive than the inorganic detectors.

In general, two types of etched track detectors have been used. The first consists of combinations of suitable fissile elements and fission-fragment detectors such as polycarbonate foils. This type of detector represents one of the most sensitive, accurate and simple methods for integrating fast-neutron doses. It has been used around medical accelerators as ordinary soda-lime-silica glass in which 1% of uranium in the form of uranium oxide has been mixed (Löfgren and Spring, 1970), and Lexan® (polycarbonate plastic) sandwiched between depleted uranium foils (Kehrer and Robinson, 1972; Wilenzick *et al.*, 1973). Figure 37 shows an example of the track detectors used by Wilenzick *et al.*

The second type depends upon the direct interaction of fast neutrons with a sensitive polymer foil, and is a less expensive and simpler system than the previous one. This system has been used with polycarbonate foils (Sohrabi and Morgan, 1979).

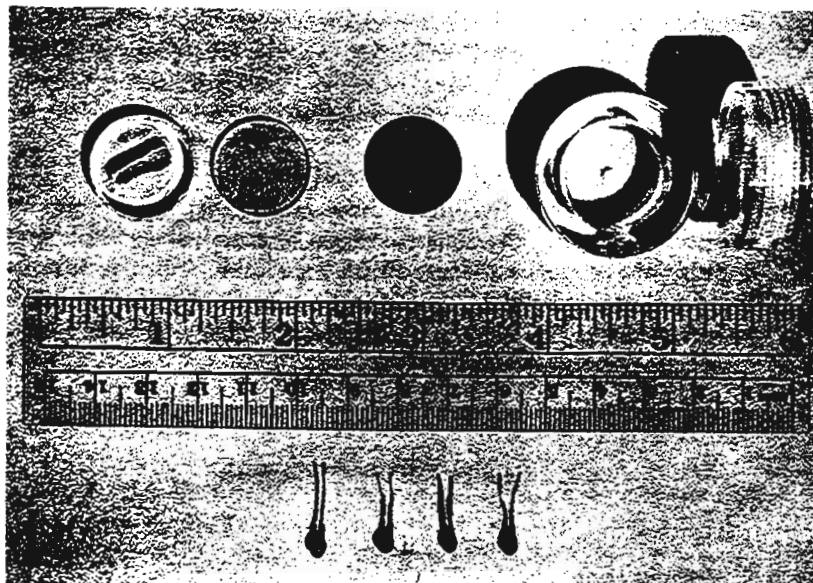


Fig. 37. Photograph of four silicon diode dosimeters (at bottom) and track detector components consisting of Lucite® case, uranium foil, Lexan® disc and lucite retainer (Wilenzick *et al.*, 1973).

4.3.2 Fission-Fragment Track-Etching Dosimeters

An extensive discussion and review of these dosimeters has been published (Becker, 1973). The use of these systems can be divided into three parts: exposure, etching and counting. Table 12 contains some etching procedures that have been suggested for fission-fragment detectors (from Becker, 1973). Both inorganic and organic materials have been used and a wide variety of etching conditions have been reported. The data are chosen somewhat arbitrarily and optimum etching conditions, if they exist, may differ from those indicated. Each system must, therefore, be evaluated separately. For example, Wilenzick *et al.* etched their Lexan dosimeters in 28% KOH for 60 minutes at 60°C using ultrasonic agitation, which is different from the technique recommended in Table 12 (Wilenzick *et al.*, 1973). The counting method dictates the etching method used. If a microscope is used, then the tracks must be clearly visible using an appropriate magnification. Table 13 lists some methods for automatic track counting with the most elegant method being based on the counting of electrical discharges occurring through the etched perforations in the foils (Cross, 1970; Cross and Tommasino, 1970). However, for most applications

TABLE 12—Recommended etching conditions for fission-fragment track etching in some dielectrics

Material	Etchant Composition, etching time, and temperature (°C)
A. Inorganics	
Mica (lepidolite)	15% HF, 20 s, 50° 48% HF, 3–70 s, 23°
Mica (muscovite)	{ 20% HF, 2 h, 23° 20% HF, 12 min, 52° 15% HF, 20 min, 50° 48% HF, 10–40 min, 23°
Mica (phlogopite)	{ 20% HF, 5 min, 23° 15% HF, 1 min, 50° 48% HF, 1–5 min, 23°
Quartz (SiO_2)	48% HF, 24 h, 23°
Borate glass	H_2O , 1 min, 23°
Obsidian (vulcanic glass)	48% HF, 30 s, 23°
Phosphate glass	48% HF, 5–20 min, 23°
Silica glass (fused quartz)	48% HF, 1 min, 23°
Soda-lime glass (microscope slide, window glass)	5% HF, 2 min, 23°
B. Organics	
Cellulose acetate (Kodacel®, Triafol T®)	{ 28% KOH, 30 min, 60° NaCO_3 , 30 min, 100°
Cellulose acetate butyrate (Triafol B®)	{ 6.25 N NaOH, 12 min, 70° (KMnO_4 , NaClO)
Cellulose nitrate (DaiCell®, Nixon-Baldwin)	{ 6.25 N NaOH, 2 min, 70° 6.25 N NaOH, 4 min, 55° 6.25 N NaOH, 2–4 h, 23° 28% KOH, 30 min, 23° (KMnO_4 , NaClO , $\text{K}_2\text{Cr}_2\text{O}_7$) 28% KOH, 100 min, 60°
Cellulose propionate (Cellidor®)	{ 6.25 N NaOH + 15% NaClO (2:1 to 1:3), 40°
Cellulose triacetate (Kodacel TA401®, Triafol NT®)	{ 28% KOH, 60 min, 60° NaOH , 1 h, 40°
Cormophenol (Ambrothene®, Phenoplaste®)	
Ionomeric polyethylene (Surlyn®)	{ 10g $\text{K}_2\text{Cr}_2\text{O}_7$ + 35 cm³ 30% H_2SO_4 , 1 h, 50° KMnO_4 (25% aq), 1.5 h, 100°
Polyimide (H-film)	{ 6.25 N NaOH, 20 min, 50°, 33 cm³ 30% H_2SO_4 + $\text{K}_2\text{Cr}_2\text{O}_7$ (10g), 2 h, 85°
Polycarbonate (Lexan®, Makrofol®, Kimfol®, Merlin®)	{ (6.25 N NaOH), 2 h, 23° 2.5 N NaOH + 4% Benax, 20 min, 70°
Polyethylene	{ 10g $\text{K}_2\text{Cr}_2\text{O}_7$ + 35 cm³ 30% H_2SO_4 , 30 min, 85° 10g $\text{K}_2\text{Cr}_2\text{O}_7$ + 5 cm³ 30% H_2SO_4 + 29 g H_2O , 90° { 6.25 N NaOH, 10 min, 70° KMnO_4 (25%), 1 h, 55°
Polyethylene terephthalate (Mylar®, Chronar®, Melinex®)	

TABLE 12—Continued

Material	Etchant Composition, etching time, and temperature (°C)
Polymethylmethacrylate (Plexiglas®, Lucite®)	KMnO ₄ (sat), 50 min, 85°
Polyoxymethylene (Delrin®)	5% KMnO ₄ , 10 h, 60°
Polyphenoxide	KMnO ₄ , (25% aq), 4 min, 100°
Polystyrene	$\left\{ \begin{array}{l} \text{KMnO}_4 \text{ (sat)}, 2.5 \text{ h}, 85^\circ \\ 10 \text{ g } \text{K}_2\text{Cr}_2\text{O}_7 + 35 \text{ cm}^3, 30\% \text{ H}_2\text{SO}_4, 3 \text{ h}, 85^\circ \end{array} \right.$
Polyvinylacetochloride	KMnO ₄ (25% aq), 30 min, 100°
Polyvinylchloride	$\left\{ \begin{array}{l} \text{KMnO}_4 \text{ (sat)}, 2.5 \text{ h}, 85^\circ \\ \text{KMnO}_4 \text{ (25% aq)}, 2 \text{ h}, 55^\circ \end{array} \right.$
Polyvinyl toluene	KMnO ₄ (sat aq), 30 min, 100°
Silicone-polycarbonate copolymer	6.25 NaOH, 20 min, 50°
Silicone-cellulose copolymer	8N NaOH + Benax, 3 h, 85°

TABLE 13—Some methods for automatic track or etch fit counting in solids

Microscopic techniques	Macroscopic techniques	
	For low track densities	For high track densities
1. Electrooptical scanning devices	1. Dye, gas, or reactive chemical penetration through perforations in membranes	1. Light scattering at etched surface
2. Microdensitometry	2. Light penetration through one-side etched, other-side aluminized thin foils	2. UV penetration through perforated foils
3. Measurement of scattered light in dark-field microscope	3. Electric discharges (sparks) through perforations <ul style="list-style-type: none"> a. Pulse-counting type b. Integral intensity 	3. Light absorption thin dyed foils
	4. Particle or electron penetration through perforated foils	4. Dielectric constant or resistance across perforated foil
		5. Fraunhofer diffraction of laser light

visual counting with a microscope is quite suitable. A precision reticle and stage micrometer will enable an accurate measurement of track number per unit area.

It has been observed that the track density for the neutron energy of interest can be equated to the neutron fluence by a constant, weighted by the fission cross section of the fissile material (Becker, 1965; 1966). This is because the detection efficiency of organic detectors, as well as the range and energy distribution of the fission products in the common fissile materials, are relatively constant. For fission-foil thicknesses that exceed the maximum range of the fission fragments (about 10 mg/cm^2) and that do not significantly depress the neutron flux by absorption, the sensitivity of the dosimeter is always approximately 1.16×10^{-5} tracks/neutron-barn) (Prêtre *et al.*, 1968).

The detectors can be calibrated against a neutron source, e.g., Am-Be (Löfgren and Spring, 1970) or ^{252}Cf (Wilenzick *et al.*, 1973). The fluence response curve for the uranium-Lexan® dosimeter is shown in Figure 38. For these measurements, a conversion from fluence to dose was made using the ^{252}Cf conversion factor of $3.0 \pm 0.1 \times 10^{-9}$ rad $\text{n}^{-1} \text{cm}^2$ (Stone *et al.*, 1970). Between 4 and 300 rad, the sensitivity of track detectors was found to be approximately linear with dose, with 3.46×10^{-6} tracks per incident neutron of ^{252}Cf . This value is consistent with the sensitivity given above (Prêtre *et al.*, 1968) using an effective cross-section of ^{252}Cf above the 1.5 MeV (n,f) threshold of 0.54 barns and assuming that 55.3% of the ^{252}Cf neutrons have energies greater than that value (Prince, 1969).

4.3.2.1 Photofission Corrections. The registration of tracks from photofission reactions in uranium is a serious problem that is encountered with the use of track detectors in intense photon fields (Kehrer and Robinson, 1972). The cross-section for photofission, which competes with neutron-induced fission at photon energies above approximately 7 MeV, has a maximum value of 175 mb at 14.3 MeV (Caldwell *et al.*, 1980). Since the average cross section for the ^{238}U (n,f) reaction above 1.5 MeV is 540 mb, it is evident that the (γ ,f) process is significant. Consequently, neutron measurements in the primary photon beam cannot be made with track detectors, and in order to use track detectors outside of the primary beam, it is necessary to correct for photofission tracks produced by accelerator leakage photons.

4.3.3 Direct Interaction Track-etch Dosimeters

Two types of direct interaction track-etch dosimeters have been used. Sohrabi and Morgan (1978) have studied the basic characteristics

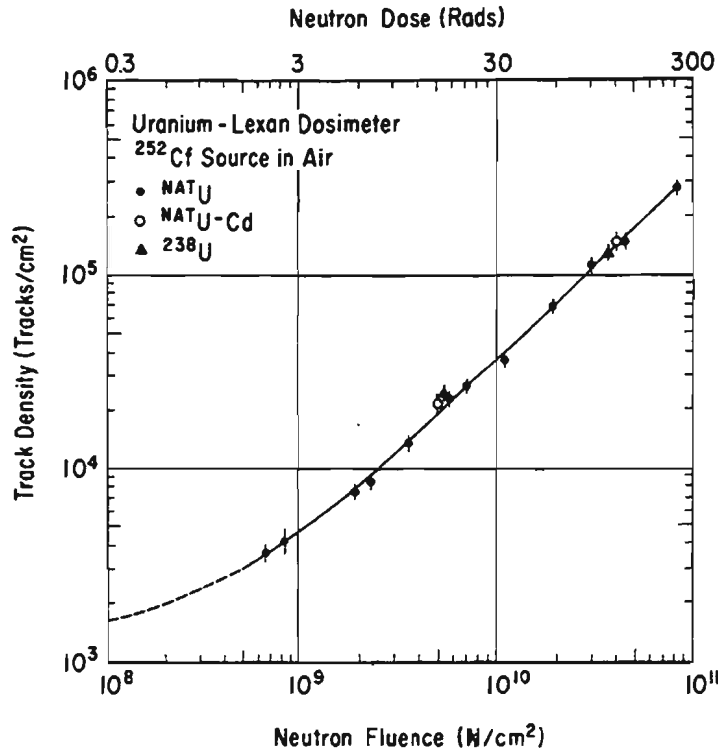


Fig. 38. Calibration curve for uranium-Lexan® track dosimeters, as measured with a ^{252}Cf neutron source in air. Experimental points (\pm one standard error) are shown for foils of natural uranium, cadmium-covered natural uranium, and highly depleted uranium ^{238}U . The solid curve is a least-squares fit to the data points. The dashed segment of the curve is an extrapolation of the computer fit into the region of low track densities where experimental data could not be obtained reliably because of the low neutron fluence and the track density background.

of polycarbonate for neutron dosimetry using the electrochemical etching (ECE) method (Tommasino, 1970; Tommasino and Armellini, 1973). Polycarbonate is composed of hydrogen, carbon and oxygen atoms and under neutron bombardment the fast neutrons produce charged recoil and (n,α) particle tracks by interacting with the atomic constituents of the polymer. The carbon and oxygen recoils and alpha particles leave damaged regions which become observable after suitable etching. However, there is no evidence that protons register in polycarbonate and it is generally considered insensitive to protons. In the ECE method, the foils are held in the etchant and an AC high voltage is applied across the chamber through two stainless-steel electrodes.

Figure 39 shows a microphotograph of fast-neutron recoil particle tracks in a $250 \mu\text{m}$ thick polycarbonate foil electrochemically etched in 28% KOH solution at 25°C applying 800 V for a field strength of 32 kV cm^{-1} at 2 kHz for 4 hours.

The dosimeters have a response approximately proportional to neutron dose-equivalent from 1 MeV up to 20 MeV. The track density can, therefore, be converted to neutron dose equivalent by a conversion factor of 105 tracks per cm^2 per rem. There is no post-irradiation fading, but care must be taken in selecting a polymer that has a negligible or reproducible low-background track density, since defects such as cracks or scratches will be amplified by the ECE method. In general, the foils should be masked on both sides, in which case a background track density of approximately 1 track per cm^2 is found.

In these polymers, the sensitivity to photon radiation will be enhanced if the photon dose is high enough to simulate the threshold dose delivered to the polymer by a charged particle along its trajectory. The critical dose has been calculated to be about 7.5×10^6 rad in polycarbonate (Katz and Kobetich, 1968). When the photon dose approaches this value, the surface or bulk etching rate will be enhanced. Photonuclear reactions have also been investigated but, due

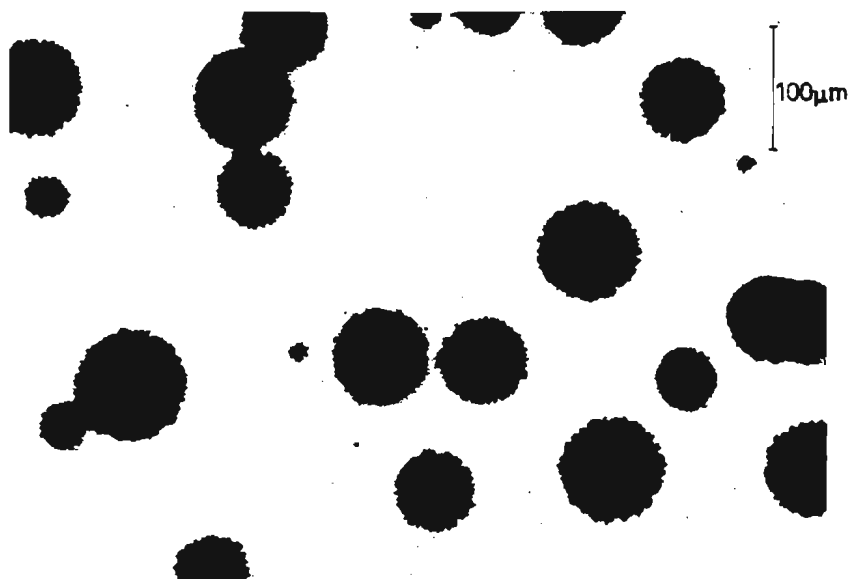


Fig. 39. Micrograph of fast-neutron induced recoil particle tracks in $250 \mu\text{m}$ thick polycarbonate foils electrochemically etched in 28% KOH solution at 25°C applying 800 V at 2 kHz for 4 h.

to the very small mass in the polymer and the threshold energies and cross-sections involved, contributions from photonuclear reactions are considered insignificant.

A new carbonate plastic known as CR-39 has been developed which, when used as a nuclear track detector and properly treated, is capable of detecting recoil protons. Using the ECE parameters employed for the polycarbonate foils described above, the shape of the etched tracks in CR-39 differs slightly from that for the polycarbonate foils. By pre-etching in 6N KOH for five hours at 60°C, the neutron-induced track density can be increased by a factor of 50 to 100 over that obtained with no pre-etching. This should allow the CR-39 plastic to detect fast-neutron doses as low as 10 mrem (Sohrabi and Morgan, 1979). The pre-etching also significantly improves the quality of the background. The threshold of this detector is approximately 100 keV, so that the energy threshold is reduced by a factor of 10 or more compared with that of the more conventional detectors.

4.4 Diodes

Neutron-induced nuclear reactions, elastic scattering of heavy charged particles, and, to a much smaller degree, high energy electrons can produce measurable changes in the electrical properties of various semiconductors. The most common type of radiation damage is the displacement of lattice atoms. The vacancies created and the displaced atoms disrupt the conductivity of excess charge carriers in the base of the junction. Thus, a measure of the change in conductance can be correlated with the neutron damage in the crystal. A means of monitoring the damage is to measure the increase in forward voltage at a constant current. The detectors are small p-i-n silicon diodes enclosed in silicon rubber and coatings of epoxy resin (see Figure 37).

The change in forward voltage of a diode can be measured by applying a constant current of 25 mA ($\pm 0.1\%$) before and after exposure to neutrons and observing the potential drop with a 4-figure digital voltmeter. A low current level and a rapid read-out procedure must be utilized to minimize heating of the diode while still providing acceptable sensitivity to small voltage differences. The precision of the read-out system is better than $\pm 3\%$, based upon the reproducibility of multiple readings. Because of fading effects from ambient annealing, it is necessary to maintain a fixed post-exposure read-out time. For a given dose, the minimum spread in diode response occurs at 48 h after the end of exposure; consequently, that time should be used for all

measurements. The pre-exposure voltage dependence of the diode response can be eliminated by normalizing the neutron induced voltage change to the pre-exposure voltage.

The voltage sensitivity of the diodes as a function of neutron dose is shown in Figure 40 (Wilenzick *et al.*, 1973). The calibration curve for the track detectors is also shown for comparison. For a monitoring current of 25 mA, the diode sensitivity to primary fission neutrons is 1.28 mV per tissue rad over the range of 3-100 rad. A nonlinear calibration curve extends the range to more than 10^3 rad.

The photon and electron responses of silicon-diode neutron detectors have been investigated (McCall *et al.*, 1978a; Almond, 1975). The main mechanism for producing a response in the diode has been shown

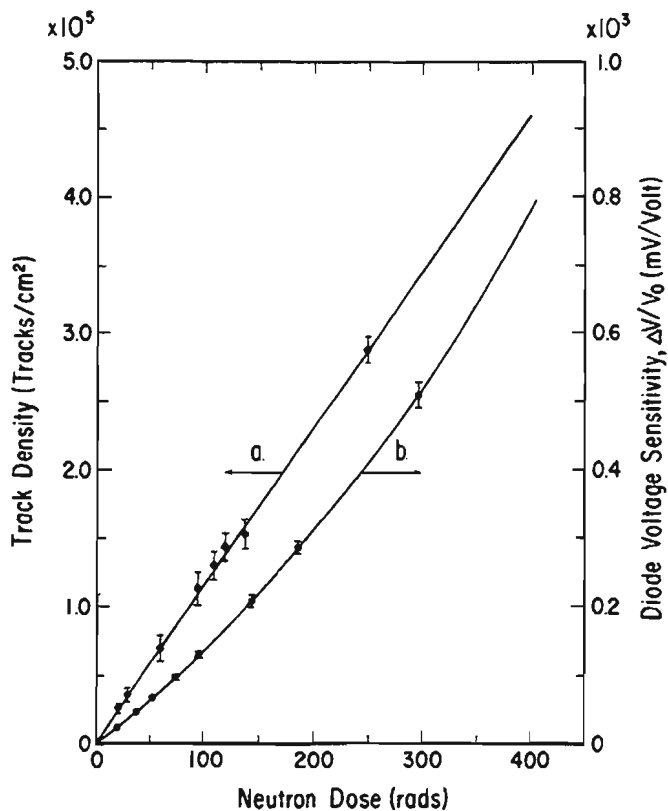


Fig. 40. Comparison of calibration curves for track detectors (a) and silicon (b), as measured with a ^{252}Cf neutron source in air. The diode voltage sensitivity, $\Delta V/V_0$, is the change in diode forward voltage before and after irradiation, divided by the pre-irradiation voltage (Wilenzick *et al.*, 1973).

to be the displacement of silicon atoms by scattering of electrons, although in very high photon fluxes, the photoneutron reaction may also be detectable. The diode systems are, therefore, not suitable for measurement of neutrons directly in the photon beam but do give good agreement with other methods outside the main photon beam.

4.5 Ionization Detectors

4.5.1 *Introduction*

Ionization detectors include ionization chambers, proportional counters and Geiger-Müller counters. In essence, these detectors consist of a gas between a pair of electrodes. Radiation causes ionization in the gas and the resulting charge is collected by the electrodes under the influence of an applied electric field. When the applied voltage to the electrodes is low, the ionization is merely collected by the electrodes and the detector is called an ionization chamber. When the voltage is increased, the electrons from the original ionization become energetic enough to produce further secondary ionization giving rise to gas amplification. If the size of the resulting electronic pulse is proportional to the original ionization, the detector is called a proportional counter. However, if the voltage is high enough that an avalanche of charge is generated by the original ionization—regardless of its size—the detector is called a Geiger-Müller counter. These three modes of operation impart different detection characteristics to these detectors. For instance, the Geiger-Müller counter is much more rugged, requires simpler electronics and can detect much lower levels of radiation than the ionization chamber; but it is not a dose-measuring device. In practice, the different requirements in radiation measurements have led to completely different designs of these detectors. A more detailed description of gaseous devices for biomedical applications is given in ICRU Report 26 (ICRU, 1977).

4.5.2 *Ionization Chambers*

Ionization chambers containing air and air-equivalent walls or tissue-equivalent gas and walls are routinely used for the quantification of radiation levels in connection with radiobiological applications. When the radiation contains both photons and neutrons, it is a common practice to use two ionization chambers; ideally, a photon-

detecting device which is insensitive to neutrons and a neutron-detecting device which is insensitive to photons. However, such devices do not exist and one must resort to detectors which respond predominantly to one or the other radiation.

The use of an ionization chamber outside the shield of a medical linear accelerator has been reported (Schulz, 1978). The ionization chamber was made with thin aluminum walls and was filled with either argon or propane to obtain a predominantly photon or photon plus neutron response, respectively. The results of the measurement were used to estimate the photon and neutron absorbed dose rates and a calculated quality factor was used to obtain the neutron dose equivalent rate. The results obtained with the argon/propane ionization chamber have been shown to be in reasonable agreement with those of several other methods (Nath *et al.*, 1979). The results of this comparison are given in Table 14. It would be very difficult to detect neutrons with the argon/propane ionization chamber inside the treatment room because of the high photon field (Schulz, 1978).

Conventional air-filled ionization chamber survey meters are often used to measure the photon dose rate outside of the shielded accelerator room, especially at the door. In this use, it is assumed (often unstated) that the ionization chamber measures only photons and that the response to neutrons is negligible. This is probably true since the n/γ ratio outside the shield is usually small and the neutrons are predominantly of low energy. In addition, it is a conservative assumption since it can only cause an over-estimate of the photon dose rate.

TABLE 14—Comparison of various methods for neutron measurements far from the treatment beam of a 25 MeV linear accelerator

Method	Q	Dose Equivalent Rate mrem/h	Reference
<i>Outside the treatment room—doors closed</i>			
Multisphere Spectrometer	7.0	0.33	Nath <i>et al.</i> , 1979
Nemo* (PuBe Calibration)	—	0.51	Nath <i>et al.</i> , 1979
Nemo* (Cf Calibration)	—	0.62	Nath <i>et al.</i> , 1979
Ionization Chamber	7.1 ^b	0.35 ^c	Schulz, 1978
<i>Outside treatment room—doors open</i>			
Moderated Au Foil	—	150	McCall, 1977
Ionization Chamber	7.1 ^b	62	Schulz, 1978
<i>In the maze</i>			
Multisphere Spectrometer	5.4	1560	Nath <i>et al.</i> , 1979
Moderated Au Foil		1488	McCall, 1977

Note: The photon dose rate was 400 rad/min at a distance of 105 cm.

* A commercial 10 inch sphere rem meter.

^b McCall, 1977.

^c Corrected by a factor of 2.64 for difference in location of detectors.

It should be noted that the photons outside the door of the accelerator room are mostly neutron capture gamma rays. These gamma rays will not only occur during the approximately 2 microsecond accelerator pulse but will be spread out in time for hundreds of microseconds as the thermal neutrons diffuse before capture (Dinter and Tesch, 1976). Therefore, measurement difficulties due to the pulsed nature of the radiation are not as severe outside as inside the room.

4.5.3 Proportional Counters

Proportional counters, with filling gases such as boron trifluoride or ^3He , are often used inside moderators to detect the thermalized neutrons. These fillings are used because the capture of thermal neutrons by ^{10}B or ^3He gives rise to energetic charged particles which result in large electronic signals and provide good discrimination against the relatively small signals produced by photons.

Special spherical proportional counters having walls of tissue-equivalent plastic and filled with a counting gas at low pressure have been developed (Rossi and Rosenzweig, 1955a; 1955b). These counters can process the pulse-height distribution of their signals to yield the absorbed dose as a function of linear energy transfer (LET). It should be noted that in a pulsed field, the proportional counter may register several particles at once, especially if they are electrons. Since quality factors are based on LET (ICRP, 1962), these counters can provide the average quality factor for a radiation field without the knowledge of its energy spectrum. LET spectrometers have been used to monitor stray radiation around proton accelerators (Phillips *et al.*, 1965). The only known use of LET spectrometers around an electron accelerator involved a version built into a survey meter (McCaslin *et al.*, 1977). Compact LET spectrometers have now been developed which use microelectronic data processing to facilitate their application in routine radiation monitoring applications (Quam *et al.*, 1982; Erkkila *et al.*, 1982). There is no known use of tissue equivalent proportional counters inside an accelerator room.

4.5.4 Geiger-Müller Counters

G-M counters are inherently slow with a recovery time of 50 to 300 μs . If they are used to count direct radiation from the accelerator, they can never record more than one count per machine pulse. Thus, in the

4.5 IONIZATION DETECTORS / 93

monitoring of low radiation levels (less than one count per pulse), the effect of dead time must be taken into account. G-M counters could possibly cause the existence of a hazardous situation to go unnoticed if radiation levels were high enough that the counter was only recording accelerator repetition rate, when it should be indicating much higher levels. No use of G-M counters to measure neutrons from electron accelerators is known.

5. Literature Review

In this section a limited selection of neutron measurements around medical electron accelerators is presented. There are so many possible variables (beam size, plane of measurement, distance from the beam, room size, etc.) that it is difficult to present the data in comparable categories. For this reason, the selected data have been limited to measurements in the patient plane, out of the photon beam and no more than 100 cm from the isocenter. The data are presented in Tables 15 and 16 for betatrons and linear accelerators, respectively. The column labelled "method" refers to the method of measurement used, and the code letters are identified in each table. Measurements reported in the literature that are not listed in Tables 15 and 16 are omitted only because there was insufficient information to fit them into the tables, and no reflection on the quality of those measurements is intended.

TABLE 15—*Neutron measurements around betatrons*

Entry	Manufacturer ^a and Mode	Photon Mode Energy	Distance from Isocenter in Patient Plane	Neutron Leakage per Photon Rad at the Isocenter			Method ^b	References	
				Mev	cm	Dose Equivalent rem	Absorbed Dose rad	Fluence n/cm ²	
1	A C	23	30	—	—	—	3.0×10^4	A	Laughlin, 1951
2	Non-commercial	45	50	—	—	—	3.1×10^2	A	Hsieh, 1956
3	BBC	35	20	1×10^{-4}	—	—	—	A	Axton and Bardell, 1972
4	Siemens	19	30	—	—	—	5.5×10^4	C	Wilenzick <i>et al.</i> , 1973
5	A C	25	10	—	—	4.05×10^{-4}	1.01×10^6	A	McGinley <i>et al.</i> , 1976
6	BBC	45	10	—	—	3.95×10^{-4}	9.95×10^4	A	McGinley <i>et al.</i> , 1976
7	Shimadzu	23	15	—	—	2.9×10^{-4}	—	D	Fox and McAllister, 1977
8	A C	25	25	6.0×10^{-4}	—	—	—	F	Sohrabi and Morgan, 1979
9	BBC	45	25	6.4×10^{-5}	—	—	—	F	Sohrabi and Morgan, 1979
10	A C	25	12	—	—	—	4.2×10^4	D	McGinley and Sohrabi, 1979
11	BBC	45	12	—	—	—	3.96×10^4	D	McGinley and Sohrabi, 1979
12	A C	25	15	—	—	2.2×10^{-3}	—	C	Oliver, 1976
13	BBC	32	15	—	—	$< 10^{-6}$	—	C	Oliver, 1976
14	BBC	45	15	—	—	3.5×10^{-4}	—	C	Oliver, 1976
15	Siemens	42	15	—	—	2.1×10^{-3}	—	C	Oliver, 1976
16	A C	23	100	1.6×10^{-3}	—	—	—	B	Rogers and VanDyk, 1981
17	A C	25	50	1.5×10^{-3}	—	—	5.8×10^4	A	McCall, 1982

^a Code for manufacturer: A C-Allis Chalmers; BBC-Brown-Boveri; CGR-Compagnie Générale de Radiologie.^b A. Moderated activation foils; B. Activation foils in remmeter moderator; C. Silicon diodes; D. Bare activation foils; E. Bonner spectrometer; F. Moderated TLD's.

TABLE 16—Neutron measurements around linear accelerators

Entry	Manufacturer ^a and Model	Photon Mode Energy	Distance from Isocenter in Patient Plane	Neutron Leakage per Photon Rad at the Isocenter			Method ^b	References	
				MeV	cm	Dose Equivalent REM	Absorbed Dose RAD	Fluence n/cm ²	
1	MEL	16	20			2.5×10^{-5}	—	—	Axton and Bardell, 1972
2	CGR-Sagittaire	25	30			—	—	1.9×10^5	Wilenzick <i>et al.</i> , 1973
3	Philips/MEL SL75-20	16	20			2.5×10^{-4}	—	—	Atherton, 1975
4	Varian Clinac 18	10	10			—	6.03×10^{-5}	1.52×10^4	McGinley <i>et al.</i> , 1976
5	CGR-Sagittaire	25	100			3.3×10^{-3}	3.3×10^{-4}	—	Merbach, 1975
6	Varian Clinac 18	10	100			1×10^{-4}	1×10^{-5}	3.2×10^3	Deye and Young, 1977
7	CGR-Sagittaire	25	50			2.09×10^{-3}	2.48×10^{-4}	—	Holeman <i>et al.</i> , 1977
8	CGR-Saturne	18	100			8.7×10^{-4}	—	—	Drouet <i>et al.</i> , 1977
9	Phillips SL/75-20	18	10			—	1.4×10^{-4}	4.1×10^4	Gur <i>et al.</i> , 1978b
10	Phillips SL/75-10	8	60			3.8×10^{-5}	—	—	Nemec and Roth, 1978
11	Varian Clinac 18	10	30			—	—	3.8×10^3	McGinley and Sohrabi, 1979
12	CGR-Sagittaire	25	50			3.8×10^{-3}	—	—	Nath <i>et al.</i> , 1979
13	Varian Clinac 20	15	50			2.3×10^{-4}	—	—	Tochilin and LaRiviere, 1979
14	Varian Clinac 20	19	50			6.3×10^{-4}	—	—	Tochilin and LaRiviere, 1979
15	CGR-Sagittaire	25	100			2.04×10^{-3}	—	—	Anderson and Hwang, 1980

16	AECL-Therac 20	18	100	—	1.5×10^{-4}	—	C	Grant, 1978
17	Varian Clinac 18	10	15	—	6.3×10^{-5}	—	C	Oliver, 1976
18	Toshiba LMR-15	14	15	—	9.8×10^{-5}	—	C	Oliver, 1976
19	Siemens-Mevatron XX	15	15	—	1.2×10^{-4}	—	C	Oliver, 1976
20	Varian Clinac 35	25	15	—	5.9×10^{-4}	—	C	Oliver, 1976
21	AECL/CGR Therac 20	18	100	2.1×10^{-3}	—	—	B	Rogers and VanDyk, 1981
22	Varian Clinac 18	10	100	4×10^{-5}	—	—	B	Rogers and VanDyk, 1981
23	CGR-Sagittaire	25	100	4.1×10^{-3}	—	—	B	Rogers and VanDyk, 1981
24	Varian Clinac 35	25	100	3.1×10^{-3}	—	—	B	Rogers and VanDyk, 1981
25	Siemens-Mevatron XX	20.4	50	2.6×10^{-3}	—	—	B	Rogers and VanDyk, 1981
26	Varian Clinac 2500	24	50	9.9×10^{-4}	—	6.5×10^4	A	McCall, 1982
27	Siemens Mevatron XX	15	50	2.5×10^{-4}	—	1.9×10^4	A	McCall, 1982
28	Varian Clinac 2500	24	50	6.3×10^{-4}	—	5.0×10^4	A	La Riviere, 1982b
29	AECL Saturne	18	50	2.5×10^{-3}	—	1.4×10^5	A	McCall, 1982
30	AECL Saturne	18	50	2.0×10^{-3}	—	1.2×10^5	A	McCall, 1982
31	AECL Saturne	18	50	0.8×10^{-3}	—	—	D	Bading <i>et al.</i> , 1982

^a Code for manufacturer: MEL-M.E.L. Equipment Co. (Division of Phillips); CGR-Compagnie Générale de Radiologie; AECL-Atomic Energy of Canada Limited.

^b A. Moderate activation foils; B. Activation foils in remmeter moderator; C. Silicon diodes; D. Bare activation foils; E. Bonner spectrometer; F. Moderated TLD's.

REFERENCES

- AAPM (1982). American Association of Physicists in Medicine. *Report of the AAPM Task Group on Neutrons from High Energy X-ray Medical Accelerators Part I—Recommendations Regarding Risk to Patients.* (American Association of Physicists in Medicine, New York). Published with minor revisions as Nath *et al.*, 1984, q.v.
- ADAMS, G. D., AND PALUCH, I. R. (1965). "Neutron measurements relating to patients treated with x-rays from 70-MeV synchrotron," *Phys. Med. Biol.* **10**, 335.
- ADAMS, G. D., ALMY, G. M., DANCOFF, S. M., HANSON, A. O., KERST, D. W., KOCH, H. W., LANZL, E. F., LANZL, L. H., LAUGHLIN, J. S., QUASTLER, H., RIESEN, D. E., ROBINSON, C. S., AND SKAGGS, L. S. (1948). "Techniques for the application of the betatron to medical therapy," *Am. J. Roentgenol. Radium Ther.* **60**, 2, 153.
- AHRENS, J., BORCHERT, H., CZOCK, K. H., EPPLER, H. B., GIMM, H., GUNDRUM, H., KROENING, M., RIEHN, P., SITA RAM, G., ZIEGLER, A., AND ZIEGLER, B. (1975). "Total nuclear photon absorption cross sections for some light elements," *Nucl. Phys.* **A251**, 479.
- ALLEN, P. D. AND CHAUDHRI, M. A. (1982). "The dose contribution due to photonuclear reactions during radiotherapy," *Med. Phys.* **9**, 904.
- ALMOND, P. R. (1975). "Some applications of particle accelerators to cancer research and treatment," *Phys. Rep.* **17C**, 1.
- ALMOND, P. R. (1979). "Neutron leakage from current machines," page 129 in *Proceedings of a Conference on Neutrons from Medical Accelerators*, NBS Special Publication 554, Heaton, H. T. and Jacobs, R. Eds. (Government Printing Office, Washington).
- ALMOND, P. R. (1981). Personal communication.
- ALSMILLER, R. G., JR., AND MORAN, H. S. (1966). *Electron-Photon Cascade Calculations and Neutron Yields from Electrons in Thick Targets*, Oak Ridge National Laboratory, Report No. ORNL-TM-1502; also see, *Nucl. Instrum. Methods* **48**, 109 (1967).
- ALVAREZ, R. A., BERMAN, B. L., LASHER, D. R., PHILLIPS, T. W., AND FULTZ, S. C. (1971). "Photoneutron cross sections for ^{23}Na and ^{25}Mg ," *Phys. Rev. C4*, 1673.
- ALVAREZ, R. A., BERMAN, B. L., LEWIS, F. H., AND MEYER, P. (1973a). "Photoneutron cross sections for ^{55}Mn ," page 545 in *Proceedings of the International Conference on Photonuclear Reactions and Applications*, Berman, B. L., Ed. Report CONF-730301 (National Technical Information Service, Springfield, Virginia).

- ALVAREZ, R. A., BERMAN, B. L., LEWIS, F. H., AND MEYER, P. (1973b). "Photoneutron cross sections for ^{59}Co ," page 547 in *Proceedings of the International Conference on Photonuclear Reactions and Applications*, Berman, B. L., Ed. Report CONF-730301 (National Technical Information Service, Springfield, Virginia).
- ANDERSON, D. W., AND HWANG, C. C. (1983). "Accelerator room photoneutron and photon background measurements using thermoluminescent dosimeters," *Health Phys.* **44**, 115.
- ANDERSON, I. Ö., AND BRAUN, J. (1962). "A neutron rem counter for uniform sensitivity from 0.025 eV to 10 MeV," page 87 in *Neutron Dosimetry*, Vol. II IAEA Publication STI/PUB/69 (International Atomic Energy Agency, Vienna).
- ATHERTON, L. (1975). "Note on neutron measurements—16 MeV linear accelerator," International Electrochemical Commission Internal Report.
- AWSCHALOM, M. (1967). "The use of the multisphere neutron detector for dosimetry of mixed radiation fields" page 289 in *Neutron Monitoring* IAEA Publication STI/PUB/136 (International Atomic Agency, Vienna).
- AXTON, E. J., AND BARDELL, A. G. (1972). "Neutron production from electron accelerators used for medical purposes," *Phys. Med. Biol.* **17**, 293.
- AXTON, E. J., AND BARDELL, A. G. (1978). "Photoneutron production in neutron detectors in high energy x-ray beams," *Nucl. Instrum. Methods* **155**, 563.
- AXTON, E. J., AND BARDELL, A. G. (1979). "Neutron production from electron accelerators used for medical purposes," page 109 in *Proceedings of a Conference on Neutrons from Electron Medical Accelerators*, NBS Special Publication 554, Heaton, H. T. and Jacobs, R. Eds. (Government Printing Office, Washington).
- BADING, J. R., ZEITZ, L., AND LAUGHLIN, J. S. (1982). "Phosphorus activation neutron dosimetry and its application to an 18-MV radiotherapy accelerator," *Med. Phys.* **9**, 835.
- BARBER, W. C., AND GEORGE, W. D. (1959). "Neutron yields from targets bombarded by electrons," *Phys. Rev.* **116**, 1551.
- BARBIER, M. (1969). *Induced Radioactivity* (North-Holland Publishing Company, Amsterdam).
- BARRETT, R. F., BIRKELUND, J. R., THOMAS, B. J., LAM, K. S., AND THIES, H. H. (1973). "Systematics of nuclear level density parameters of nuclei deficient in one neutron," *Nucl. Phys.* **A210**, 355.
- BECKER, K. (1965). *Nuclear Track Registration in Dosimeter Glasses for Neutron Dosimetry in Mixed Radiation Fields*, report USNRDL-TR-904 (National Technical Information Service, Springfield, Virginia).
- BECKER, K. (1966). "Nuclear track registration in dosimeter glasses for neutron dosimetry in mixed radiation fields," *Health Phys.* **12**, 769.
- BECKER, K. (1973). *Solid State Dosimetry* (Chemical Rubber Publ. Co., Cleveland).
- BEIL, H., BERGERE, R., AND VEYSSIERE, A. (1969). "Detection system for photoneutrons utilizing a large scintillator capable of analyzing simultane-

- ously the reactions ($\gamma, \chi m$)," Nucl. Instrum. Methods **67**, 293.
- BEIL, H., BERGÈRE, R., CARLOS, P., LEPRÉTRE, A., DE MINIAC, A., AND VEYSSIÈRE, A. (1974). "A study of the photoneutron contribution to the giant dipole resonance in doubly even Mo isotopes," Nuc. Phys. **A227**, 427.
- BERGER, M. J., AND SELTZER, S. M. (1964). *Tables of Energy Losses and Ranges of Electrons and Positrons*, Report NASA SP-3012 (National Aeronautics and Space Administration, Washington).
- BERGER, M. J., AND SELTZER, S. M. (1982). *Stopping Powers and Ranges of Electrons and Positrons*, Report NBS IR 82-2550 (National Bureau of Standards, Washington).
- BERGÈRE, R., BEIL, H., AND VEYSSIÈRE, A. (1968). "Photoneutron cross sections of La, Tb, Ho and Ta," Nuc. Phys. **A121**, 463.
- BERGÈRE, R., BEIL, H., CARLOS, P., AND VEYSSIÈRE, A. (1969). "Photoneutron cross sections of I, Ce, Sm, Er, and Lu," Nuc. Phys. **A133**, 417.
- BERMAN, B. L. (1975). "Atlas of photoneutron cross sections obtained with monoenergetic photons," At. Data Nucl. Data Tables. **15**, 319.
- BERMAN, B. L., AND FULTZ, S. C. (1975). "Measurements of the giant dipole resonance with monoenergetic photons," Rev. Mod. Phys. **47**, 713.
- BERMAN, B. L., FULTZ, S. C., CALDWELL, J. T., KELLY, M. A., AND DIETRICH, S. S. (1970). "Photoneutron cross sections for ^{138}Ba and ^{14}N ," Phys. Rev. **C2**, 2318.
- BERTOZZI, W., PAOLINI, F. R., AND SARGENT, C. P. (1958). "Time of flight measurement of photoneutron energy spectra," Phys. Rev. **110**, 790.
- BLATT, J. M., AND WEISSKOPF, V. F. (1952). page 365 in *Theoretical Nuclear Physics* (John Wiley and Sons, Inc., New York).
- BNL, 1979. Brookhaven National Laboratory *ENDF/B Summary Documentation, BNL-NCS-17541 (ENDF-201)*, 3rd Edition (ENDF/B-V), R. Kinsey, Ed. (National Nuclear Data Center, Brookhaven National Laboratory, Upton, N. Y.).
- BRAHME, A., MONTELUS, A., NORDELL, B., REUTHAL, M., AND SVENSSON, H. (1980). "Investigations of the possibility of using photoneutron beams for radiation therapy," Phys. Med. Biol. **25**, 1111.
- BRAMBLETT, R. L., EWING, R. I., AND BONNER, T. W. (1960). "A new type of neutron spectrometer," Nucl. Instrum. Methods **9**, 1.
- BRENNER, M. (1965). "Fast neutron measurements by means of threshold detectors in the presence of 32 MeV x-rays," Soc. Sci. Fenn. Comm. Phys. Math. **31**, #3, 1.
- BURRUS, W. R. (1962). "Bonner spheres and threshold detectors for neutron spectroscopy," page 296 in *Neutron Physics Division Annual Report*, ORNL 3360 (Oak Ridge National Laboratory, Oak Ridge, Tennessee).
- BUSH, R. S. (1980). *Malignancies of the Ovary, Uterus and Cervix*, Vol. 2, page 202, (Year Book Medical Publishers, Chicago).
- CALDWELL, J. T. (1967). *Experimental Investigation of Particular Final-State Decay Modes Following Photo-Particle Reactions in ^{16}O* , Lawrence Radiation Laboratory Report UCRL-50287 (National Technical Information Service, Springfield, Virginia).

- CALDWELL, J. T., DOWDY, E. J., BERMAN, B. L., ALVAREZ, R. A., AND MEYER, P. (1980). "Giant resonance for the actinide nuclei: Photoneutron and photofission cross sections for ^{235}U , ^{236}U , ^{238}U and ^{232}Th ," Phys. Rev. **C21**, 1215.
- COOK, B. C., BAGLIN, E. E., BRADFORD, J. N., AND GRIFFIN, J. E. (1966). " $\text{C}^{12}(\gamma, n)\text{C}^{11}$ cross section to 65 MeV," Phys. Rev. **143**, 724.
- CROSS, W. G. (1970). "Developments in threshold detectors for personnel dosimeters," page 117 in *Nuclear Accident Dosimetry Systems*, International Atomic Energy Agency publication STI/PUB/241 (International Atomic Energy Agency, Vienna).
- CROSS, W. G., AND TOMMASINO, L. (1970). "Rapid reading technique for nuclear particle damage tracks in thin foils," Radiat. Eff. **5**, 85.
- DEYE, J. A., AND YOUNG, F. D. (1977). "Neutron production from a 10 MV medical linac," Phys. Med. Biol. **22**, 90.
- DINTER, H., AND TESCH, K. (1976). "Moderated rem meters in pulsed neutron fields," Nucl. Instrum. Methods **136**, 389.
- DISTENFELD, C., BISHOP, W., AND COLVETT, D. (1967). "Thermoluminescent neutron-dosimetry system," page 457 in *Luminescence Dosimetry USAEC Symposium Series 8*. (National Technical Information Service, Springfield, Virginia).
- DROUET, J., MOREAU, J. C., QUECHON, H., AND TABOT, L. (1977). *Compte Rendu des Mesures Effectuees Aupres d'un Accelerateur Saturne de la CGR-MeV a Buc*, Saclay Report D. CEN-S/SPR/SRI/77-507 GRA-092 JD/58 (Centre d'Etudes Nucleaires de Saclay, France).
- DUDZIAK, D. J. (1969). "Fast neutron biological dose attenuation by lead and polyethylene shields," Nucl. Appl. **6**, 63.
- EISENHAUER, C. (1965). "An image source technique for calculating reflection of gamma-rays or neutrons," Health Phys. **11**, 1145.
- EISENHAUER, C., SCHWARTZ, R., AND JOHNSON, T. (1982). "Measurement of neutrons reflected from the surfaces of a calibration room," Health Phys. **42**, 489.
- ERKKILA, B. H., WAECHTER, D. A., AND VASILIK, D. G. (1982). "A portable neutron spectrometer/dosimeter" Proc. Ninth DOE Workshop on Personnel Neutron Dosimetry, Pacific Northwest Laboratory Report PNL-SA-10714 (Richland, Washington).
- ERNST, W., AND OVADIA, J. (1956). "Contaminant dose from incident neutrons associated with 22.5 MeV x-rays from a betatron," Radiology **66**, 105.
- FAST, R. W., FLOURNOY, P. A., TICKLE, R. S., AND WHITEHEAD, W. D. (1960). "Photoneutron cross sections of Li, N and A," Phys. Rev. **118**, 535.
- FOX, J. G., AND MCALLISTER, J. D. (1977). "Fast neutrons from a 25-MeV betatron," Med. Phys. **4**, 387.
- FRENCH, R. L., AND WELLS, M. B. (1964). "An angle-dependent albedo for fast neutron-reflection calculations," Nucl. Sci. Eng. **19**, 441.
- FROST, D., AND MICHEL, L. (1964). "Additional component dose of neutrons in therapy using fast electrons and also ultra-hard x rays," Strahlentherapie **124**, 321.

- FROST, D., AND MICHEL, L. (1967). "Über die Zusatzdosis infolge Gewebeaktivierung bei der Therapie mit schnellen Elektronen sowie energiereicher Bremsstrahlung," *Strahlentherapie* **132**, 228.
- FULTZ, S. C., CALDWELL, J. T., BERMAN, B. L., BRAMBLETT, R. L., AND HARVEY, R. R. (1966). "Photoneutron cross sections for ^{12}C and ^{27}Al ," *Phys. Rev.* **143**, 790.
- FULTZ, S. C., BERMAN, B. L., CALDWELL, J. T., BRAMBLETT, R. L., AND KELLEY, M. A. (1969) "Photoneutron cross sections for Sn^{110} , Sn^{117} , Sn^{118} , Sn^{119} , Sn^{120} , Sn^{124} , and indium," *Phys. Rev.* **186**, 1255.
- FULTZ, S. C., ALVAREZ, R. A., BERMAN, B. L., KELLEY, M. A., LASHER, D. R., PHILLIPS, T. W., AND MCELHINNEY, J. (1971). "Photoneutron cross sections for ^{24}Mg , ^{28}Mg , and natural magnesium," *Phys. Rev. C4*, No. 1, 149.
- FULTZ, S. C., ALVAREZ, R. A., BERMAN, B. L., AND MEYER, P. (1974). "Photoneutron cross sections for ^{59}Ni and ^{60}Ni ," *Phys. Rev. C10*, 608.
- GELLIE, R. W., LOKAN, K. H., SHERMAN, N. K., JOHNSON, R. G. AND LODGE, J. I. (1972). "Photoneutron cross sections in ^{14}N ," *Can. J. Phys.* **50**, 1689.
- GILBERT, A., AND CAMERON, A. G. W. (1965). "A composite nuclear-level density formula with shell corrections," *Can. J. Phys.* **43**, 1446.
- GLASGOW, G. P. (1980). "Residual radioactivity in radiation therapy treatment aids irradiated on medical linear accelerators," *Proceedings of Health Physics Society Midyear Symposium on Medical Health Physics* (Hyannis, MA, Dec. 8-12).
- GLAZUNOV, SAVIN, M. V., SAFINA, I. N., FOMUSHKIN, E. F., AND KHOKHLOV, YU. A. (1964). "Photoneutron spectra of platinum, bismuth, lead and uranium," *Zh. Eksp. Teor. Fiz.* **46**, 1906, *Sov. Phys. JETP* **19**, 1284.
- GRANT, W. H. III (1978). "Neutron leakage for Therac 20," unpublished report.
- GUR, D., BUKOVITZ, A. G., ROSEN, J. C., AND HOLMES, B. G. (1978a). "The use of activated aluminum foils for determination of fast neutron contaminations in photon beams." *Phys. Med. Biol.* **23**, 1183.
- GUR, D., ROSEN, J. C., BUKOVITZ, A. G., AND GILL, A. W. (1978b). "Fast and slow neutrons in an 18-MV photon beam from a Philips SL75-20 linear accelerator," *Med. Phys.* **5**, 221.
- GUR, D., BUKOVITZ, A. G., ROSEN, J. C., AND HOLMES, B. G. (1979). "Relative measurements of fast neutron contamination in 18-MV photon beams from two linear accelerators and a betatron," *Med. Phys.* **6**, 140.
- HANKINS, D. E. (1968a). *The Multisphere Neutron-Monitoring Technique*, USAEC Report LA-3700 (Los Alamos Scientific Laboratory, Los Alamos, New Mexico).
- HANKINS, D. E. (1968b). "The substitution of a BF_3 tube for the LiI crystal in neutron rem-meters," *Health Phys.* **14**, 518.
- HANKINS, D. E., AND PEDERSON, R. A. (1963). *A Comparison of the Neutron Dose Rates Obtained with the Single-Sphere Instrument, Multisphere Method, and Hurst Proportional Counter*, USAEC Report LAMS-2977 (Los Alamos Scientific Laboratory, Los Alamos).

- HANSEN, E. C., BARTOLETTI, C. S., AND DAITCH, P. B. (1975). "Analog Monte Carlo studies of electron-photon cascades and the resultant production and transport of photoneutrons in finite three-dimensional systems," *J. Appl. Phys.* **46**, 1109.
- HARVEY, R. A., HASS, L. L., AND LAUGHLIN, J. S. (1952). "Effects of x-ray and electron beam from the betatron on head and neck cancer," page 440 in *Proc. 2nd Natl. Cancer Conf.*, Vol. I. (American Cancer Society, New York).
- HERTEL, N. E., JOHNSON, R. H., DORNING, J. J., AND WEHRING, B. W. (1979). "Measurements and analysis of neutron transport through iron," page 563 in *Proceedings of the International Conference on Nuclear Cross Sections for Technology*. NBS Special Publication 594 (National Technical Information Service, Springfield, Virginia).
- HOFFMAN, R. J., AND NATH, R. (1982). "On the sources of radiation exposure of technologists in a radiotherapy center with high energy x-ray accelerators," *Health Phys.* **42**, 525.
- HOLDEN, N. E. (1977). *Isotopic Composition of the Elements and their Variation in Nature; A Preliminary Report*, Report BNL-NCS-50605 (Brookhaven National Laboratory).
- HOLEMAN, G. R., PRICE, K. W., FRIEDMAN, L. F., AND NATH, R. (1977). "Neutron spectral measurements in an intense photon field associated with a high-energy x-ray radiotherapy machine," *Med. Phys.* **4**, 508.
- HORSLEY, R. J., JOHNS, H. E., AND HASLAM, R. N. H. (1953). "Energy absorption in human tissue by nuclear processes with high-energy x-rays," *Nucleonics* **11**, (#2), 28.
- HOWERTON, R. J. (1958). *Semi-Empirical Neutron Cross Sections 0.5-15 MeV*, UCRL-5351 (Lawrence Berkeley Laboratory, Berkeley, California).
- HSIEH, C. L. (1956). "The stray radiation levels of a 45 MeV travelling wave linear electron accelerator," *Br. J. Radiol.*, Vol **XXIX**, 201.
- HUGHES, W. L., NUSSBAUM, G. H., CONNOLLY, R., EMANI, B., AND REILLY, P. (1979). "Tissue perfusion rate determined from the decay of ^{15}O activity after photon irradiation *in situ*," *Science* **204**, 1215.
- IAEA (1965). International Atomic Energy Agency. *In-Pile Dosimetry*, IAEA Technical Report Series No. 46 (International Atomic Energy Agency, Vienna).
- IAEA (1970). International Atomic Energy Agency. *Neutron Fluence Measurements*, IAEA Technical Report Series No. 107 (International Atomic Energy Agency, Vienna).
- ICRP (1962). International Commission on Radiological Protection, *Report of Committee IV on Protection against Electromagnetic Radiation above 3 MeV and Electrons, Neutrons and Protons*, ICRP Publication 4 (Pergamon Press, Oxford).
- ICRP (1973). International Commission on Radiological Protection. *Report of Committee 3 on Data for Protection against Ionizing Radiation from External Sources Supplement to ICRP Publication 15*, ICRP Publication 21 (Pergamon Press, Oxford).

104 / REFERENCES

- ICRU (1969). International Commission on Radiation Units and Measurements, *Neutron Fluence, Neutron Spectra and Kerma*. ICRU Report 13 (International Commission on Radiation Units and Measurements, Bethesda, Maryland).
- ICRU (1977). International Commission on Radiation Units and Measurements, *Neutron Dosimetry for Biology and Medicine*, ICRU Report 26 (International Commission on Radiation Units and Measurements, Bethesda, Maryland).
- ICRU (1984). International Commission on Radiation Units and Measurements, *Stopping Powers For Electrons and Positrons*, ICRU Report 37 (International Commission on Radiation Units and Measurements, Bethesda, Maryland)
- ING, H., AND SHORE R. A. (1982). "Unwanted radiation produced by leakage neutrons from medical electron accelerators," *Med. Phys.* **9**, 34.
- ING, H., NELSON, W. R., AND SHORE, R. A. (1982). "Unwanted photon and neutron radiation resulting from collimated photon beams interacting with the body of radiotherapy patients," *Med. Phys.* **9**, 27.
- JOHNS, H. E. (1979). "Advantages and properties of high energy photon beams," page 17 in *Proceedings of a Conference on Neutrons from Electron Medical Accelerators*, NBS Special Publication 554, Heaton, H. T. and Jacobs, R., Eds. (U.S. Government Printing Office, Washington).
- JONES, L. W., AND TERWILLIGER, K. M. (1953) "Photoneutron production excitation functions to 320 MeV," *Phys. Rev.* **91**, 699.
- KATZ, R., AND KOBETICH, E. J. (1968). "Formation of etchable tracks in dielectrics," *Phys. Rev.* **170**, 401.
- KEHRER, M. L. AND ROBINSON, J. E. (1972). "A simple technique for making neutron measurements," *Int. J. Appl. Radiat. Isot.* **23**, 141.
- KENNEY, G. N. (1981). Personal communication.
- KERSEY, R. W. (1979). Estimation of neutron and gamma radiation doses in the entrance mazes of SL75-20 linear accelerator treatment rooms," *Medicamundi* **24**, 151.
- KNEISSL, U., KUHL, G., LEISTER, K. H., AND WELLER, A. (1975). "Photoneutron cross sections for ^9Be obtained with quasi-monoenergetic photons," *Nucl. Phys.* **A247**, 91.
- KNEISSL, U., LEISTER, K. H., NEIDEL, H. O., AND WELLER, A. (1976). "A study of the photoneutron reactions in ^{10}B and ^{11}B ," *Nucl. Phys.* **A264**, 30.
- KUCHNIR, F. T., AXEL, P., CRIEGEE, L., DRAKE, D. M., HANSON, A. O. AND SUTTON, D. C. (1967). "Neutron spectra from monoenergetic photons on bismuth," *Phys. Rev.* **161**, 1236.
- KUSHELEVSKY, A. P., AND SHANI, G. (1976). "Photoneutron production in detectors in high energy x-ray beams," *Nucl. Instrum. Methods* **137**, 71.
- LARIVIERE, P. D. (1980). Personal communication. (Varian Associates, Palo Alto, California).
- LARIVIERE, P. D. (1982a). "Capture gamma radiation at the entrance to a medical accelerator treatment room," page 239 in *Proceedings of 3rd International Symposium of the British Society for Radiological Protection Vol. I*,

- (National Radiological Protection Board, Harwell, Didcot, Oxon, United Kingdom).
- LARIVIERE, P. D. (1982b). Varian Internal Report Rad. Physics # 11-81. (Varian Associates, Palo Alto, California).
- LAUGHLIN, J. S. (1951). "Physical considerations in the use of a 23-MeV medical betatron," Nucleonics 8 (#4), 5.
- LAUGHLIN, J. S., REID, A., ZEITZ, L., AND DING, J. (1979). "Unwanted neutron contribution to megavoltage x-ray and electron therapy," page 1 in *Proceedings of a Conference on Neutrons from Medical Accelerators*, NBS Special Publication 554, Heaton, H. T. and Jacobs, R. Eds. (U.S. Government Printing Office, Washington).
- LBL (1973). Lawrence Berkeley Laboratory. *Instrumentation for Environmental Monitoring, Vol. 3 Radiation Report LBL-1, Vol. 3* (University of California, Berkeley, California).
- LEDERER, C. M., AND SHIRLEY, V. S. (1978). *Table of Isotopes, 7th Ed.* (Wiley, New York).
- LEPRÉTRE, A., BEIL, R., BERGÈRE, P., CARLOS, P., FAGOT, J., DE MINIAC, A., AND VEYSSIÈRE, A. (1981). "Measurements of the total photonuclear cross sections from 30 MeV to 140 MeV for Sn, Ce, Ta, Pb and U nuclei," Nucl. Phys. A367, 237.
- LEVINGER, J. S., AND BETHE, H. A. (1950). "Dipole transitions in the nuclear photo effect," Phys. Rev. 78, 115.
- LÖFGREN, K., AND SPRING, E. (1970). "Neutron radiation produced by the 32 MeV roentgen beam of a medical betatron," Acta Radiol. 9, 247.
- MAERKER, R. E., AND MUCKENTHALER, F. J. (1967a). "Neutron fluxes in concrete ducts arising from incident thermal neutrons: Calculation and experiment," Nucl. Sci. Eng. 29, 444.
- MAERKER, R. E., AND MUCKENTHALER, F. J. (1967b). "Neutron fluxes in concrete ducts arising from incident epicadmium neutrons," Nucl. Sci. Eng. 30, 340.
- MAERKER, R. E., CLAIBORNE, H. C., AND CLIFFORD, C. E. (1968). "Neutron attenuation in rectangular ducts," page 517 in *Engineering Compendium on Radiation Shielding, Vol. I*, Jaeger, R. C., Ed. (Springer-Verlag, New York).
- MARBACH, J. R. (1975). "Neutron Leakage from the Sagittaire linear accelerator at the University of Indiana at Indianapolis," unpublished report.
- MAYNEORD, W. V., MARTIN, J. H., AND LAYNE, D. A. (1949). "Production of radioactivity in animal tissues by high-energy x-rays," Nature 164, 728.
- MC CALL, R. C. (1977). Unpublished data.
- MC CALL, R. C. (1978). Internal Report to Varian dated April 1, 1978.
- MC CALL, R. C. (1979). Unpublished data.
- MC CALL, R. C. (1982). McCall Associates (report unpublished).
- MC CALL, R. C., AND SWANSON, W. P. (1979). "Neutron sources and their characteristics," page 75 in *Proceedings of a Conference on Neutrons from Electron Medical Accelerators*, NBS Special Publication 554, Heaton, H. T. and Jacobs, R. Eds. (U.S. Government Printing Office, Washington).
- MC CALL, R. C., JENKINS, T. M., AND TOCHILIN, E. (1976). *High Energy*

- Photon Response of Moderated Neutron Detectors*, Report SLAC-PUB-1768 (Stanford Linear Accelerator Center, Stanford, California).
- MCCALL, R. C., JENKINS, T. M., AND OLIVER, JR., G. D. (1978a). "Photon and electron response of silicon-diode neutron detectors," *Med. Phys.* **5**, 37.
- MCCALL, R. C., MCINTYRE, R. O., AND TURNBULL, W. G. (1978b). "Improvement of linear accelerator depth dose curves," *Med. Phys.* **5**, 518.
- MCCALL, R. C., JENKINS, T. M., AND SHORE, R. A. (1979). "Transport of accelerator produced neutrons in a concrete room," *IEEE Trans, Nucl. Sci.* **NS-26**, #1, 1593.
- MCCALL, R. C., JENKINS, T. M., SHORE, R. A. AND LARIVIERE, P. D. (1980). "Personnel hazards from medical electron accelerator photoneutrons," page 193 in *Proceeding of the 5th International Congress of the International Radiation Protection Association*, Vol. I, (Pergamon Press, Oxford, England.)
- MCCASLIN, J. B., SMITH A. R., STEPHENS, L. D., THOMAS, R. H., JENKINS, T. M., WARREN, G. J., AND BAUM, J. W. (1977). "An intercomparison of dosimetry techniques in radiation fields at two high energy accelerators," *Health Phys.* **33**, 611.
- MCGINLEY, P. H., AND SOHRABI, M. (1979). "Neutron contamination in the primary beam," page 99 in *Proceedings of a Conference on Neutrons from Electron Medical Accelerators*, NBS Special Publication 554, Heaton, H. T. and Jacobs, R., Eds. (U.S. Government Printing Office, Washington).
- MCGINLEY, P. H., WOOD, M., MILLS, M., AND RODRIGUEZ, R. (1976). "Dose levels due to neutrons in the vicinity of high-energy medical accelerators," *Med. Phys.* **3**, 397.
- MC GUIRE, S. A. (1966). *A Dose Monitoring Instrument for Neutrons from Thermal to 100 MeV*, USAEC Report LA-3435 (Los Alamos Scientific Laboratory, Los Alamos, New Mexico).
- MC NEILL, K. G., JURY, J. W., AND HEWITT, J. S. (1970). "Fine structure in the photoneutron spectra from praseodymium-141 and lead," *Can. J. Phys.* **48**, 950.
- MUTCHLER, G. S. (1966). *The Angular Distributions and Energy Spectra of Photoneutrons from Heavy Elements*, Ph.D. Thesis, Report MIT-2098-224 (Massachusetts Institute of Technology, Cambridge, Massachusetts).
- NAS (1972). National Academy of Sciences-National Research Council, *The Effects on Populations of Exposure to Low Levels of Ionizing Radiation*, Report of the Advisory Committee on the Biological Effects of Ionizing Radiation (National Academy of Sciences-National Research Council, Washington).
- NAS (1980). National Academy of Sciences-National Research Council, *The Effects on Populations of Exposure to Low Levels of Ionizing Radiation*, Report of the Advisory Committee on the Biological Effects of Ionizing Radiation (National Academy of Sciences-National Research Council, Washington).
- NATH, R., PRICE, K. W., AND HOLEMAN, G. R. (1979). "Mixed photon-neutron field measurements," page 87 in *Proceedings of a Conference on Neutrons from Electron Medical Accelerators*, NBS Special Publication 554,

- Heaton, H. T. and Jacobs, R. Eds. (U.S. Government Printing Office, Washington).
- NATH, R., EPP, E. R., LAUGHLIN, J. S., SWANSON, W. P., AND BOND, V. P. (1984). "Neutrons from high-energy x-ray medical accelerators: An estimate of risk to the radiotherapy patient," *Med. Phys.* **11**, 231.
- NCRP (1936). National Committee on Radiation Protection. *X-Ray Protection*, NCRP Report No. 3 Published as NBS Handbook 20 (out of print). Superseded by NCRP Reports No. 33, 35, 36 and 49.
- NCRP (1964). National Council on Radiation Protection and Measurements, *Shielding for High-Energy Electron Accelerator Installations*, NCRP Report No. 31, Published as NBS Handbook 97 (out of print). Superseded by NCRP Report 51.
- NCRP (1968). National Council on Radiation Protection and Measurements. *Medical X-Ray and Gamma-Ray Protection for Energies Up to 10 MeV. Equipment Design and Use*. NCRP Report No. 33. (National Council on Radiation Protection and Measurements, Bethesda, Maryland.).
- NCRP (1971). National Council on Radiation Protection and Measurements, *Protection against Neutron Sources*, NCRP Report No. 38, (National Council on Radiation Protection and Measurements, Bethesda, Maryland).
- NCRP (1976). National Council on Radiation Protection and Measurements *Structural Shielding Design and Evaluation for Medical Use of X-rays and Gamma Rays of Energies Up to 10 MeV*, NCRP Report No. 49 (National Council on Radiation Protection and Measurements, Bethesda, Maryland).
- NCRP (1977). National Council on Radiation Protection and Measurements, *Radiation Protection Design Guidelines for 0.1-100 MeV Particle Accelerator Facilities*, NCRP Report No. 51 (National Council on Radiation Protection and Measurement, Bethesda, Maryland).
- NEMEC, H. W., AND ROTH, J. (1978). "Dosisverteilung der Photonen und Neutronen ausserhalb des Bestrahlungsfeldes eines 8-MeV-Linearbeschleunigers," *Strahlentherapie* **154**, 380.
- NEWTON, T. D. (1956). "Shell effects on the spacing of nuclear levels," *Can. J. Phys.* **34**, 804.
- O'BRIEN, K., SANNA, R., AND MCLAUGHLIN, J. (1965). "Inference of accelerator stray neutron spectra from various measurements," page 286 in *Symposium Proceedings, USAEC First Symposium on Accelerator Radiation Dosimetry and Experience*, USAEC Report CONF-651109 (National Technical Information Service, Springfield, Virginia).
- OLIVER, G. D., JR. (1976). Revised data from "Fast neutron contamination in x-ray beams of medical accelerators from 19 to 45 MV," presented at the annual meeting of the American Association of Physicists in Medicine (1974).
- OVERLY, J. C., HOLEMAN, G. R., PARKER, P. D., AND BROMLEY, D. A. (1967). "Radiation shielding for an MP tandem accelerator installation," *Nucl. Instrum. Methods* **53**, 56.
- PATTERSON, H. W., AND THOMAS, R. H. (1973). *Accelerator Health Physics*, (Academic Press, New York).

- PATTERSON, H. W., AND WALLACE, R. (1958). *A Method of Calibrating Slo. Neutron Detectors*, Report UCRL-8359 (Lawrence Berkeley Laboratory, Berkeley, California).
- PENFOLD, A. S., AND LEISS, J. E. (1958). *Analysis of Photo Cross Sections*. Physics Research Laboratory Report, (University of Illinois, Champaign Illinois).
- PHILLIPS, L. F., CHAMPAGNE, R. J., AND SCALSKY, E. D. (1965). "Linear energy transfer spectra and effective quality factors in stray radiation areas at the Brookhaven National Laboratory proton synchrotrons," Proceedings of the USAEC First Symposium on Accelerator Radiation Dosimetry and Experience, USAEC Report CONF-651109, (National Technical Information Service, Springfield, Virginia).
- POCHIN, E. E. (1978). *Why be Quantitative about Radiation Risk Estimates*, Lauriston S. Taylor Lectures in Radiation Protection and Measurements, Lecture No. 2 (National Council on Radiation Protection and Measurements, Bethesda, Maryland).
- POHLIT, W. (1959). "Zur Frage der bei Betatronbestrahlung in Phantom auftretenden Neutronenverteilung," Strahlentherapie 110, 240.
- POHLIT, W. (1960), "Die Messung der Neutronenstreustrahlung an einem 35 MeV-Betatron," Strahlentherapie 113, 469.
- PRESTON, M. A. (1962). Page 523 in *Physics of the Nucleus* (Addison-Wesley Publishing Co., Inc., Reading, Massachusetts).
- PRÊTRE, S., TOCHILIN, E., AND GOLDSTEIN, N. (1968). "A standardized method for making neutron fluence measurements by fission fragment tracks in plastic. A suggestion for an emergency neutron dosimeter with rad response," page 491 in *Proceedings of 1st International Congress on Radiation Protection* (Pergamon Press, Oxford).
- PRICE, W. J. (1958). *Nuclear Radiation Detection* (McGraw-Hill, New York).
- PRICE, K. W., NATH, R., AND HOLEMAN, G. R. (1978a). "Fast and thermal neutron profiles for a 25-MV x-ray beam," Med. Phys. 5, 285.
- PRICE, K. W., HOLEMAN, G. R., AND NATH, R. (1978b). A technique for determining fast and thermal neutron flux densities in intense high-energy (8-30 MeV) photon fields," Health Phys. 35, 341.
- PRINCE, A. (1969). *Nuclear and Physical Properties of Californium-252*, Report BNL-50168. (Brookhaven National Laboratory, New York).
- QUAM, W., DEL DUCA, T., PLAKE, W., AND GRAVES, G. (1982). "Pocket neutron rem meter," Proc. Ninth DOE Workshop of Personnel Neutron Dosimetry. Pacific Northwest Laboratory Report PNL-SA-10714 (Pacific Northwest Laboratory, Richland, Washington).
- QUASTLER, H., ADAMS, G. D., ALMY, G. M. DANCOFF, S. M. HANSON, A. O., KERST, D. W., KOCH, H. W., LANZL, L. M., LAUGHLIN, J. S., RIESEN, D. E., ROBINSON, C. S., AUSTIN, V. T., KERLEY, T. G., LANZL, E. F., MCCLURE, G. Y., THOMPSON, E. A., AND SKAGGS, L. S. (1949). "Techniques for application of the betatron to medical therapy," Am. J. Roentgenol. Radium Ther. 61, No. 5, 591.
- RAWLINSON, J. A. (1979). "Scattered radiation relative to leakage radiation in high energy x-ray beams," page 25 in *Proceedings of a Conference on Neutrons from Medical Accelerators*, NBS Special Publication 554, Heaton,

REFERENCES / 109

- H. T., and Jacobs, R. Eds. (U.S. Government Printing Office, Washington).
- RAWLINSON, J. A., AND JOHNS, H. E. (1977). Letter to the Editor, *Med. Phys.* **4**, 456.
- ROGERS, D. W. O., AND VANDYK, G. (1981). "Use of a neutron remmeter to measure leakage neutrons from medical accelerators," *Med. Phys.* **8**, 163.
- ROSSI, H. H., AND ROSENZWEIG, W. (1955a). "A device for the measurement of dose as a function of specific ionization," *Radiology* **64**, 404.
- ROSSI, H. H., AND ROSENZWEIG, W. (1955b). "Measurement of neutron dose as a function of linear energy transfer," *Radiat. Res.* **2**, 417.
- SANNA, R. S. (1976). *Modification of an Iterative Code for Unfolding Neutron Spectra from Multisphere Data*, ERDA Report-HASL-311 (Health and Safety Laboratory, New York).
- SCHMIDT, F. A. R. (1970). *The Attenuation Properties of Concrete for Shielding of Neutrons of Energy less than 15 MeV*, Report ORNL-RSIC-26 (Oak Ridge National Laboratory, Oak Ridge, Tennessee).
- SCHULZ, R. J. (1978). "Argon/propane combination-chamber dosimetry for mixed x-ray/neutron fields," *Med. Phys.* **5**, 525.
- SELPF, W. E. (1973). "Albedos, ducts and voids," page 313 in *Reactor Shielding for Nuclear Engineers*, Schaeffer, N. M., Ed., TID-25951, (National Technical Information Service, Springfield, Virginia).
- SHURE, K., O'BRIEN, J. A., AND ROTHBERG, D. M. (1969). "Neutron dose rate attenuation by iron and lead," *Nucl. Sci. Eng.* **35**, 371.
- SKAGGS, L. S., ALMY, G. M., KERST, D. W., AND LANZL, L. H. (1946). "Removal of the electron beam from the betatron," *Phys. Rev.* **70**, 95.
- SKAGGS, L. S., ALMY, G. M., KERST, D. W., AND LANZL, L. H. (1948). "Development of the betatron for electron therapy," *Radiology* **50**, 167.
- SKAGGS, L. S., LANZL, L. H., AND AVERY, R. T. (1958). "A new approach to electron therapy," page 312 in *Second United Nations International Conference on Peaceful Uses of Atomic Energy, Isotopes in Medicine*, Vol. 26 (United Nations, New York).
- SMITH, A. R. (1960). *A Cobalt Neutron-Flux Integrator*, Report UCRL-9212 (Lawrence Berkeley Laboratory, Berkeley, California).
- SOHRABI, M., AND MORGAN, K. Z. (1978). "A new polycarbonate fast neutron personnel dosimeter," *Am. Ind. Hyg. Assn. J.* **39** #6, 438.
- SOHRABI, M., AND MORGAN K. Z., (1979). "Neutron dosimetry in high energy x-ray beams of medical accelerators," *Phys. Med. Biol.* **24**, 756.
- SONG, Y. T. (1965). *Fast Neutron Streaming through Two-Legged Concrete Ducts*, Report NCEL-R354, (Naval Civil Engineering Laboratory, Port Hueneme, California).
- SONG, Y. T., HUDDLESTON, C. M., AND CHILTON, A. B. (1971). "Neutron streaming through ducts-analysis of experimental results," *Nucl. Sci. & Eng.* **44**, 252.
- SPENCER, L. V., AND DIAZ, J. A. (1964). *Neutron Penetration in Ducts and other Cavities*, NBS Report 8541 (National Bureau of Standards, Washington, D.C.).
- SPENCER, L. V., DIAZ, J. A., AND MOSES, E., (1964). *Neutron Penetration in Cylindrical Ducts*, NBS Report 8542 (National Bureau of Standards, Washington, D. C.).

110 / REFERENCES

- SPRING, E., AND VÄYRYNEN, T. (1970). "Measurement of changes in the oxygen and carbon concentration of tissues during fractionated high energy x-ray treatment," *Phys. Med. Biol.* **15**, 23.
- STEPHENS, L. D., AND SMITH, A. R. (1958). *Fast-Neutron Surveys Using Indium-Foil Activation*, Report UCRL-8418 (Lawrence Berkeley Laboratory, Berkeley, CA).
- STEVENSON, G. R. (1967). *Neutron Spectrometry from 0.025 eV to 25 GeV*, Report RHEL/R-154 (National Technical Information Service, Springfield, Virginia).
- STONE, D. R., WAGNER, E. G., JONES, T. D., AND SHINPAUGH, W. H. (1970). "Calculated and experimentally determined neutron dose conversion factors for Californium," *Health Phys.* **18**, 69.
- STRAKER, E. A., STEVENS, P. N., IRVING, D. C., AND CAIN, V. R. (1970). *The MORSE Code-A Multigroup Neutron and Gamma Ray Monte Carlo Transport Code*, Report ORNL—4585 (Oak Ridge National Laboratory, Oak Ridge, Tennessee).
- STRAKER, E. A., STEVENS, P. N., IRVING, D. C., AND CAIN, V. R. (1976). *MORSE-CG, General Purpose Monte-Carlo Multigroup Neutron and Gamma-Ray Transport Code With Combinatorial Geometry*, Report CCC-203, (Radiation Shielding Information Center, Oak Ridge, TN).
- STRANDEN, E. (1977a). "Activity induced in patients by high energy x-ray therapy," *Phys. Med. Biol.* **22**, 348.
- STRANDEN, E. (1977b). "Neutron doses to patients in high energy x-ray therapy," *Phys. Med. Biol.* **22**, 1011.
- SUND, R. E., BAKER, M. P., KULL, L. A., AND WALTON, R. B. (1968). "Measurements of the $^{63}\text{Cu}(\gamma, n)$ and $(\gamma, 2n)$ cross sections," *Phys. Rev.* **176**, 1366.
- SWANSON, W. P. (1978). "Calculation of neutron yields released by electrons incident on selected materials," *Health Phys.* **35**, 353.
- SWANSON, W. P. (1979). "Improved calculation of photoneutron yield released by incident electrons," *Health Phys.* **37**, 347.
- SWANSON, W. P. (1980). "Estimate of risk in radiation therapy due to unwanted neutrons," *Med. Phys.* **7**, 141.
- TAUMANN, L. (1980). Personal communication. Siemens Medical Laboratories, Inc.
- TOCHILIN, E., AND LARIVIERE, P. D. (1979). "Neutron leakage characteristics related to room shielding," page 145 in *Proceedings of a Conference on Neutrons from Electron Medical Accelerators*, NBS Special Publication 554, Heaton, H.T. and Jacobs, R. Eds. (U.S. Government Printing Office, Washington)
- TOMMASINO, L. (1970). "Electrochemical etching of damaged track detectors by H. V. pulse and sinusoidal waveforms," page 213 in *Proc. of 7th Int. Colloq. on Corpuscular Photogr. Solid Detectors*, Barcelona. Article available as RT/PROT (71) 1 (National Technical Information Service, Springfield, Virginia)
- TOMMASINO, L., AND ARMELLINI, C. (1973). "New etching technique for damaged track detectors," *Radiat. Eff.* **20**, 253.

- TSAI, Y. S. (1974). "Pair production and bremsstrahlung of charged leptons," *Rev. Mod. Phys.* **46**, 829.
- UNSCEAR (1977). United National Scientific Committee on the Effects of Atomic Radiation *Sources and Effects of Ionizing Radiation*. Report to the General Assembly, with Annexes Publ. E771X1, (United Nations, New York).
- UNSCEAR (1982) United National Scientific Committee on the Effects of Atomic Radiation, *Ionizing Radiation: Sources and Biological Effects*. United Nations Publication Sales No: E.82 IX.8 (United Nations, New York).
- VANDYK, G. (1981). Personal communication, Atomic Energy of Canada, Ltd.
- VEYSSIÈRE, A., BEIL, H., BERGÈRE, R., CARLOS, P., AND LEPRÉTRE, A. (1970). "Photoneutron cross sections of ^{208}Pb and ^{197}Au ," *Nucl. Phys.* **A159**, 561.
- VEYSSIÈRE, A., BEIL, H., BERGÈRE, R., CARLOS, P., LEPRÉTRE, A., AND DE MINIAC, A. (1974). "A study of the photoneutron contribution to the giant dipole resonance of s-d shell nuclei," *Nucl. Phys.* **A227**, 513.
- VEYSSIÈRE, A., BEIL, H., BERGÈRE, R., CARLOS, P., LEPRÉTRE, A., AND DE MINIAC, A. (1975). "A study of the giant dipole resonance in the $A = 190$ transition region," *J. Phys. (Paris) Lett.* **36**, L267.
- WACHSMANN, F., BARTH, G., LANZL, L. H., AND CARPENTER, J. W. J. (1962). Page 155 in *Moving Field Radiation Therapy*, (The University of Chicago Press, Chicago, Illinois).
- WAPSTRA, A. H., AND BOS, K. (1977). "The 1977 atomic mass evaluation," *At. Data Nucl. Data Tables* **19** 177.
- WATKINS, G. L., AND HOLEMAN, G. R. (1968). "The evaluation of an iterative technique's use in unfolding neutron spectra data," *Health Phys.* **15**, 535.
- WEINSTEIN, M. S., O'BRIEN, K. AND HAJNAL, F. (1969). *Procedures for Estimating the Errors in Neutron Spectra from Bonner Multisphere Measurements*, USAEC Report HASL-TM-69-4 (Health and Safety Laboratory, New York).
- WILENZICK, R. M., ALMOND, P. R., OLIVER, G. D., AND DEALMEIDA, C. E. (1973) "Measurement of fast neutrons produced by high energy x-ray beams of medical electron accelerators," *Phys. Med. Biol.* **18**, 396.
- WORSNOP, R. (1979) Personal communication.
- YOUNG, D. A. (1958). "Etching of radiation damage in lithium fluoride," *Nature* **182**, 375.

The NCRP

The National Council on Radiation Protection and Measurements is a nonprofit corporation chartered by Congress in 1964 to:

1. Collect, analyze, develop, and disseminate in the public interest information and recommendations about (a) protection against radiation and (b) radiation measurements, quantities, and units, particularly those concerned with radiation protection;
2. Provide a means by which organizations concerned with the scientific and related aspects of radiation protection and of radiation quantities, units, and measurements may cooperate for effective utilization of their combined resources, and to stimulate the work of such organizations.
3. Develop basic concepts about radiation quantities, units, and measurements, about the application of those concepts, and about radiation protection;
4. Cooperate with the International Commission on Radiological Protection, the International Commission on Radiation Units and Measurements, and other national and international organizations, governmental and private, concerned with radiation quantities, units, and measurements and with radiation protection.

The Council is the successor to the unincorporated association of scientists known as the National Committee on Radiation Protection and Measurements and was formed to carry on the work begun by the Committee.

The Council is made up of the members and the participants who serve on the eighty-one scientific committees of the Council. The scientific committees, composed of experts having detailed knowledge and competence in the particular area of the committee's interest, draft proposed recommendations. These are then submitted to the full membership of the Council for careful review and approval before being published.

The following comprise the current officers and membership of the Council:

Officers

<i>President</i>	WARREN K. SINCLAIR
<i>Vice President</i>	S. JAMES ADELSTEIN
<i>Secretary and Treasurer</i>	W. ROGER NEY
<i>Assistant Secretary</i>	EUGENE R. FIDELL
<i>Assistant Treasurer</i>	JAMES F. BERG

Members

SEYMOUR ABRAHAMSON	THOMAS A. LINCOLN
S. JAMES ADELSTEIN	RAY D. LLOYD
ROY E. ALBERT	ARTHUR C. LUCAS
PETER R. ALMOND	CHARLES W. MAYS
EDWARD L. ALPEN	ROGER O. MCCLELLAN
JOHN A. AUXIER	JAMES E. MC LAUGHLIN
WILLIAM J. BAIR	BARBARA J. MCNEIL
JOHN D. BOICE, JR.	THOMAS F. MEANEY
VICTOR P. BOND	CHARLES B. MEINHOLD
ROBERT L. BRENT	MORTIMER L. MENDELSON
ANTONE BROOKS	WILIAM A. MILLS
REYNOLD F. BROWN	DADE W. MOELLER
THOMAS F. BUDINGER	A. ALAN MOGHISI
MELVIN W. CARTER	ROBERT D. MOSELEY, JR.
GEORGE W. CASARETT	JAMES V. NEEL
RANDALL S. CASWELL	WESLEY NYBORG
ARTHUR B. CHILTON	MARY ELLEN O'CONNOR
GERALD D. DODD	FRANK L. PARKER
PATRICIA W. DURBIN	ANDREW K. POZNANSKI
JOE A. ELDER	NORMAN C. RASMUSSEN
MORTIMER M. ELKIND	WILLIAM C. REINIG
THOMAS S. ELY	CHESTER R. RICHMOND
EDWARD R. EPP	JAMES S. ROBERTSON
R. J. MICHAEL FRY	LEONARD A. SAGAN
ROBERT A. GOEPP	WILLIAM J. SCHULL
ROBERT O. GORSON	GLENN E. SHELINE
ARTHUR W. GUY	ROY E. SHORE
ERIC J. HALL	WARREN K. SINCLAIR
NAOMI H. HARLEY	LEWIS V. SPENCER
JOHN W. HEALY	JOHN B. STORER
JOHN M. HESLEP	ROY C. THOMPSON
SEYMOUR JABLON	JOHN E. TILL
DONALD G. JACOBS	ARTHUR C. UPTON
A. EVERETTE JAMES, JR.	GEORGE L. VOELZ
BERND KAHN	EDWARD W. WEBSTER
JAMES G. KEREIAKES	GEORGE M. WILKENING
CHARLES E. LAND	H. RODNEY WITHERS
GEORGE R. LEOPOLD	

*Honorary Members**LAURISTON S. TAYLOR, Honorary President*

EDGAR C. BARNES	JOHN H. HARLEY	ROBERT J. NELSEN
AUSTIN M. BRUES	LOUIS H. HEMPELMANN,	HARALD H. ROSSI
FREDERICK P. COWAN	JR.	WILLIAM G. RUSSELL
JAMES F. CROW	PAUL C. HODGES	JOHN H. RUST
MERRIL EISENBUD	GEORGE V. LEROY	EUGENE L. SAENGER
ROBLEY D. EVANS	WILFRID B. MANN	J. NEWELL STANNARD
RICHARD F. FOSTER	KARL Z. MORGAN	HAROLD O. WYCKOFF
HYMER L. FRIEDELL	RUSSELL H. MORGAN	

Currently, the following subgroups are actively engaged in formulating recommendations:

- SC-1: Basic Radiation Protection Criteria
- SC-3: Medical X-Ray, Electron Beam and Gamma-Ray Protection for Energies Up to 50 MeV (Equipment Performance and Use)
- SC-16: X-Ray Protection in Dental Offices
- SC-18: Standards and Measurements of Radioactivity for Radiological Use
- SC-38: Waste Disposal
 - Task Group on Krypton-85
 - Task Group on Carbon-14
 - Task Group on Disposal of Accident Generated Waste Water
 - Task Group on Disposal of Low-Level Waste
 - Task Group on the Actinides
 - Task Group on Xenon
 - Task Group on Definitions of Radioactive Waste
- SC-40: Biological Aspects of Radiation Protection Criteria
 - Task Group on Atomic Bomb Survivor Dosimetry
 - Subgroup on Biological Aspects of Dosimetry of Atomic Bomb Survivors
- SC-44: Radiation Associated with Medical Examinations
- SC-45: Radiation Received by Radiation Employees
- SC-46: Operational Radiation Safety
 - Task Group I on Warning and Personnel Security Systems
 - Task Group 2 on Uranium Mining and Milling—Radiation Safety Programs
 - Task Group 3 on ALARA for Occupationally Exposed Individuals in Clinical Radiology
 - Task Group 4 on Calibration of Instrumentation
 - Task Group 5 on Maintaining Personnel Exposure Records
 - Task Group 6 on Radiation Protection for Allied Health Personnel
- SC-47: Instrumentation for the Determination of Dose Equivalent
- SC-48: Apportionment of Radiation Exposure
- SC-52: Conceptual Basis of Calculations of Dose Distributions
- SC-53: Biological Effects and Exposure Criteria for Radiofrequency Electromagnetic Radiation
- SC-54: Bioassay for Assessment of Control of Intake of Radionuclides
- SC-55: Experimental Verification of Internal Dosimetry Calculations
- SC-57: Internal Emitter Standards
 - Task Group 2 on Respiratory Tract Model

- Task Group 3 on General Metabolic Models
- Task Group 6 on Bone Problems
- Task Group 7 on Thyroid Cancer Risk
- Task Group 8 on Leukemia Risk
- Task Group 9 on Lung Cancer Risk
- Task Group 10 on Liver Cancer Risk
- Task Group 11 on Genetic Risk
- Task Group 12 on Strontium
- Task Group 13 on Neptunium
- SC-59: Human Radiation Exposure Experience
- SC-61: Radon Measurements
- SC-63: Control of Exposure to Ionizing Radiation from Accident or Attack
- SC-64: Radionuclides in the Environment
 - Task Group 5 on Public Exposure to Nuclear Power
 - Task Group 6 on Screening Models
 - Task Group 7 on Contaminated Soil as a Source of Radiation Exposure
- SC-65: Quality Assurance and Accuracy in Radiation Protection Measurements
- SC-67: Biological Effects of Magnetic Fields
- SC-68: Microprocessors in Dosimetry
- SC-69: Efficacy Studies in Diagnostic Radiology
- SC-70: Quality Assurance and Measurement in Diagnostic Radiology
- SC-71: Radiation Exposure and Potentially Related Injury
- SC-72: Radiation Protection in Mammography
- SC-74: Radiation Received in the Decontamination of Nuclear Facilities
- SC-75: Guidance on Radiation Received in Space Activities
- SC-76: Effects of Radiation on the Embryo-Fetus
- SC-77: Guidance on Occupational and Public Exposure Resulting from Diagnostic Nuclear Medicine Procedures
- SC-78: Practical Guidance on the Evaluation of Human Exposures to Radiofrequency Radiation
- SC-79: Extremely Low-Frequency Electric and Magnetic Fields
- SC-80: Radiation Biology of the Skin (Beta-Ray Dosimetry)
- SC-81: Assessment of Exposure from Therapy
- Committee on Public Education
- Ad Hoc Committee on Policy in Regard to the International System of Units
- Ad Hoc Committee on Comparison of Radiation Exposures
- Study Group on Comparative Risk
 - Task Group on Comparative Carcinogenicity of Pollutant Chemicals
 - Task Force on Occupational Exposure Levels
- Ad Hoc Group on Model Used for Assessing Transport of Low Level Radioactive Waste
- Ad Hoc Group on Medical Evaluation of Radiation Workers

In recognition of its responsibility to facilitate and stimulate cooperation among organizations concerned with the scientific and related aspects of radiation protection and measurement, the Council has created a category of NCRP Collaborating Organizations. Organizations or groups of organizations that are national or international in scope and are concerned with scientific problems involving radiation quantities, units, measurements and effects, or radiation protection may be admitted to collaborating status by the Council. The present

Collaborating Organizations with which the NCRP maintains liaison are as follows:

American Academy of Dermatology
American Association of Physicians in Medicine
American College of Nuclear Physicians
American College of Radiology
American Dental Association
American Industrial Hygiene Association
American Institute of Ultrasound in Medicine
American Insurance Association
American Medical Association
American Nuclear Society
American Occupational Medical Association
American Podiatric Medical Association
American Public Health Association
American Radium Society
American Roentgen Ray Society
American Society of Radiologic Technologists
American Society for Therapeutic Radiology and Oncology
Association of University Radiologists
Atomic Industrial Forum
Bioelectromagnetics Society
College of American Pathologists
Federal Communications Commission
Federal Emergency Management Agency
Genetics Society of America
Health Physics Society
National Bureau of Standards
National Electrical Manufacturers Association
Radiation Research Society
Radiological Society of North America
Society of Nuclear Medicine
United States Air Force
United States Army
United States Department of Energy
United States Department of Housing and Urban Development
United States Department of Labor
United States Environmental Protection Agency
United States Navy
United States Nuclear Regulatory Commission
United States Public Health Service

The NCRP has found its relationships with these organizations to be extremely valuable to continued progress in its program.

Another aspect of the cooperative efforts of the NCRP relates to the special liaison relationships established with various governmental organizations that have an interest in radiation protection and measurements. This liaison relationship provides: (1) an opportunity for

participating organizations to designate an individual to provide liaison between the organization and the NCRP; (2) that the individual designated will receive copies of draft NCRP reports (at the time that these are submitted to the members of the Council) with an invitation to comment, but not vote; and (3) that new NCRP efforts might be discussed with liaison individuals as appropriate, so that they might have an opportunity to make suggestions on new studies and related matters. The following organizations participate in the special liaison program:

Defense Nuclear Agency
Federal Emergency Management Agency
National Bureau of Standards
Office of Science and Technology Policy
Office of Technology Assessment
United States Air Force
United States Army
United States Coast Guard
United States Department of Energy
United States Department of Health and Human Services
United States Department of Labor
United States Department of Transportation
United States Environmental Protection Agency
United States Navy
United States Nuclear Regulatory Commission

The NCRP values highly the participation of these organizations in the liaison program.

The Council's activities are made possible by the voluntary contribution of time and effort by its members and participants and the generous support of the following organizations:

Alfred P. Sloan Foundation
Alliance of American Insurers
American Academy of Dental Radiology
American Academy of Dermatology
American Association of Physicists in Medicine
American College of Radiology
American College of Radiology Foundation
American Dental Association
American Hospital Radiology Administrators
American Industrial Hygiene Association
American Insurance Association
American Medical Association
American Nuclear Society
American Occupational Medical Association
American Osteopathic College of Radiology

American Podiatric Medical Association
American Public Health Association
American Radium Society
American Roentgen Ray Society
American Society of Radiologic Technologists
American Society for Therapeutic Radiology and Oncology
American Veterinary Medical Association
American Veterinary Radiology Society
Association of University Radiologists
Atomic Industrial Forum
Battelle Memorial Institute
Center for Devices and Radiological Health
College of American Pathologists
Commonwealth of Pennsylvania
Defense Nuclear Agency
Edison Electric Institute
Edward Mallinckrodt, Jr. Foundation
Electric Power Research Institute
Federal Emergency Management Agency
Florida Institute of Phosphate Research
Genetics Society of America
Health Physics Society
James Picker Foundation
National Aeronautics and Space Administration
National Association of Photographic Manufacturers
National Bureau of Standards
National Cancer Institute
National Electrical Manufacturers Association
Radiation Research Society
Radiological Society of North America
Society of Nuclear Medicine
United States Department of Energy
United States Department of Labor
United States Environmental Protection Agency
United States Navy
United States Nuclear Regulatory Commission

To all of these organizations the Council expresses its profound appreciation for their support.

Initial funds for publication of NCRP reports were provided by a grant from the James Picker Foundation and for this the Council wishes to express its deep appreciation.

The NCRP seeks to promulgate information and recommendations based on leading scientific judgement on matters of radiation protection and measurement and to foster cooperation among organizations concerned with these matters. These efforts are intended to serve the public interest and the Council welcomes comments and suggestions on its reports or activities from those interested in its work.

NCRP Publications

NCRP publications are distributed by the NCRP Publications Office. Information on prices and how to order may be obtained by directing an inquiry to:

NCRP Publications
7910 Woodmont Avenue
Suite 800
Bethesda, MD 20814-3095

The currently available publications are listed below.

NCRP Reports

No.	Title
8	<i>Control and Removal of Radioactive Contamination in Laboratories</i> (1951)
22	<i>Maximum Permissible Body Burdens and Maximum Permissible Concentrations of Radionuclides in Air and in Water for Occupational Exposure</i> (1959) [Includes Addendum 1 issued in August 1963]
23	<i>Measurement of Neutron Flux and Spectra for Physical and Biological Applications</i> (1960)
25	<i>Measurement of Absorbed Dose of Neutrons, and of Mixtures of Neutrons and Gamma Rays</i> (1961)
27	<i>Stopping Powers for Use with Cavity Chambers</i> (1961)
30	<i>Safe Handling of Radioactive Materials</i> (1964)
32	<i>Radiation Protection in Educational Institutions</i> (1966)
35	<i>Dental X-Ray Protection</i> (1970)
36	<i>Radiation Protection in Veterinary Medicine</i> (1970)
37	<i>Precautions in the Management of Patients Who Have Received Therapeutic Amounts of Radionuclides</i> (1970)
38	<i>Protection Against Neutron Radiation</i> (1971)
40	<i>Protection Against Radiation from Brachytherapy Sources</i> (1972)
41	<i>Specification of Gamma-Ray Brachytherapy Sources</i> (1974)
42	<i>Radiological Factors Affecting Decision-Making in a Nuclear Attack</i> (1974)

- 44 *Krypton-85 in the Atmosphere—Accumulation, Biological Significance, and Control Technology* (1975)
- 46 *Alpha-Emitting Particles in Lungs* (1975)
- 47 *Tritium Measurement Techniques* (1976)
- 49 *Structural Shielding Design and Evaluation for Medical Use of X Rays and Gamma Rays of Energies Up to 10 MeV* (1976)
- 50 *Environmental Radiation Measurements* (1976)
- 51 *Radiation Protection Design Guidelines for 0.1-100 MeV Particle Accelerator Facilities* (1977)
- 52 *Cesium-137 from the Environment to Man: Metabolism and Dose* (1977)
- 54 *Medical Radiation Exposure of Pregnant and Potentially Pregnant Women* (1977)
- 55 *Protection of the Thyroid Gland in the Event of Releases of Radioiodine* (1977)
- 57 *Instrumentation and Monitoring Methods for Radiation Protection* (1978)
- 58 *A Handbook of Radioactivity Measurements Procedures*, 2nd ed. (1985)
- 59 *Operational Radiation Safety Program* (1978)
- 60 *Physical, Chemical, and Biological Properties of Radioeuropium Relevant to Radiation Protection Guidelines* (1978)
- 61 *Radiation Safety Training Criteria for Industrial Radiography* (1978)
- 62 *Tritium in the Environment* (1979)
- 63 *Tritium and Other Radionuclide Labeled Organic Compounds Incorporated in Genetic Material* (1979)
- 64 *Influence of Dose and Its Distribution in Time on Dose-Response Relationships for Low-LET Radiations* (1980)
- 65 *Management of Persons Accidentally Contaminated with Radionuclides* (1980)
- 67 *Radiofrequency Electromagnetic Fields—Properties, Quantities and Units, Biophysical Interaction, and Measurements* (1981)
- 68 *Radiation Protection in Pediatric Radiology* (1981)
- 69 *Dosimetry of X-Ray and Gamma-Ray Beams for Radiation Therapy in the Energy Range 10 keV to 50 MeV* (1981)
- 70 *Nuclear Medicine—Factors Influencing the Choice and Use of Radionuclides in Diagnosis and Therapy* (1982)
- 71 *Operational Radiation Safety—Training* (1983)
- 72 *Radiation Protection and Measurement for Low-Voltage Neutron Generators* (1983)

- 73 *Protection in Nuclear Medicine and Ultrasound Diagnostic Procedures in Children* (1983)
- 74 *Biological Effects of Ultrasound: Mechanisms and Clinical Implications* (1983)
- 75 *Iodine-129: Evaluation of Releases from Nuclear Power Generation* (1983)
- 76 *Radiological Assessment: Predicting the Transport, Bioaccumulation, and Uptake by Man of Radionuclides Released to the Environment* (1984)
- 77 *Exposures from the Uranium Series with Emphasis on Radon and Its Daughters* (1984)
- 78 *Evaluation of Occupational and Environmental Exposures to Radon and Radon Daughters in the United States* (1984)
- 79 *Neutron Contamination from Medical Electron Accelerators* (1984)
- 80 *Induction of Thyroid Cancer by Ionizing Radiation* (1985)
- 81 *Carbon-14 in the Environment* (1985)
- 82 *SI Units in Radiation Protection and Measurements* (1985)
- 83 *The Experimental Basis for Absorbed-Dose Calculations in Medical Uses of Radionuclides* (1985)
- 84 *General Concepts for the Dosimetry of Internally Deposited Radionuclides* (1985)
- 85 *Mammography—A User's Guide* (1986)
- 86 *Biological Effects and Exposure Criteria for Radiofrequency Electromagnetic Fields* (1986)
- 87 *Use of Bioassay Procedures for Assessment of Internal Radionuclide Deposition* (1987)
- 88 *Radiation Alarms and Access Control Systems* (1986)
- 89 *Genetic Effects from Internally Deposited Radionuclides* (1987)
- 90 *Neptunium: Radiation Protection Guidelines* (1988)
- 92 *Public Radiation Exposure from Nuclear Power Generation in the United States* (1987)
- 93 *Ionizing Radiation Exposure of the Population of the United States* (1987)
- 94 *Exposure of the Population in the United States and Canada from Natural Background Radiation* (1987)
- 95 *Radiation Exposure of the U.S. Population from Consumer Products and Miscellaneous Sources* (1987)
- 96 *Comparative Carcinogenicity of Ionizing Radiation and Chemicals* (1989)
- 97 *Measurement of Radon and Radon Daughters in Air* (1988)
- 98 *Guidance on Radiation Received in Space Activities* (1989)
- 99 *Quality Assurance for Diagnostic Imaging* (1988)

122 / NCRP PUBLICATIONS

- 100 *Exposure of the U.S. Population from Diagnostic Medical Radiation* (1989)
- 101 *Exposure of the U.S. Population from Occupational Radiation* (1989)
- 102 *Medical X-Ray, Electron Beam and Gamma-Ray Protection for Energies Up to 50 MeV (Equipment Design, Performance and Use)* (1989)
- 103 *Control of Radon in Houses* (1989)
- 104 *The Relative Biological Effectiveness of Radiations of Different Quality* (1990)
- 105 *Radiation Protection for Medical and Allied Health Personnel* (1989)
- 106 *Limit for Exposure to "Hot Particles" on the Skin* (1989)
- 107 *Implementation of the Principle of As Low As Reasonably Achievable (ALARA) for Medical and Dental Personnel* (1990)
- 108 *Conceptual Basis for Calculations of Absorbed-Dose Distributions* (1991)
- 109 *Effects of Ionizing Radiation on Aquatic Organisms* (1991)
- 110 *Some Aspects of Strontium Radiobiology* (1991)
- 111 *Developing Radiation Emergency Plans for Academic, Medical or Industrial Facilities* (1991)
- 112 *Calibration of Survey Instruments Used in Radiation Protection for the Assessment of Ionizing Radiation Fields and Radioactive Surface Contamination* (1991)
- 113 *Exposure Criteria for Medical Diagnostic Ultrasound: I. Criteria Based on Thermal Mechanisms* (1992)
- 114 *Maintaining Radiation Protection Records* (1992)
- 115 *Risk Estimates for Radiation Protection* (1993)
- 116 *Limitation of Exposure to Ionizing Radiation* (1993)
- 117 *Research Needs for Radiation Protection* (1993)
- 118 *Radiation Protection in the Mineral Extraction Industry* (1993)
- 119 *A Practical Guide to the Determination of Human Exposure to Radiofrequency Fields* (1993)
- 120 *Dose Control at Nuclear Power Plants* (1994)

Binders for NCRP reports are available. Two sizes make it possible to collect into small binders the "old series" of reports (NCRP Reports Nos. 8-30) and into large binders the more recent publications (NCRP Reports Nos. 32-120). Each binder will accommodate from five to seven reports. The binders carry the identification "NCRP Reports" and come with label holders which permit the user to attach labels showing the reports contained in each binder.

The following bound sets of NCRP reports are also available:

Volume I.	NCRP Reports Nos. 8, 22
Volume II.	NCRP Reports Nos. 23, 25, 27, 30
Volume III.	NCRP Reports Nos. 32, 35, 36, 37
Volume IV.	NCRP Reports Nos. 38, 40, 41
Volume V.	NCRP Reports Nos. 42, 44, 46
Volume VI.	NCRP Reports Nos. 47, 49, 50, 51
Volume VII.	NCRP Reports Nos. 52, 53, 54, 55, 57
Volume VIII.	NCRP Report No. 58
Volume IX.	NCRP Reports Nos. 59, 60, 61, 62, 63
Volume X.	NCRP Reports Nos. 64, 65, 66, 67
Volume XI.	NCRP Reports Nos. 68, 69, 70, 71, 72
Volume XII.	NCRP Reports Nos. 73, 74, 75, 76
Volume XIII.	NCRP Reports Nos. 77, 78, 79, 80
Volume XIV.	NCRP Reports Nos. 81, 82, 83, 84, 85
Volume XV.	NCRP Reports Nos. 86, 87, 88, 89
Volume XVI.	NCRP Reports Nos. 90, 91, 92, 93
Volume XVII.	NCRP Reports Nos. 94, 95, 96, 97
Volume XVIII.	NCRP Reports Nos. 98, 99, 100
Volume XIX.	NCRP Reports Nos. 101, 102, 103, 104
Volume XX.	NCRP Reports Nos. 105, 106, 107, 108
Volume XXI.	NCRP Reports Nos. 109, 110, 111
Volume XXII.	NCRP Reports Nos. 112, 113, 114
Volume XXIII.	NCRP Reports Nos. 115, 116, 117, 118

(Titles of the individual reports contained in each volume are given above.)

NCRP Commentaries

No.	Title
1	<i>Krypton-85 in the Atmosphere—With Specific Reference to the Public Health Significance of the Proposed Controlled Release at Three Mile Island</i> (1980)
2	<i>Preliminary Evaluation of Criteria for the Disposal of Transuranic Contaminated Waste</i> (1982)
3	<i>Screening Techniques for Determining Compliance with Environmental Standards—Releases of Radionuclides to the Atmosphere</i> (1986), Revised (1989)
4	<i>Guidelines for the Release of Waste Water from Nuclear Facilities with Special Reference to the Public Health Significance of the Proposed Release of Treated Waste Waters at Three Mile Island</i> (1987)

- 5 *Review of the Publication, Living Without Landfills* (1989)
- 6 *Radon Exposure of the U.S. Population—Status of the Problem* (1991)
- 7 *Misadministration of Radioactive Material in Medicine—Scientific Background* (1991)
- 8 *Uncertainty in NCRP Screening Models Relating to Atmospheric Transport, Deposition and Uptake by Humans* (1993)
- 9 *Considerations Regarding the Unintended Radiation Exposure of the Embryo, Fetus or Nursing Child* (1994)
- 10 *Advising the Public about Radiation Emergencies: A Document for Public Comment* (1994)

Proceedings of the Annual Meeting

No.	Title
1	<i>Perceptions of Risk</i> , Proceedings of the Fifteenth Annual Meeting held on March 14–15, 1979 (including Taylor Lecture No. 3) (1980)
3	<i>Critical Issues in Setting Radiation Dose Limits</i> , Proceedings of the Seventeenth Annual Meeting held on April 8–9, 1981 (including Taylor Lecture No. 5) (1982)
4	<i>Radiation Protection and New Medical Diagnostic Approaches</i> , Proceedings of the Eighteenth Annual Meeting held on April 6–7, 1982 (including Taylor Lecture No. 6) (1983)
5	<i>Environmental Radioactivity</i> , Proceedings of the Nineteenth Annual Meeting held on April 6–7, 1983 (including Taylor Lecture No. 7) (1983)
6	<i>Some Issues Important in Developing Basic Radiation Protection Recommendations</i> , Proceedings of the Twentieth Annual Meeting held on April 4–5, 1984 (including Taylor Lecture No. 8) (1985)
7	<i>Radioactive Waste</i> , Proceedings of the Twenty-first Annual Meeting held on April 3–4, 1985 (including Taylor Lecture No. 9) (1986)
8	<i>Nonionizing Electromagnetic Radiations and Ultrasound</i> , Proceedings of the Twenty-second Annual Meeting held on April 2–3, 1986 (including Taylor Lecture No. 10) (1988)
9	<i>New Dosimetry at Hiroshima and Nagasaki and Its Implications for Risk Estimates</i> , Proceedings of the Twenty-third Annual Meeting held on April 8–9, 1987 (including Taylor Lecture No. 11) (1988)

- 10 *Radon*, Proceedings of the Twenty-fourth Annual Meeting held on March 30–31, 1988 (including Taylor Lecture No. 12) (1989)
- 11 *Radiation Protection Today—The NCRP at Sixty Years*, Proceedings of the Twenty-fifth Annual Meeting held on April 5–6, 1989 (including Taylor Lecture No. 13) (1990)
- 12 *Health and Ecological Implications of Radioactively Contaminated Environments*, Proceedings of the Twenty-sixth Annual Meeting held on April 4–5, 1990 (including Taylor Lecture No. 14) (1991)
- 13 *Genes, Cancer and Radiation Protection*, Proceedings of the Twenty-seventh Annual Meeting held on April 3–4, 1991 (including Taylor Lecture No. 15) (1992)
- 14 *Radiation Protection in Medicine*, Proceedings of the Twenty-eighth Annual Meeting held on April 1–2, 1992 (including Taylor Lecture No. 16) (1993)

Lauriston S. Taylor Lectures

No.	Title
1	<i>The Squares of the Natural Numbers in Radiation Protection</i> by Herbert M. Parker (1977)
2	<i>Why be Quantitative about Radiation Risk Estimates?</i> by Sir Edward Pochin (1978)
3	<i>Radiation Protection—Concepts and Trade Offs</i> by Hymer L. Friedell (1979) [Available also in <i>Perceptions of Risk</i> , see above]
4	<i>From “Quantity of Radiation” and “Dose” to “Exposure” and “Absorbed Dose”—An Historical Review</i> by Harold O. Wyckoff (1980)
5	<i>How Well Can We Assess Genetic Risk? Not Very</i> by James F. Crow (1981) [Available also in <i>Critical Issues in Setting Radiation Dose Limits</i> , see above]
6	<i>Ethics, Trade-offs and Medical Radiation</i> by Eugene L. Saenger (1982) [Available also in <i>Radiation Protection and New Medical Diagnostic Approaches</i> , see above]
7	<i>The Human Environment—Past, Present and Future</i> by Merril Eisenbud (1983) [Available also in <i>Environmental Radioactivity</i> , see above]
8	<i>Limitation and Assessment in Radiation Protection</i> by Harald H. Rossi (1984) [Available also in <i>Some Issues Important in Developing Basic Radiation Protection Recommendations</i> , see above]

- 9 *Truth (and Beauty) in Radiation Measurement* by John H. Harley (1985) [Available also in *Radioactive Waste*, see above]
- 10 *Biological Effects of Non-ionizing Radiations: Cellular Properties and Interactions* by Herman P. Schwan (1987) [Available also in *Nonionizing Electromagnetic Radiations and Ultrasound*, see above]
- 11 *How to be Quantitative about Radiation Risk Estimates* by Seymour Jablon (1988) [Available also in *New Dosimetry at Hiroshima and Nagasaki and its Implications for Risk Estimates*, see above]
- 12 *How Safe is Safe Enough?* by Bo Lindell (1988) [Available also in *Radon*, see above]
- 13 *Radiobiology and Radiation Protection: The Past Century and Prospects for the Future* by Arthur C. Upton (1989) [Available also in *Radiation Protection Today*, see above]
- 14 *Radiation Protection and the Internal Emitter Saga* by J. Newell Stannard (1990) [Available also in *Health and Ecological Implications of Radioactively Contaminated Environments*, see above]
- 15 *When is a Dose Not a Dose?* by Victor P. Bond (1992) [Available also in *Genes, Cancer and Radiation Protection*, see above]
- 16 *Dose and Risk in Diagnostic Radiology: How Big? How Little?* by Edward W. Webster (1992) [Available also in *Radiation Protection in Medicine*, see above]
- 17 *Science, Radiation Protection and the NCRP* by Warren K. Sinclair (1993)

Symposium Proceedings

The Control of Exposure of the Public to Ionizing Radiation in the Event of Accident or Attack, Proceedings of a Symposium held April 27–29, 1981 (1982)

NCRP Statements

No.	Title
1	"Blood Counts, Statement of the National Committee on Radiation Protection," <i>Radiology</i> 63 , 428 (1954)
2	"Statements on Maximum Permissible Dose from Television Receivers and Maximum Permissible Dose to the Skin of the Whole Body," <i>Am. J. Roentgenol., Radium Ther. and Nucl. Med.</i> 84 , 152 (1960) and <i>Radiology</i> 75 , 122 (1960)

- 3 *X-Ray Protection Standards for Home Television Receivers, Interim Statement of the National Council on Radiation Protection and Measurements* (1968)
- 4 *Specification of Units of Natural Uranium and Natural Thorium, Statement of the National Council on Radiation Protection and Measurements* (1973)
- 5 *NCRP Statement on Dose Limit for Neutrons* (1980)
- 6 *Control of Air Emissions of Radionuclides* (1984)
- 7 *The Probability That a Particular Malignancy May Have Been Caused by a Specified Irradiation* (1992)

Other Documents

The following documents of the NCRP were published outside of the NCRP Report, Commentary and Statement series:

- Somatic Radiation Dose for the General Population*, Report of the Ad Hoc Committee of the National Council on Radiation Protection and Measurements, 6 May 1959, Science, February 19, 1960, Vol. 131, No. 3399, pages 482-486
- Dose Effect Modifying Factors In Radiation Protection*, Report of Subcommittee M-4 (Relative Biological Effectiveness) of the National Council on Radiation Protection and Measurements, Report BNL 50073 (T-471) (1967) Brookhaven National Laboratory (National Technical Information Service, Springfield, Virginia)

The following documents are now superseded and/or out of print:

NCRP Reports

No.	Title
1	<i>X-Ray Protection</i> (1931) [Superseded by NCRP Report No. 3]
2	<i>Radium Protection</i> (1934) [Superseded by NCRP Report No. 4]
3	<i>X-Ray Protection</i> (1936) [Superseded by NCRP Report No. 6]
4	<i>Radium Protection</i> (1938) [Superseded by NCRP Report No. 13]
5	<i>Safe Handling of Radioactive Luminous Compound</i> (1941) [Out of Print]
6	<i>Medical X-Ray Protection Up to Two Million Volts</i> (1949) [Superseded by NCRP Report No. 18]

- 7 *Safe Handling of Radioactive Isotopes* (1949) [Superseded by NCRP Report No. 30]
- 9 *Recommendations for Waste Disposal of Phosphorus-32 and Iodine-131 for Medical Users* (1951) [Out of Print]
- 10 *Radiological Monitoring Methods and Instruments* (1952) [Superseded by NCRP Report No. 57]
- 11 *Maximum Permissible Amounts of Radioisotopes in the Human Body and Maximum Permissible Concentrations in Air and Water* (1953) [Superseded by NCRP Report No. 22]
- 12 *Recommendations for the Disposal of Carbon-14 Wastes* (1953) [Superseded by NCRP Report No. 81]
- 13 *Protection Against Radiations from Radium, Cobalt-60 and Cesium-137* (1954) [Superseded by NCRP Report No. 24]
- 14 *Protection Against Betatron-Synchrotron Radiations Up to 100 Million Electron Volts* (1954) [Superseded by NCRP Report No. 51]
- 15 *Safe Handling of Cadavers Containing Radioactive Isotopes* (1953) [Superseded by NCRP Report No. 21]
- 16 *Radioactive-Waste Disposal in the Ocean* (1954) [Out of Print]
- 17 *Permissible Dose from External Sources of Ionizing Radiation* (1954) including *Maximum Permissible Exposures to Man, Addendum to National Bureau of Standards Handbook 59* (1958) [Superseded by NCRP Report No. 39]
- 18 *X-Ray Protection* (1955) [Superseded by NCRP Report No. 26]
- 19 *Regulation of Radiation Exposure by Legislative Means* (1955) [Out of Print]
- 20 *Protection Against Neutron Radiation Up to 30 Million Electron Volts* (1957) [Superseded by NCRP Report No. 38]
- 21 *Safe Handling of Bodies Containing Radioactive Isotopes* (1958) [Superseded by NCRP Report No. 37]
- 24 *Protection Against Radiations from Sealed Gamma Sources* (1960) [Superseded by NCRP Reports No. 33, 34 and 40]
- 26 *Medical X-Ray Protection Up to Three Million Volts* (1961) [Superseded by NCRP Reports No. 33, 34, 35 and 36]
- 28 *A Manual of Radioactivity Procedures* (1961) [Superseded by NCRP Report No. 58]
- 29 *Exposure to Radiation in an Emergency* (1962) [Superseded by NCRP Report No. 42]
- 31 *Shielding for High-Energy Electron Accelerator Installations* (1964) [Superseded by NCRP Report No. 51]
- 33 *Medical X-Ray and Gamma-Ray Protection for Energies up to 10 MeV—Equipment Design and Use* (1968) [Superseded by NCRP Report No. 102]

- 34 *Medical X-Ray and Gamma-Ray Protection for Energies Up to 10 MeV—Structural Shielding Design and Evaluation Handbook* (1970) [Superseded by NCRP Report No. 49]
- 39 *Basic Radiation Protection Criteria* (1971) [Superseded by NCRP Report No. 91]
- 43 *Review of the Current State of Radiation Protection Philosophy* (1975) [Superseded by NCRP Report No. 91]
- 45 *Natural Background Radiation in the United States* (1975) [Superseded by NCRP Report No. 94]
- 48 *Radiation Protection for Medical and Allied Health Personnel* (1976) [Superseded by NCRP Report No. 105]
- 53 *Review of NCRP Radiation Dose Limit for Embryo and Fetus in Occupationally-Exposed Women* (1977) [Out of Print]
- 56 *Radiation Exposure from Consumer Products and Miscellaneous Sources* (1977) [Superseded by NCRP Report No. 95]
- 58 *A Handbook of Radioactivity Measurements Procedures*, 1st ed. (1978) [Superseded by NCRP Report No. 58, 2nd ed.]
- 66 *Mammography* (1980) [Out of Print]
- 91 *Recommendations on Limits for Exposure to Ionizing Radiation* (1987) [Superseded by NCRP Report No. 116]

NCRP Proceedings

No.	Title
2	<i>Quantitative Risk in Standards Setting</i> , Proceedings of the Sixteenth Annual Meeting held on April 2–3, 1980 [Out of Print]

Index

- Accelerators 2–4, 95–97
 Betatrons 2, 95
 Linear 3, 96, 97
 Microtrons 4
- Activation 69, 70
 Accelerator and treatment aids 69
 Patient 70
 Walls 70
- Albedo 49, 54, 55
- Average Energy 31, 40, 43–48, 50, 51, 57, 58
- Betatrons 2, 95
- Bonner Multisphere Spectrometer 79
- Bremsstrahlung-Weighted Cross Section 13–17
- Conversion Factors 44, 45, 46, 48
- Cookbook Method 46–48
- Cross Sections for Photoneutron Production 5, 7, 9–12
- Detectors 73–97
 Activation 73–81
 Diodes 88–90
 Etched track 81–88
 Geiger-Müller 90, 92
 Ionization chamber 90, 91
 Moderated foils 78, 79
 Photon interference 77, 79, 85, 87, 89, 91
 Proportional counters 90, 92
 Rem meters 78
 Thermal neutron 75
 Threshold 74–78
- Dipole Sum Rule 5, 8
- Doors 57–59
- Dose 63–67
 Head leakage 63–67
 Induced radioactivity in patient 63, 66, 67
 Neutrons produced in the patient 63–67
 Scattered photons 63–67
- Electroproduction of Neutrons 5, 9, 13, 14, 15
- Equivalent Quantum, Cross Section Per 13–17
- Etched Track Detectors 81–88
- Geiger-Müller Counters 90, 92
- Giant Resonance 2, 5–12, 31
 Cross section 5, 7, 9–12
 Mean energy 5, 7, 8, 31
 Strength 5, 7, 8
- Half-Energy Layer (HEL) 40, 43
- Half-Value Layer (HVL) or Tenth-Value Layer (TVL) 50–52, 64
- Hazards from Neutrons 61–72
 Exposures during installation 71
 Operating personnel risk 68
 Patient risk 61–68
- Induced Radioactivity (see Activation & Detectors, Activation)
- Ionization Chambers 90, 91
- Leakage Radiation 63–67, 94–97
- Level Density Parameter 27, 31–33
- Linear Accelerators 3, 96, 97
- Maze Design 52, 53
- Microtrons 4
- Moderated Foil Detectors 78, 79
- Neutron Capture Gamma-Rays 56–58, 92
- Neutron Measurements 73–97
 Activation detectors 73–81
 Comparison of methods 80, 91
 Data collection 80, 81
 Diodes 88–90
 Experimental results 95–97
 Etched track detectors 81–88
 Geiger-Müller counters 90, 92
 Ionization chambers 90, 91

- Neutron Measurements (Continued)**
- Moderated foil detectors 78, 79
 - Photon interference 85, 87, 89, 91
 - Proportional counters 90, 92
 - Rem meters 78
 - Results on various accelerators 94-97
 - Spectral 79
 - Thermal 75
 - Threshold detectors 74-77
- Neutron Production (see Photoproduction of Neutrons, Electroproduction of Neutrons)**
- Neutron Removal Cross Sections 43
 - Neutron Scattering 34-37, 39, 46, 47
 - Cross section 34, 35
 - Effect on Spectra 34-37, 39, 47
 - Elastic 34
 - Inelastic 34-36
 - Nonelastic 34
 - Neutron Transport 34-43, 46-49, 52-59
 - In accelerator head 34-43, 48
 - In concrete rooms 46-48
 - In mazes 52-59
 - Nuclear Temperature 28, 32, 33
- Operating Personnel Risk 68-71**
- Activation 69, 70
 - Door leakage 68
- Patient Risk 61-68**
- Personnel Dosimeters 68**
- Personnel Exposures 69-72**
- Photofission 1, 17, 85**
- Threshold energy 1
- Photoproduction of Neutrons 1, 5-9, 13-33, 38-48, 57-60, 63**
- Average energy of photoneutrons 39-48, 57
 - Cross sections 13, 14, 17, 18, 22, 23
- Photoproduction of Neutrons (Continued)**
- Direct interaction neutrons 28, 30
 - In patient 63
 - Minimizing 59, 60
 - Spectra 26-33, 38-42
 - Threshold (separation) energy 1, 6, 19, 20, 21
 - Yield 15-18, 22-26, 29, 30
- Proportional Counters 90, 92**
- Rem Meters 78**
- Resonance Reactions 2**
- Scattered Photon Dose to Patient 63, 67**
- Separation Energy (see Threshold Energy)**
- Shielding 42-44, 49-59**
- Albedo 55
 - Borated materials 41, 58
 - Combined materials 52
 - Concrete 50-52, 57, 58
 - Doors 57-59
 - Heavy metals 34-44
 - Maze design 52-59
 - Monoeenergetic neutrons 50
 - Polyethylene 50-52, 57-59
 - Tenth-value layer (TVL) (or half value layer) 50-52, 57, 64
 - Wood 59
- Stopping Power 16, 17**
- Tenth-Value Layer (or half value layer) 50-52, 57, 64**
- Capture gamma-rays 57
 - Neutrons 50-52, 57, 64
- Threshold Detectors 74-78**
- Threshold Energy 1, 6, 19-21**
- Yield of Photoneutrons 15-18, 22-26, 29, 30**